Technical Report Documentation Page

1. Report No. FHWA/TX-00/1709-1	2. Government Accession No.	3. Recipient's Catalog No.
4. Title and Subtitle MULTI-BOX BEAM BRIDGES WITH COMPOSITE DECK		5. Report Date April 1999 Resubmitted: July 1999
		6. Performing Organization Code
7. Author(s) Harry L. Jones		8. Performing Organization Report No. Report 1709-1
9. Performing Organization Name and Address Texas Transportation Institute The Texas A&M University System College Station, TX 77843-3135		10. Work Unit No. (TRAIS)
		11. Contract or Grant No. Project No. 0-1709
12. Sponsoring Agency Name and Address Texas Department of Transportation Research and Technology Transfer Office P. O. Box 5080 Austin, TX 78763-5080		13. Type of Report and Period Covered Research: Sept. 1, 1996 – Aug. 31, 1998
		14. Sponsoring Agency Code

15. Supplementary Notes
Research performed in cooperation with the Texas Department of Transportation and the U.S. Department of Transportation, Federal Highway Administration.
Research Project Title: Load Transfer Properties of Cast-in-Place Deck on Multi-beam Box Beam Bridges

16. Abstract

This report describes the study of lateral distribution factors and control of longitudinal cracking in multi-beam prestressed concrete box girder bridges with composite concrete deck slab. Researchers developed recommended values for lateral distribution factors for 22 different Texas Department of Transportation (TxDOT) bridge configurations. Formulas and tables for predicting the maximum values of transverse moment in the deck slab from American Association of State Highway and Transportation Officials (AASHTO) truck loadings are presented. Recommendations for control of longitudinal deck cracking are made.

17. Key Words Box, Beam, Multi-beam, Bridge, Concrete, Prestressed, Lateral, Distribution, Factor, Longitudinal, Cracking	18. Distribution Statement No restrictions. This document is available to the public through NTIS: National Technical Information Service 528 Port Royal Rd. Springfield, Virginia 22161		
19. Security Classif.(of this report) Unclassified	20. Security Classif.(of this page) Unclassified	21. No. of Pages 136	22. Price

Form DOT F 1700.7 (8-72) **Reproduction of completed page authorized**

MULTI-BOX BEAM BRIDGES WITH COMPOSITE DECK

by

Harry L. Jones
Associate Research Engineer
Texas Transportation Institute

Report 1709-1
Project Number 0-1709
Research Project Title: Load Transfer Properties of Cast-in-Place Deck
on Multi-beam Box Beam Bridges

Sponsored by the
Texas Department of Transportation
In Cooperation with the
U.S. Department of Transportation
Federal Highway Administration

April 1999
Resubmitted: July 1999

TEXAS TRANSPORTATION INSTITUTE
The Texas A&M University System
College Station, Texas 77843-3135

DISCLAIMER

The contents of this report reflect the views of the author, who is responsible for the facts and accuracy of the data presented herein. The contents do not necessarily reflect the official views or policies of the Texas Department of Transportation (TxDOT) or the U.S. Department of Transportation, Federal Highway Administration. This report does not constitute a standard, specification, or regulation. In addition, the above assumes no liability for its contents or use thereof.

ACKNOWLEDGMENTS

This project was sponsored by the Texas Department of Transportation in cooperation with the U.S. Department of Transportation, Federal Highway Administration. The assistance of Brian Merrill, TxDOT project director, is gratefully acknowledged. The vehicle used in load testing was provided at no charge by TXI Transportation in Dallas.

TABLE OF CONTENTS

TABLE OF CONTENTS (continued)

LISTS OF FIGURES

LISTS OF FIGURES (continued)

LIST OF TABLES

CHAPTER ONE ■ INTRODUCTION

The prestressed concrete multi-beam box girder bridge is often the structure of choice when vertical clearance and/or speed of construction are important factors. This bridge type has been used in Texas at least since the late 1960s (Ybanez, 1990). The vast majority of box beam sections used in the state are standard shapes developed by Texas Department of Transportation (TxDOT). In addition to these standard sections, some bridges were built with an American Association of State Highway Transportation Officials - Prestressed Concrete Institute (AASHTO - PCI) shape which differs from the TxDOT standard shapes in several important ways. For approximately 30 years multi-beam box girder bridges in Texas were constructed with a concrete shear key between adjacent beams to cause them to act as a unit in sharing live loads. Transverse post tensioning was also used as a device to tie the beams together laterally.

Experience with this type bridge has shown there is a tendency for longitudinal cracking to develop in the asphalt riding surface over the shear keys. The cracks result from longitudinal cracking in the shear key concrete itself and can potentially lead to staining of concrete on the underside of the bridge due to water leakage through the asphalt/shear key as well as possible corrosion of transverse post tension strands, if present. Additionally, the presence of longitudinal cracks has raised questions concerning the integrity and adequacy of the shear key to serve as a mechanism for sharing live load forces among adjacent beams.

Beginning in the late 1980s, a new detail for multi-beam box girder bridges was instituted in Texas in which a structural composite concrete deck slab was added to the top of the boxes. This detail typically called for a 4 in. thick slab, although slabs of up to 8 in. were used in some cases. In order to reduce dead load and possibly cost, bridges of this construction were sometimes built without the concrete shear key. This was accomplished by using a thin piece of sheet metal to span between adjacent beam flanges, creating a void beneath the slab where the concrete shear key would normally be placed. This new detail almost immediately resulted in problems. Longitudinal cracks having the same general pattern as those found in bridges with only concrete shear keys (and no composite deck) now were developing in the concrete deck slab over the shear key area. The

problem seemed to be more severe in bridges which had no concrete in the shear keyway, but cracking was reported to be occurring in both kinds of construction. With a cracked deck slab and possibly no shear key available to distribute live load forces among box beams, questions arose as to whether individual boxes were being designed to resist the forces they actually experienced. In addition, there remained the potential problem of leakage of water between beams through the cracks in the deck, as well as the potentially new problem of corrosion of deck steel and transverse post tensioning, if present.

These circumstances led TxDOT to initiate a project to examine these issues, concentrating on the composite deck slab construction detail. This report presents the results of that project and offers recommendations for modification of TxDOT practices with regard to design and construction of this bridge type.

LITERATURE REVIEW

Methods of Analysis

Published works on multi-beam bridges extend back to at least the 1950s. The preponderance of those works, including Walther [1957], Duberg et al. [1960], Arya et al. [1961], Pool [1963], Cusens and Pama [1965], and Powell et al. [1969] deal with methods of analysis that determine the forces in the individual beams induced by vehicular loads on the bridge structure. Each of these analysis methods assume the presence of some type of lateral connection between adjacent beams. Pool treated this connection as a continuous hinge, capable of transmitting vertical shear, lateral thrust, and axial force, but no transverse moment. Powell generalized this approach by assuming a series of four continuous springs at the juncture of adjacent beams and thus allowed for the presence of vertical shear, lateral thrust, axial force, and transverse moment. Jones and Boaz [1986] extended Powell's work to allow for the analysis of skewed structures and discrete rather than continuous lateral connections.

With current commercially available structural analysis software, it is possible to develop very detailed models of multi-beam bridges. Huckelbridge et al. [1993] performed a study of load

transfer in prestressed concrete multi-beam box girder bridges used in Ohio. As a part of that study, they used solid finite elements ("3D bricks") to model each beam in a hypothetical three-beam structure. Slab and beam bridges can be analyzed using plate elements to represent the deck slab and beam elements for the beams. Zokaie et al. [1993] created a general bridge analysis computer program using these types of elements which computes live load lateral distribution factors for a variety of bridge types, including the multi-beam bridge. Unfortunately, the program assumes that beams are connected laterally with a momentless hinge and that connection occurs at the centroid level of the beams. Both these assumptions are clearly inappropriate for multi-beam bridges having a composite deck slab.

The primary difficulty with models at this level of detail is the enormous amount of effort needed to create and check a model, as well as to extract the desired analysis results. For the hundreds of analyses needed to establish general live load lateral distribution factors, such models are not practical. For this reason, the formulations of Powell and Jones and their associated computer programs were used extensively in this study. The results from these models are compared against detailed finite element models in Chapter Three as part of a project conducted to validate their ability to predict forces in the composite deck slab and longitudinal beams.

Shear Keys

There is body of evidence suggesting multi-beam bridges throughout the U.S. connected laterally with shear keys suffer problems with longitudinal cracking at the keyway. The Prestressed Concrete Institute (PCI) is currently finalizing a subcommittee report on reflective cracking in adjacent box beam bridges (PCI, 1995). This study reports longitudinal joint failure between adjacent box beams as a problem in most regions of the U.S. The report is based on national surveys of state DOTs conducted in 1988, 1990, and most recently in 1992. In the latest survey, 50 percent of the respondents (including Texas) reported leakage at the longitudinal joints. In addition, a detailed analysis of five bridges in Ohio (Huckelbridge et al., 1993) found substantial deterioration of shear keys. Hlavacs et al. [1997] reported results from tests on a full-scale portion of the Ohio multi-beam box girder bridge. Their study monitored the development and growth under cyclic

loading of longitudinal cracks in the shear keys. They found that cracking in the shear key developed almost immediately after construction and prior to any live loading, as a result of shrinkage and thermal effects. They observed that little, if any, new keyway cracking was caused by simulated truck loading, but existing cracks propagated under repeated application of these loads. Laboratory testing of multi-beam bridge models have also been reported by Arockiasamy and Reddy [1992]. Static and fatigue loadings were applied to a scale model, and various data was collected on shear key performance and beam forces.

The beam cross sections examined in these studies differ radically from the TxDOT standard box section in that the shear keys were much smaller–typically 6 in. vertically and 3/4 in. deep. It is doubtful the live load induced stresses in those shear keys are representative of those found in TxDOT bridges. However, shrinkage and thermal cracking may well be more pronounced with the larger key area. In any event, attempts at detailed theoretical analysis of shear keys have been rather limited. Kaneko et al. [1993] used a fracture mechanics approach as well as experimental results to examine the strength of a typical shear key. Works by Gulyas et al. [1995], Annamalai and Brown [1990], and Hucklebridge et al. [1995] all examine the design, performance, and testing of grouted shear keys typically used in prestressed concrete multi-box beam bridges in this country. It also appears that useful information on shear key behavior might be found in research studies dealing with the strength of joints in segmental concrete construction (Koseki and Breen, 1983).

Deck Cracking

Cracking of concrete decks in highway bridges has been studied extensively. In most cases however, the cracks investigated were transverse as opposed to the longitudinal type found in multi-beam bridges. Nonetheless, those studies provide some insight into the mechanisms and the severity of cracks found in TxDOT multi-beam bridges with composite deck slab. A recent report by Krauss and Rogalla [1996] appears to be the most comprehensive work available on the subject. It examines in qualitative terms the important effects of shrinkage, initiation of cracking, and the role of temperature changes in advancing crack growth. It also cites results from a national survey of state DOTs which suggests that typical transverse crack surface widths range from about 0 .002 in. to

0.025 in. These values provide some perspective on the crack widths found on Texas bridges inspected in this study and discussed in the next chapter.

Other References

Several other assessments of the performance of multi-beam bridges have been published. Information compiled by Dunker and Rabbat [1992] indicates over 20,000 prestressed concrete multi-beam bridges were built in this country between 1950 and 1989. Yamane et al. [1994] reviewed successful precast prestressed concrete bridge practices in Japan, citing their heavily transversely post-tensioned multi-box beam system as one which has served with little or no problems associated with longitudinal cracking at the keyway. El-Remaily et al. [1996] present a design for prestressed concrete multi-box beam bridges which draws on the successful practices followed in Japan but purports to accommodate current U.S. construction practices.

Shear Key/Composite Deck Combination

No reports describing the combined use of shear keys with cast-in-place concrete deck on multi-beam bridge systems like those investigated in this study were found.

SPECIFIC PROBLEMS TO BE ADDRESSED

This study addresses the following questions:

- What is the basic mechanism(s) which leads to objectionable longitudinal cracking of the cast-in-place composite deck slab of multi-box beam bridges?
- What steps can be taken to minimize or eliminate this mode of deck cracking?
- What is an appropriate means for determining a live load lateral distribution factor (LLDF) to be used in designing the standard TxDOT box beams in this mode of construction? How do the resulting LLDF values compare to those computed using the AASHTO load in resistance factor design (LRFD) specification?

RESEARCH APPROACH

Inspections of some multi-box beam bridges with composite deck slab were conducted. Some of these structures had integral shear keys while others did not. These inspections confirmed the presence of longitudinal cracks in most cases. The cracks varied noticeably among the structures inspected. Interestingly, longitudinal cracks in the deck slab were in some cases located over box beams as well as directly over the shear key area. These findings tended to confirm the speculation that shrinkage stresses may play a significant role in the cracking process. Details and documentation of the inspections are contained in Chapter Two.

The principal tools used in developing answers to the questions cited above were analytical models. Various models were created to predict the stress state in the composite deck slab due to vehicular live loads and for predicting the live load bending moments and shears in the beams from which live load lateral distribution factors (LLDF) could be established. After appropriate analytical validation of the various models, they were used to perform analyses on a series of bridge structures taken from current TxDOT standards. These encompassed the four TxDOT standard box sections and a range of span lengths appropriate to each, composite deck slabs from 4 to 8 in. thick, and roadway widths from 28 to 52 ft. The results of this exercise suggested that truck traffic in certain bridge configurations produced transverse stresses large enough to cause the reported pattern of longitudinal cracking, especially given the likely presence of shrinkage cracks from the outset. The analytical models were also used to explore the effectiveness of several proposals for eliminating cracking in the composite deck. These are presented in Chapter Four.

The final task in this study investigated the lateral distribution of vehicular loads among beams in the multi-beam bridge with composite deck slab. Chapter Five presents formulas for LLDFs tailored to standard TxDOT boxes, bridge geometries, and deck thicknesses. Comparisons are also drawn between these LLDFs and those computed using the latest AASHTO LRFD provisions. Finally, load tests were performed on a typical multi-box beam bridge and the data from those tests compared with the predictions of analytical models used in the study. These comparisons are reported in Chapter Three.

CHAPTER TWO ■ FIELD STUDIES

BRIDGE INSPECTIONS

Composite deck multi-box beam bridges are in service at various locations around the state. A three-day inspection tour was conducted on June 30 through July 2, 1997, to examine bridges of the subject type located in the Fort Worth area. This locale was chosen because it offered a variety of deck and shear key type combinations as well as structures subject to interstate truck traffic and others on secondary roadways with correspondingly lighter volume and mix of vehicle loads. An additional inspection of a bridge which had not yet been opened to traffic was conducted in San Antonio on July 18, 1997.

Each bridge was given a walk around, looking for signs of distress in the beams or other anomalies that might be visible from beside or beneath the structure. The remainder of inspection efforts were devoted to the bridge deck and cracking found there. Typically one lane of traffic was blocked off to provide working space for closer examination of the deck surface. No attempt was made to map the exact crack locations. Instead, a general description of longitudinal crack locations was developed, and the widths of typical cracks were measured using a crack width comparator card and "feeler" gage, which are shown in Figures 2.1 and 2.2. The narrative below summarizes the findings for the various bridges which, for convenience, have been grouped by county.

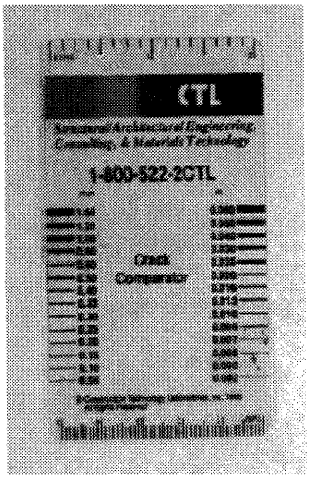

Figure 2.1. Crack Comparator Card.

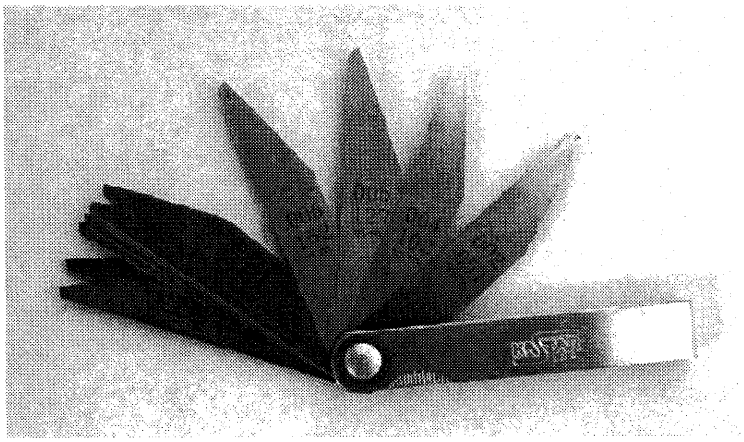

Figure 2.2. Feeler Gage.

Ellis County

- I-35 @ Waxahachie Creek - Northbound Lanes

This structure consists of seven 30 ft spans with armor joints at the juncture of spans 2 and 3 and spans 5 and 6. It is an unskewed bridge carrying interstate traffic with 38 ft roadway, 20 in. deep TxDOT boxes, arranged 8[5B20], with two traffic lanes plus a shoulder lane. The bridge has a 4 in. nominal composite deck slab with full depth concrete shear key and no transverse post tensioning. Visible longitudinal cracks in the top surface of the deck were confined to the two traffic lanes and had nominal surface widths in the range of 0.02-0.03 in. Cracks were found running longitudinally over the keyway between boxes and also over the boxes themselves, with about equal frequency.

- I-45 Underpass @ Station 1131

This underpass carries service road traffic over I-45. It consists of two 100 ft spans with a 40 ft roadway width and a mixture of 4 ft and 5 ft, 34 in. deep boxes arranged 4[4B34]+2[5B34]+ 4[4B34]. It contains two traffic lanes and has a 4 in. composite deck with full shear key and no transverse post tensioning. Longitudinal cracking was minimal, with surface crack widths in the 0.02-0.03 in. range which occurred over both keyways and boxes.

- I-45 Underpass @ Station 1252+85

This underpass carries service road traffic over I-45 and contains two 100 ft spans and a 28 ft roadway. The structure consists of six 34 in. deep boxes and two traffic lanes. It has a 4 in. composite deck, full shear key, and no transverse post tensioning. Cracking in the longitudinal direction was minimal, with cracks tending to form over boxes but not over the keyways. A sampling of surface crack widths fell in the 0.02-0.04 in. range. Figure 2.3 shows photographs of typical cracks (photo ID No. 1).

- I-45 Overpass @ Fifth Street - Northbound Lanes

The Fifth Street overpass carries I-45 traffic and consists of 35 ft-80 ft-35 ft spans carrying a 52 ft roadway. A mixture of 4 ft and 5 ft boxes arranged in a 4[5B34]+6[4B34]+2[5B34] pattern,

with phased construction consisting of 4[4B34]+2[5B34] (west side) followed by 4[5B34]+2[4B34] (east side). The structure contained three traffic lanes plus a shoulder. A 4 in. composite deck with shear key was used. The bridge has no transverse post tensioning. Longitudinal cracking was found in all lanes and occurred over both keyways and boxes. Crack widths of 0.01-0.02 in. were found in the less traveled lanes, while those in the more heavily traveled lanes were in the 0.04-0.06 in. range and tended to occur more frequently over boxes rather than keyways.

- FM 660 Overpass - Northbound Lanes

The FM 660 overpass carries I-45 traffic over FM 660 and is identical in layout, box beam configuration, and staged construction to the I-45 overpass at Fifth Street. It too has a 4 in. composite deck, shear key, and no transverse post tensioning. Longitudinal cracks were found both over the keyways (0.02-0.04 in. widths) and boxes (0.04-0.06 in. widths) in all traffic lanes and in all spans. Figure 2.4 shows typical deck cracks (photo ID No. 2). This structure also experienced a deck disintegration over an approximately 2 ft^2 area located over a keyway and at the juncture of the middle and end spans at the north end of the structure. Concrete in the affected area broke loose from the reinforcing steel mat (the bond to the steel appeared to be non-existent), producing a hole through the full thickness of the deck. Figure 2.5 shows photographs of the area.

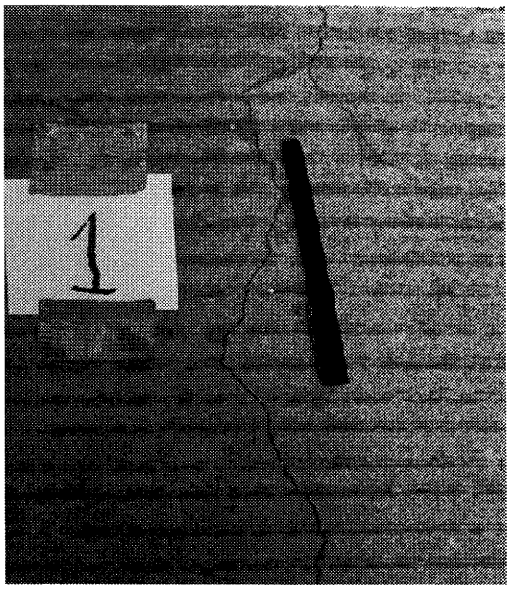

Figure 2.3. Longitudinal Deck Cracking on I-45 Underpass @ Station 1252+ 85.

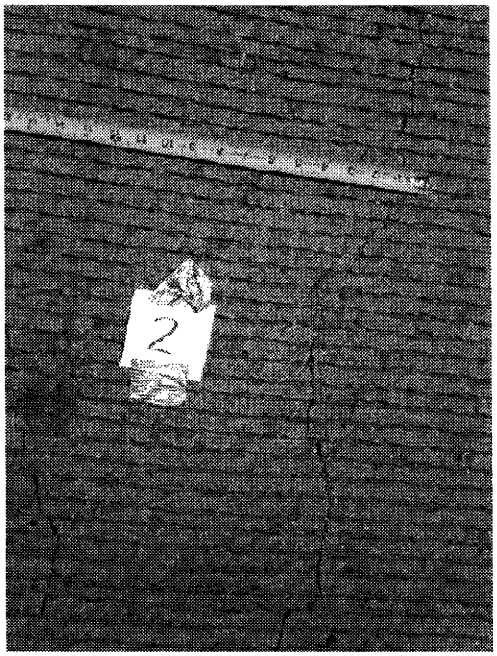

Figure 2.4. Longitudinal Deck Cracking on FM 660 Overpass.

Figure 2.5. Deck Blowout on FM 660 Overpass.

City of Arlington

- I-30 @ Cooper Street Underpass

This structure carries municipal traffic over I-30 and contains two spans of 89 ft and 101 ft. The roadway is 72 ft wide with 8 ft sidewalks on each side. Each span contains 17 TxDOT 5B34 boxes with a 4 in. composite slab and full shear key. Three lines of transverse post tensioning, located at mid-span of each span and over the interior support between spans, provide lateral connectivity. Cracks found on the surface of the deck were in the 0.01-0.02 in. range. They tended to occur over both boxes and keyways. Figure 2.6 (photo ID No. 3) shows typical cracks on this structure.

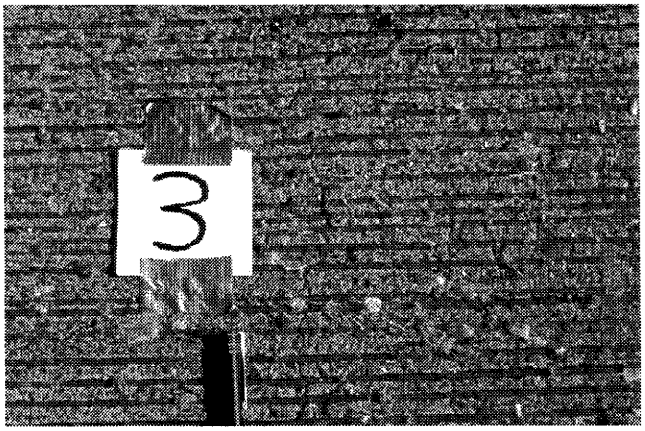

Figure 2.6. Longitudinal Deck Cracking on Cooper Street Underpass.

Parker County

- US 180 @ Willow Creek - Eastbound Lanes

The Willow Creek bridge consists of five 40 ft spans formed from seven 5B20 TxDOT boxes. Roadway width is 38 ft. An 8 in. thick composite slab without shear keys forms the deck. There is no transverse post tensioning. The beams were spread further apart than other bridges inspected, with an average distance between adjacent bottom flanges being about 4 1/4 in. Longitudinal cracks were found over keyways but were generally small–falling in the 0.002-0.007 in. wide range. Figure 2.7 (photo ID No. 4) shows some of these cracks.

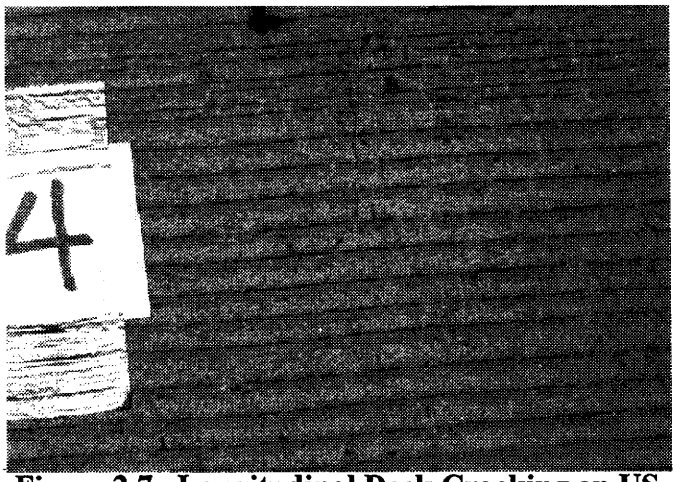

Figure 2.7. Longitudinal Deck Cracking on US 180 Bridge.

Wise County

Three pairs of bridges on US 81, a four-lane highway west of Decatur, were designed with 4 in. composite deck, no shear key, and no transverse post tensioning. After construction was under way in 1993 on the southern-most structures, concerns arose because of longitudinal cracking in the deck over the keyways. As a result, change orders were issued in 1994 to thicken the decks of the remaining bridges. It was largely as a result of these first structures that this research project was

initiated. The inspections reported below describe the current condition of the decks of these bridges.

- Business 380F Overpass - Southbound Lanes

This bridge, like the other two, carries US 81 traffic which is reputed to contain a significant proportion of truck traffic, including many hauling crushed stone (usually in a southerly direction). These vehicles tend to have weights at or near the legal limit and represent one of the more demanding live load conditions to be found in the state. The overpass has spans of 40 ft-80 ft-40 ft with a 38 ft roadway built on seven 5B34 boxes. Deck thickness is 6 3/4 in. (minimum) and 8 in. (maximum) with double mats of reinforcing steel and no transverse post tensioning. Longitudinal cracks were found over most keyways, although not always continuous from one end of a span to the other. Crack widths varied between 0.009 and 0.02 in. with the more severe cracks tending to occur over keyways closest to wheel paths. Figure 2.8 (photo ID No. 5) shows typical cracks found.

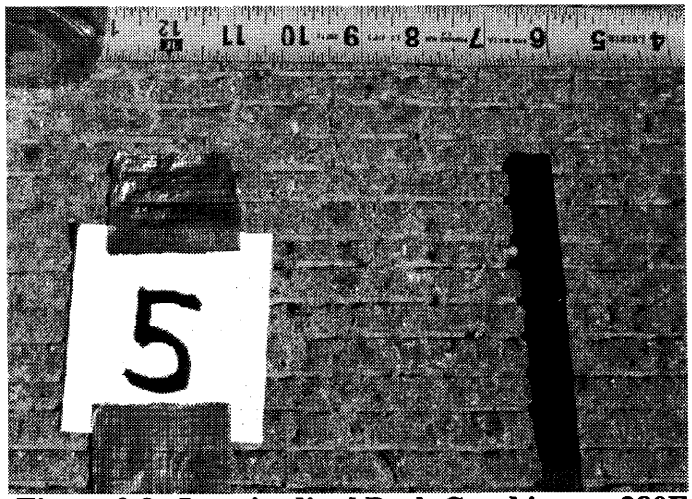

Figure 2.8. Longitudinal Deck Cracking on 380F Overpass.

- FM 51 Overpass - Southbound Lanes

The FM 51 overpass has spans of 45 ft-92 ft-45 ft on a 30 degree skew. The superstructure consists of seven 5B34 boxes with composite deck having a minimum thickness of 6 3/4 in. and a maximum thickness of 7 1/2 in., no shear key, and no post tensioning. The deck has both top and

bottom mats of reinforcing steel. Like the 380F overpass, this bridge had longitudinal cracking over some of the keyways, particularly in the center span. The largest of these was in the center span and was 0.03-0.04 in. in width. Other cracks tended to be smaller and similar in size and appearance to those on the 380F overpass. Photographs of typical cracks are shown in Figure 2.9 (photo ID No. 6).

Figure 2.9. Longitudinal Deck Cracking on FM 51 Overpass.

- FM 730 Overpass - Southbound Lanes

This structure has spans of 87 ft-104 ft-81 ft on a 39 degree skew. Eight 5B34 boxes are used in the superstructure to form an approximately 38 ft wide roadway. The deck has a 4 in. minimum thickness, no shear key, and no post tensioning. Relative to all other bridges inspected, this had the most severe deck distress. Cracking over each keyway was clearly visible. Measured crack widths ranged from 0.02-0.03 in. over keyways at the edges of the bridge to 0.06 in. and wider at keyways in wheel paths. In addition, edges of the cracks were spalling in some locations. From standing on the bridge and feeling the vibrations from passing trucks, it was apparent that dynamic amplification of forces and stresses was occurring. The center span was noticeably more flexible than any of the other bridges inspected and, not coincidently, had the largest clear span. Photographs of the deck cracks are shown in Figure 2.10 (photo ID No. 7).

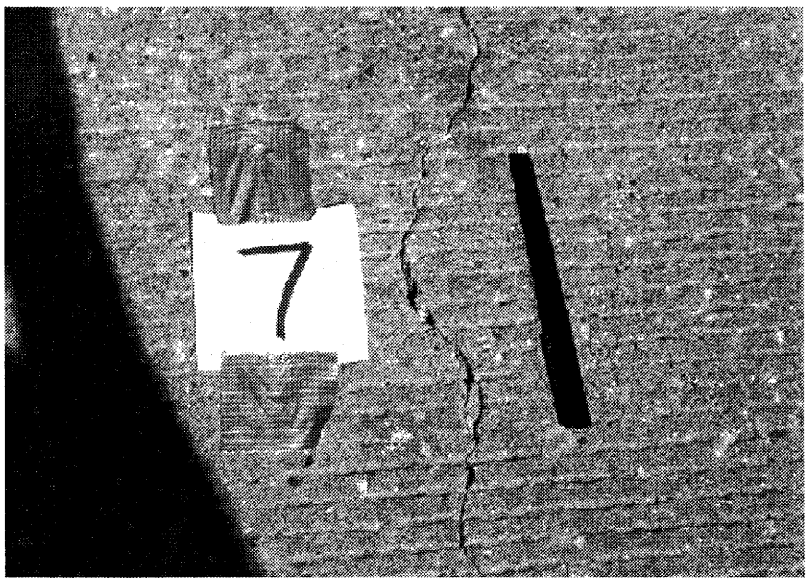

Figure 2.10. Longitudinal Deck Cracking on FM 730 Overpass.

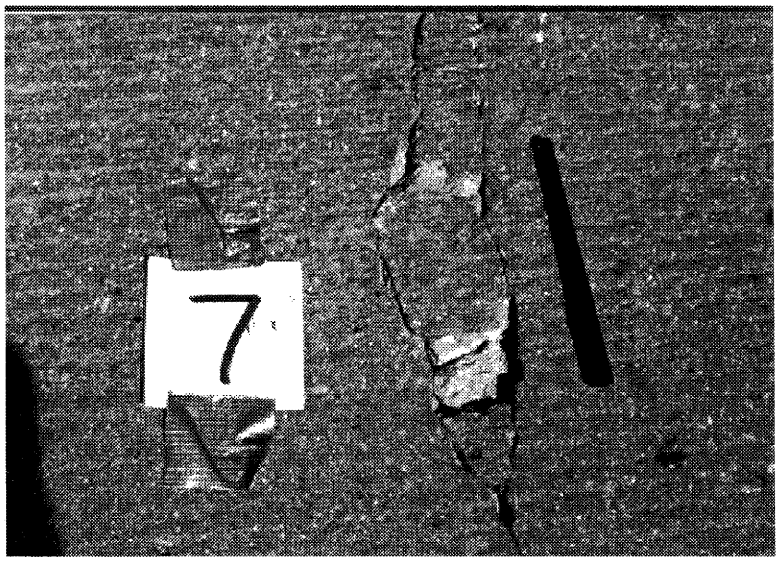

Figure 2.10. Longitudinal Deck Cracking on FM 730 Overpass (continued).

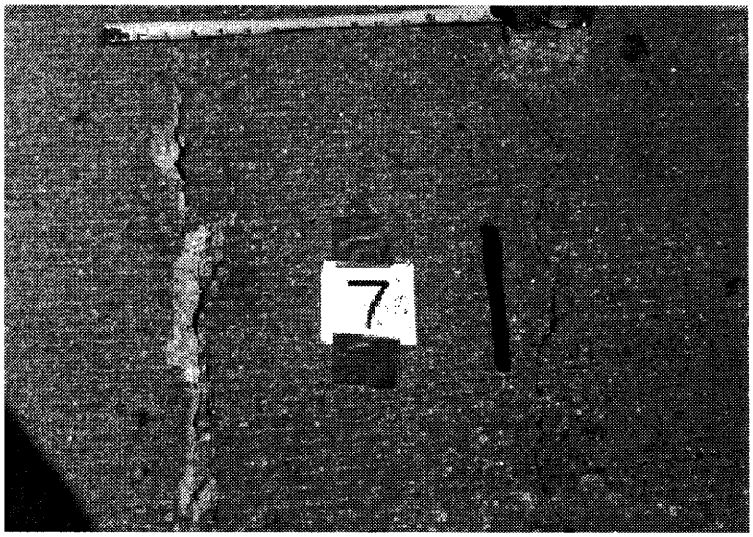

Figure 2.10. Longitudinal Deck Cracking on FM 730 Overpass (continued).

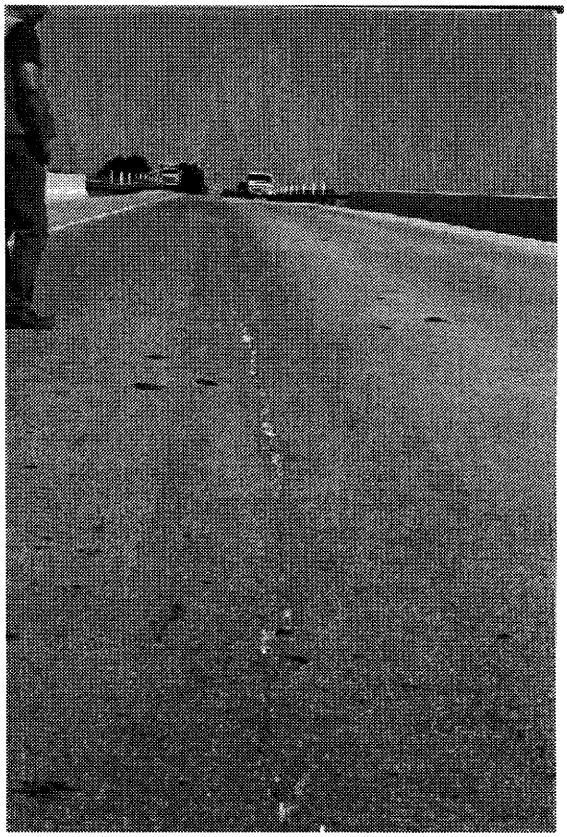

Figure 2.10. Longitudinal Deck Cracking on FM 730 Overpass (continued).

San Antonio

- IH-10 @ Wurzbach Road - Eastbound Lanes

This overpass has spans of 60 ft-55 ft-55 ft-50 ft on a 6 degree skew. It is constructed with 6[5B20]+4[4B20]+7[5B20] and has an 82 ft roadway width. The deck has a minimum thickness of 4 1/2 in. which varies to 6 in. at the ends of spans. A full shear key was used in all spans. This structure, which was not yet open to traffic, was brought to the attention of the research team through an inspector's report which indicated the presence of cracks in the deck. Inspection revealed the cracks to be quite small relative to other bridges examined, with widths consistently less than 0.002 in. They tended to occur over keyways but did not run the complete length of the span and there was a more random pattern to their path. Reports suggested the cracks were not present at the end of the 14-day curing period when the deck was first exposed to the environment and thus are likely the result of shrinkage effects.

CONCLUSIONS DRAWN FROM BRIDGE INSPECTIONS

The inspection of various bridges reported above suggests that longitudinal cracking in the composite concrete deck is the product of two effects: drying shrinkage and live load stresses. Cracks in some cases were detected in concrete placed over the top of a box beam where it should not see significant tensile stress resulting from wheel loads. This fact, combined with the restraint against free expansion of the deck concrete provided by the box beam top surface against which it is cast as well as by reinforcing bars protruding out of that surface, indicates shrinkage stresses have been at work. This notion is further supported by the development of cracks, albeit relatively small ones, in the San Antonio structure before it was opened to traffic. Because of the restraint provided by the box beam upper surface, shrinkage cracks are more likely to occur over keyways. Others report (Hlavacs, 1997; PCI, 1995) that shrinkage cracks tend to run full thickness through the element in which they occur. Thus, with a predisposition to cracking in a location where live load stresses can be tensile, there is a likelihood of significant deck deterioration if the live load tensile stresses are sufficiently large. The severity of this problem is examined in detail in Chapter Three, where it is shown that the worst conditions for transverse tensile stresses in the deck concrete occur

at keyways when no shear key is present and the span is long and possibly skewed. It is interesting to note that the worst conditions encountered in the inspections were found on the FM 730 overpass in Wise County, which possesses all these attributes.

LOAD TESTING

A series of static load tests were conducted on the northbound FM 730 overpass on US 81 in Wise County. This structure, a companion to that described in the previous section, did not have as severe a longitudinal deck cracking as the southbound bridge. It has been suggested that the differences in severity of cracking in the two bridges is due to the large number of trucks hauling crushed stone from pits located north of the structures. Trucks typically run south fully loaded and return north empty. The less severely cracked northbound bridge was chosen in an attempt to have locations on the deck surface where strain gages could be mounted that would not span a deck crack.

The tests were conducted on July 14 and 15, 1998, on the 104 ft center span shown in Figure 2.11. Traffic on the structure was diverted to the outside lane on the morning of the 14th, providing access to the inside lane for mounting strain gages on the deck. A total of four gages was mounted on the deck at mid-span and as near to locations exactly over the juncture of adjacent beams as possible (see Figure 2.12). Additionally, a single gage was mounted at mid-span on the underside of each of the eight beams of the structure. The gages used had a 2.36 in. active gage length wire sensing element mounted on polyimide backing and nominal resistance of 120 ohms.

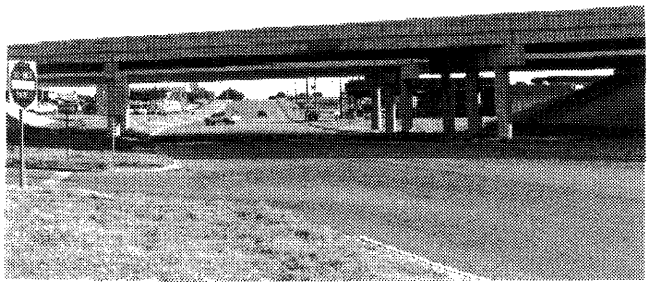

Figure 2.11. FM 730 Overpass.

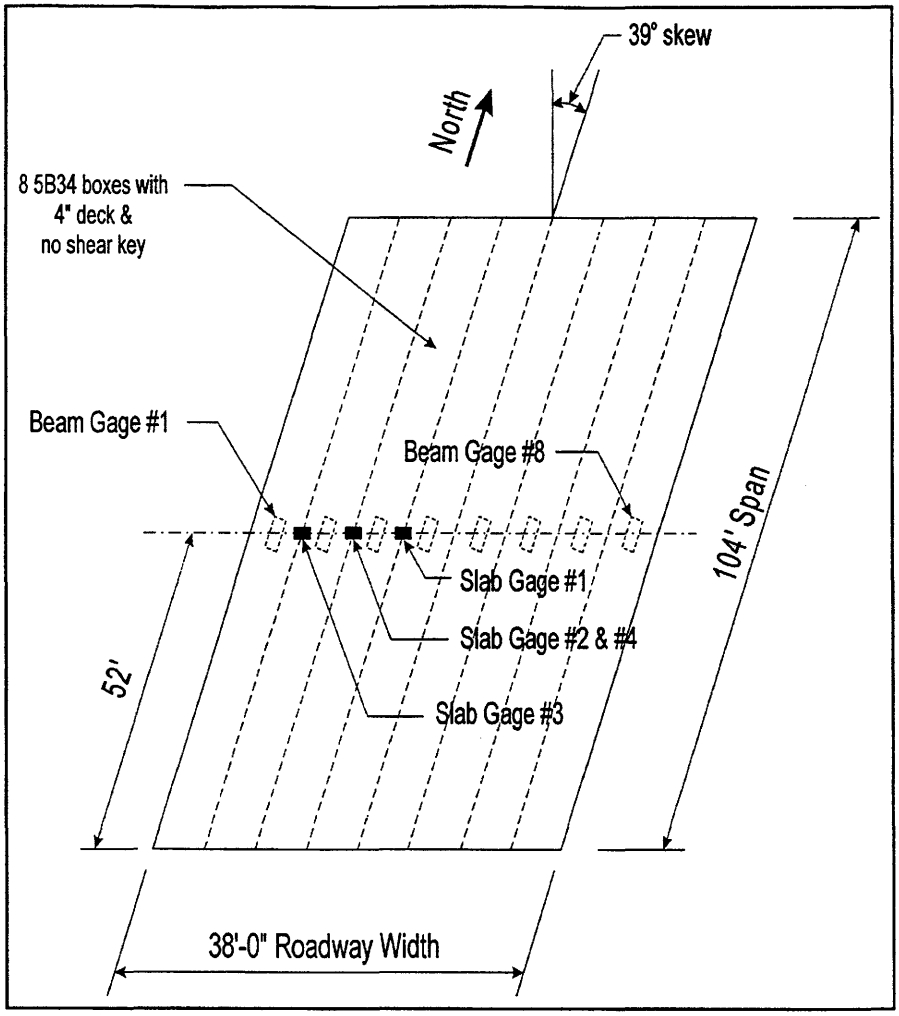

Figure 2.12. Locations of Strain Gages for Load Tests.

Each of the gages on the deck was oriented to measure strain in the transverse direction (i.e., perpendicular to the centerline of the structure) on the top of the slab, while the gages on the underside of the beams measured longitudinal strain. The gages were bonded to the concrete in a two-step process. For the deck gages, a grinder was used to remove surface grooves in the concrete and provide a smooth area for mounting. This area was then cleaned thoroughly with solvent followed by clean water. The beam surfaces were already smooth, so only cleaning was performed on them. The area was then coated with Devcon brand 5-minute epoxy which was applied and smoothed with a wood paddle. After initial set, the coated area was wiped clean and a fresh coat of epoxy added. The strain gage was then placed in the fresh epoxy and held in place using cellophane tape for several minutes until the epoxy began to harden. The last strain gage was mounted by 2:30 p.m. on the 14th. Lead wires were then attached to deck and beam gages and pulled to mid-span at

the railing where they were connected to a microcomputer-based data acquisition system. The system provided automated sweep of the 12 gages and recording of readings to file at 0.2 s intervals. Figure 2.13 is a photograph of an installed gage on the deck surface, while Figure 2.14 shows the data acquisition system.

Figure 2.13. Typical Strain Gage Mounted on Deck Concrete.

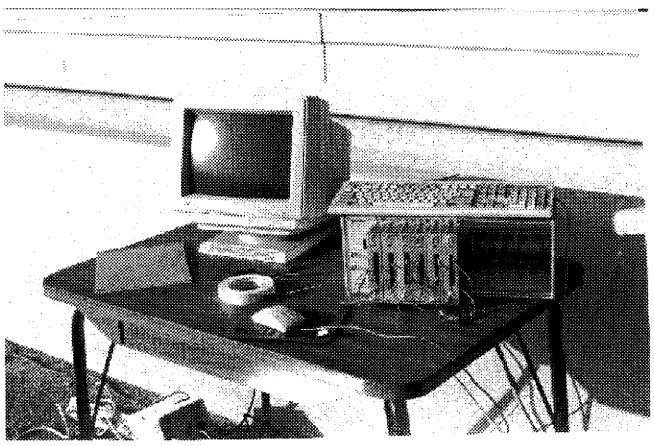

Figure 2.14. Data Acquisition System.

The strain gage and epoxy system was tested under laboratory conditions prior to their use in the field. A gage was mounted longitudinally on a concrete cylinder using the same sequence of steps and allowed to cure overnight. The following day the cylinder was loaded in axial compression in several increments up approximately one-third of its estimated compressive strength. At each increment, the load was held constant for approximately 30 minutes while strain readings were taken every 5 minutes. The readings at all stress levels were quite stable, with less than 0.1 percent drift occurring over any 30-minute interval.

A materials transport truck was provided without charge by TXI Transportation of Dallas to act as the load source and is shown in Figure 2.15. The fully loaded truck weighed 80,050 lb and had the axle spacings and weights shown in Figure 2.16. The weights assigned to the individual axles in the two-axle pairs were obtained by taking the measured weight of each axle pair and dividing it evenly between the two axles. On the morning of the 15th shortly after 8:00 a.m., the data acquisition system was powered up and readings were taken from all gages for approximately two minutes to provide a feel for the stability of the readings. Figure 2.17 shows a plot of those readings for three of the deck gages. The spikes in the plots correspond to passage of trucks across the structure in the outside lane. At approximately 9:00 a.m., TxDOT personnel diverted traffic off the northbound lanes onto the service road, and the truck was moved onto the span just north of the one being tested. A total of five loadings in three different positions on the bridge was performed, as described in Table 2.1 and Figure 2.18. In each of the five loadings, a set of readings (usually for about 20 s at 0.2 s intervals) was taken, then the truck was backed southward onto the bridge and onto the designated location which was marked with chalk on the deck surface. As soon as the truck was in position, another 20-30 s of readings were made. The difference between a gage's last reading before moving the truck onto the bridge and the first reading made afterward is the strain due to load plus whatever additional strain may have been produced by thermal effects over that period. Over the five different truck positions, the elapsed time between the last reading without load and the first reading with load varied between approximately 1.5 and 3.5 minutes. Table 2.2 contains a summary of strain readings for each of the five loadings, while comparison with theoretical values is made in the next chapter.

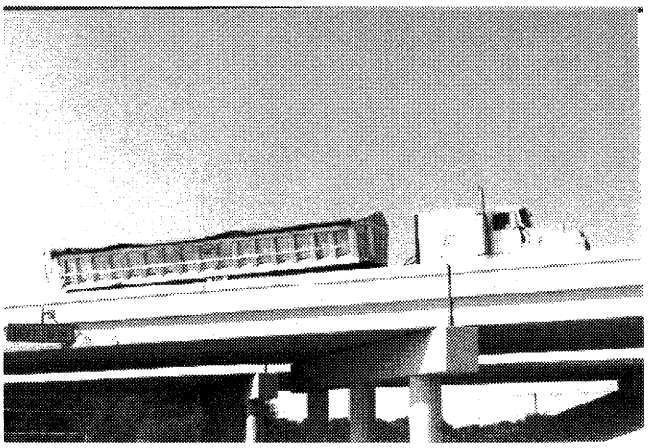

Figure 2.15. Truck Used in Load Test.

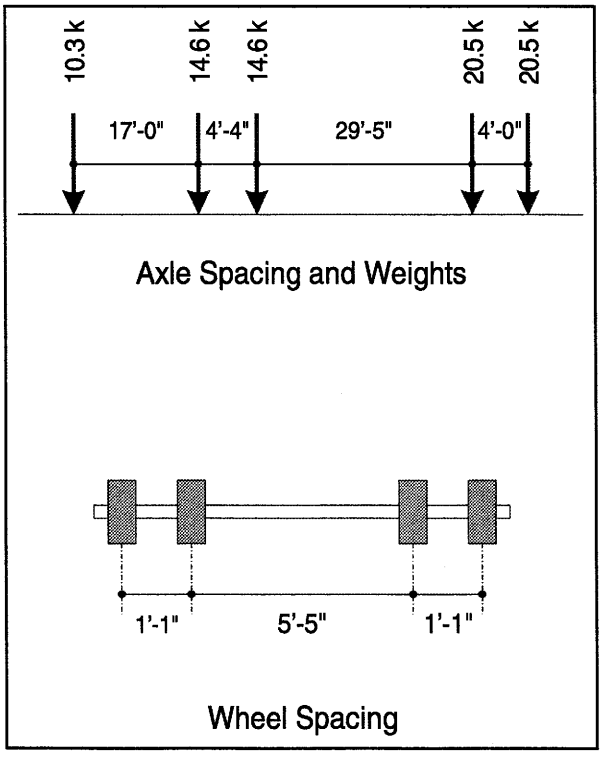

Figure 2.16. Axle Weights and Spacings.

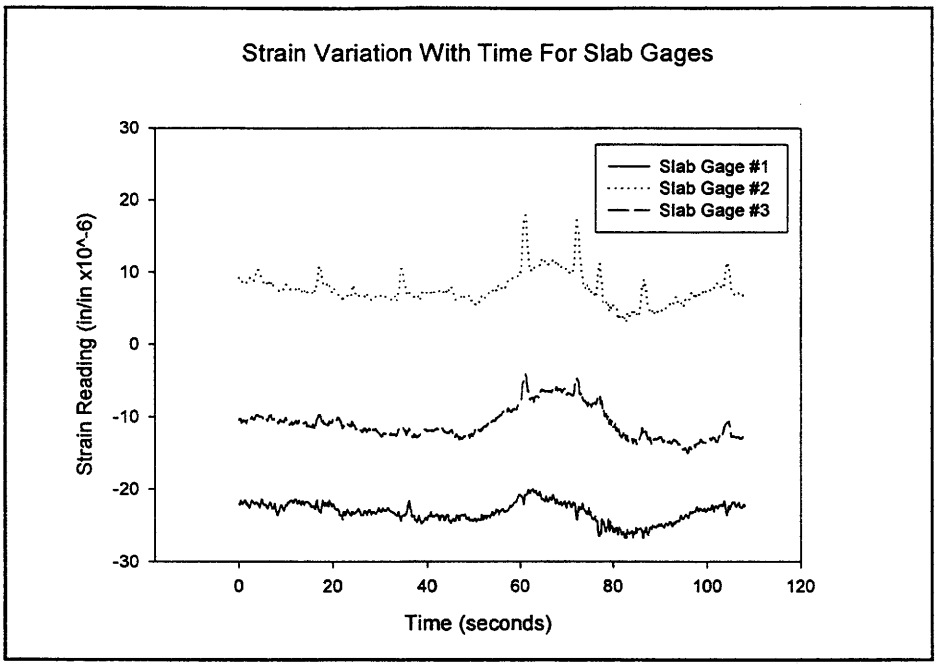

Figure 2.17. Draft of Deck Strain Gages.

Table 2.1. Position of Truck for Each Loading.

Load N°	Truck Position (Figure 2.18)
1	1
2	2
3	2
4	1
5	3

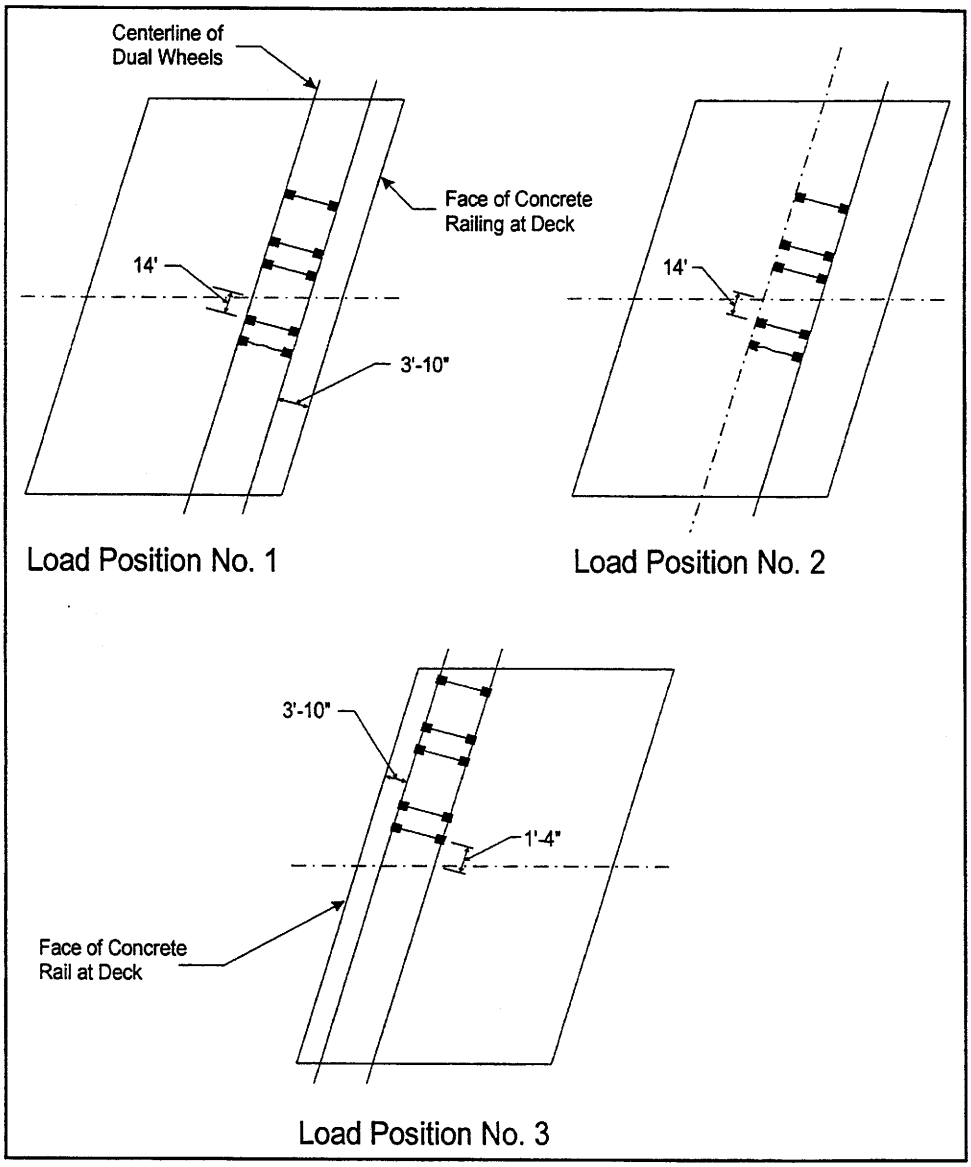

Figure 2.18. Positions of Truck for Load Test.

Table 2.2. Strain Reading (Microstrain) from Load Tests.
(See Figure 2.12 for Gage Locations)

	Slab Gages				Beam Gages							
Load N°	1	2	3	4	1	2	3	4	5	6	7	8
1	-7	-2	-10	-14	+36	+28	+24	+22	+16	+20	+7	+7
2	-30	+12	+4	+4	+17	+16	+18	+21	+8	+12	+17	+18
3	-22	+5	-9	-1	+21	+20	+18	+19	+13	+16	+11	+9
4	+1	+7	+9	-5	+43	+35	+32	+32	+24	+25	+19	+19
5	+30	-2	-6	_	+7	+7	+5	+9	+20	+30	+20	+19

CHAPTER THREE ■ NUMERICAL SIMULATION

A suitable analytical model is essential to understanding the causes of deck distress in composite multi-beam box beam bridges as well as for assessing the effectiveness of live load transfer among individual beams. Additionally, such models form the basis for developing appropriate live load lateral distribution factors for beam shear and moment design, tailored to TxDOT box sections and detailing practices. Three different analytical models implemented through three different computer codes were considered in the initial phases of this study. Each model offered certain advantages from an ease of computation, speed, or adaptability standpoint. Uncertainties about the fidelity of an analytical model to the actual structure it represents are always a concern to the analyst. At the very least, different models should give similar predictions of structural response for the same structure. If this is not the case, the assumptions underlying the two models may not be compatible and/or there may be coding errors in software implementing the model. This latter issue was a concern with one model whose coding had never been subjected to rigorous validation. Initial sections of this chapter document comparisons between the various models to ensure they gave consistent results.

The issue of an analytical model's ability to accurately predict response can be addressed to some degree by load testing a real structure. One of the tasks in this project was to gather suitable response data from a representative bridge to use in validating the analytical models. That effort was documented in Chapter Two of this report. In this chapter comparisons between those measured responses and those predicted by various analytical models are presented.

BEAM AND HINGE MODEL

The first models used in this project were primarily for predicting the forces at work in the composite deck slab at the juncture between two adjacent box beams and to predict the shears and bending moments in each of the beams in a bridge. The beam and hinge model is the least complex of those which provide this information. It is based on a series of beams laid side by side and interconnected by elastic "hinges" running longitudinally between adjacent beams. Figure 3.1 depicts this arrangement. Figures 3.2 (a) through (d) detail the "hinge" between beams. They are

in reality a set of four springs, one set associated with each of the possible modes of relative displacement between two points located directly opposite one another on adjacent beams. If the physical connection between beams is continuous, then each spring set is taken to consist of a continuous distribution of springs. Under these circumstances, the spring stiffness k_x, k_y, k_z, k_φ would

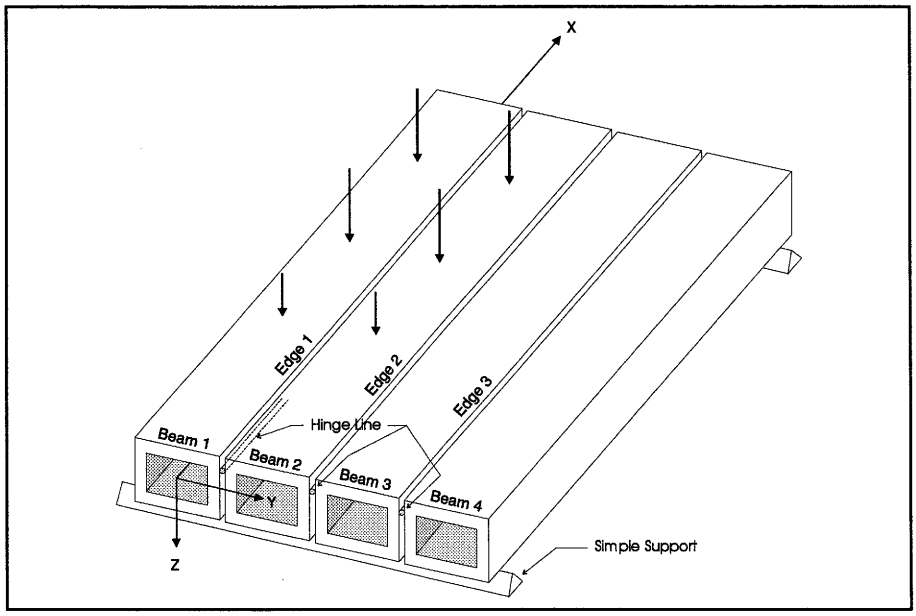

Figure 3.1. Beam and Hinge Model for Multi-beam Bridge.

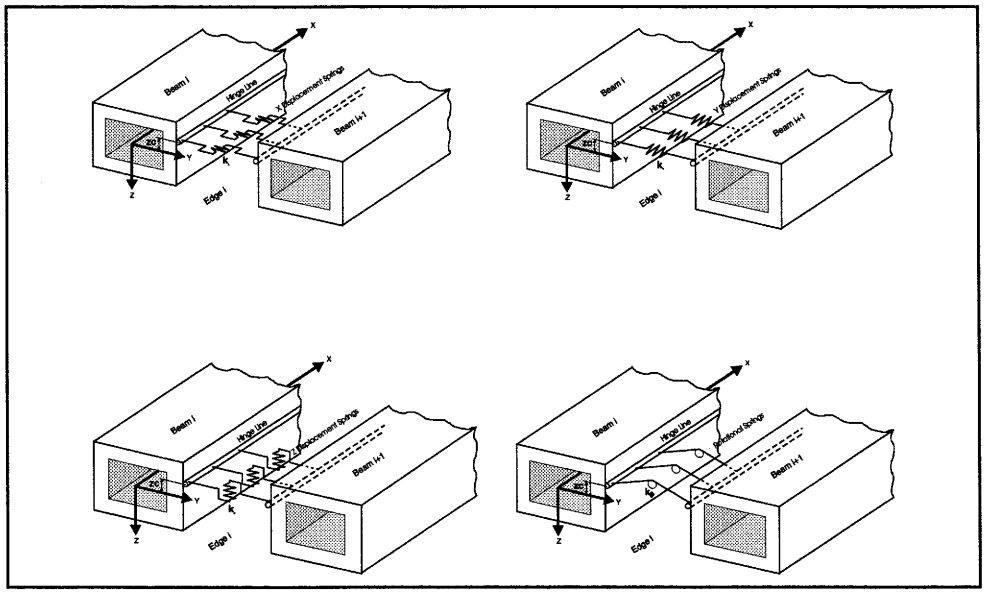

Figure 3.2. Spring Connecting Adjacent Beams at Hinge Line.

be stiffness per unit length (e.g., kips/in./in. and in.-kips/rad/in.). If the physical connection between adjacent beams is truly discrete in nature (e.g., welded plate connection sometimes used along the edges of double tee sections in multi-beam bridges), then each of the four stiffnesses would characterize a single discrete connection. When a load acts on a beam, a point on that beam will, in general, undergo displacements in the three coordinate directions shown in the figure together with a rotation about the x-axis. Such displacements are calculated using ordinary beam theory based on plane sections, remaining plane, and Saint Venant torsion theory. If the point in question lies at the hinge line of Figure 3.2, it will attempt to separate from its companion point on the adjacent beam. Such relative displacements between companion points activate the springs, which generate forces that attempt to prevent the separation. This gives rise to the forces f_x, f_y, f_z, m_c shown in Figure 3.3 for continuous springs and Figure 3.4 for discrete springs.

The AMBB Program

The basic ideas upon which the beam and hinge model is based were introduced by Duberg et al. [1960] who used a true "hinge," in effect taking k_x, k_y, k_z infinitely stiff and k_φ as zero. Powell et al. [1969] introduced the formulation with four spring sets and created a Fortran program to implement it. His formulation uses a Fourier series expansion to characterize these four components of force along the hinge line and leads to a system of 4*N linear equations for each harmonic term considered, where N is the number of beams in the bridge cross section. This results in rapid and dependable solutions which provide the magnitude of each component of hinge force as well as

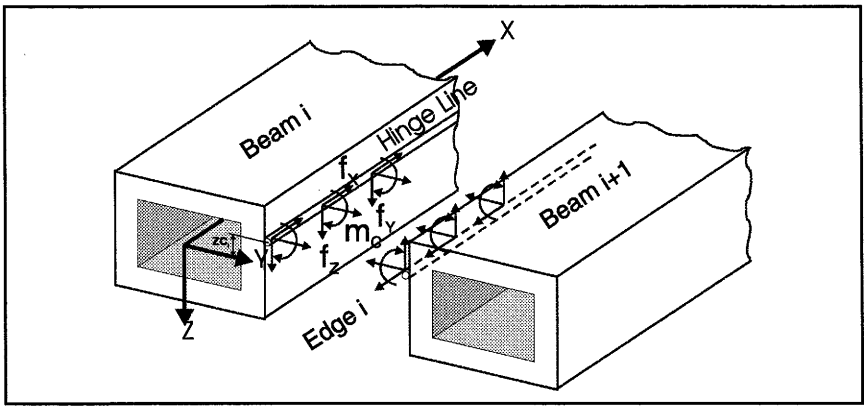

Figure 3.3. Continuous Forces Along Hinge Line.

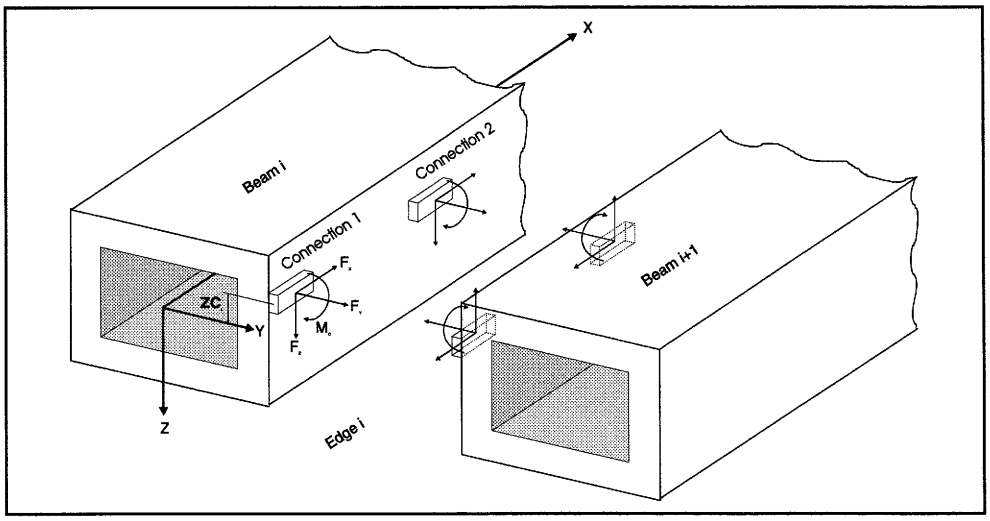

Figure 3.4. Forces at Discrete Connections Along Hinge Line.

beam bending moments about the y and z axes, beam shears in these directions, axial force, and torsional moment in any beam at any location. The program developed by Powell was modified by Jones et al. [1975] to include the automatic positioning of AASHTO trucks to compute lateral distribution factors for beam bending moments. As a part of that effort, some validation studies were performed against published analysis results available at the time. The computer code was given the acronym AMBB and delivered to TxDOT as a part of a larger effort to develop an automated design capability for prestressed concrete box girders. Among the shortcomings of AMBB are its inability to handle skewed structures and to accommodate the effects of transverse post tensioning.

The MBBA Program

In an effort to analyze multi-beam bridges with discrete connections between adjacent beams, Jones and Boaz [1986] reformulated the governing equations. The unknown quantities became the four components of connection force F_x, F_y, F_z, M_c (see Figure 3.4) at each connection along the common edge between adjacent beams in the bridge. This results in a system of linear equations equal in number to four times the total number of connections in the bridge, although the system has a substantially smaller band width that permits the use of specialized solvers and renders a solution in reasonable execution times. Two principal advantages offered by this formulation are the ability

to treat skewed bridges and to handle transverse post tensioning. The formulation also allows for more realistic modeling of the bearing pad support system used in box beam bridges by inserting springs (one in each of the three coordinate directions) at two distinct locations at each end of a beam. Unfortunately, the computer code MBBA which implements the model was never validated. Thus, initial efforts in this study centered on analyzing identical structures using both the documented AMBB and the untested MBBA programs and comparing results which should be essentially identical because of the close similarity between underlying models. In fact, the only significant difference in the models is the continuous versus discrete lateral connection assumption.

Comparison of AMBB and MBBA Results

The models of structural response represented by programs AMBB and MBBA are identical in every significant way except that the interconnection of adjacent beams in the first case is by continuous springs and in the latter case by a series of discrete springs. For a particular bridge model, as the number of discrete spring sets connecting adjacent beams along a common edge is increased and at the same time the stiffnesses of the individual springs are appropriately reduced, one would expect the analysis results from the discretely connected structure to approach those of a continuously connected structure. This fact was exploited as a means of validating the untested MBBA program against AMBB. In addition, since the composite deck slab is correctly modeled with continuous springs, it was necessary to establish some minimum number of discrete connections along a common edge that would ensure that it was "close enough" to the continuous model to give reliable results.

Numerical experimentation with MBBA was undertaken to establish how many discrete connections per edge were needed to reproduce essentially the same results as those coming from modeling the connection between beams continuously. In particular, the transverse moment component m_c (see Figure 3.3) was of primary concern because of its role in longitudinal cracking of the deck. The vertical shear component f_z was also of interest. Experimentation was performed on the two beam structure shown in Figure 3.5. First, using the continuous hinge line connection model, the two beams were joined by springs with stiffness k_x, k_y, k_z=1.0 (kips/in./in.) and k_φ=1000 (kip-in./rad/in.) and analyzed with program AMBB. The companion discretely connected model was

analyzed with MBBA for a sequence of connection frequencies. As a first pass, five equally spaced discrete connections (like that depicted in Figure 3.4) were used to join the two beams. Each discrete connection's stiffness is computed such that it mimics some length of continuous connection. For the situation in Figure 3.5, the three interior discrete connections would have stiffnesses obtained by multiplying the continuous stiffnesses by 180 in. (720 in. divided by 4). Thus, the stiffnesses K_x, K_y, K_z would each be $180 \cdot 1 = 180$ (kips/in.) and $K_\Phi = 180{,}000$ (kip-in./rad).

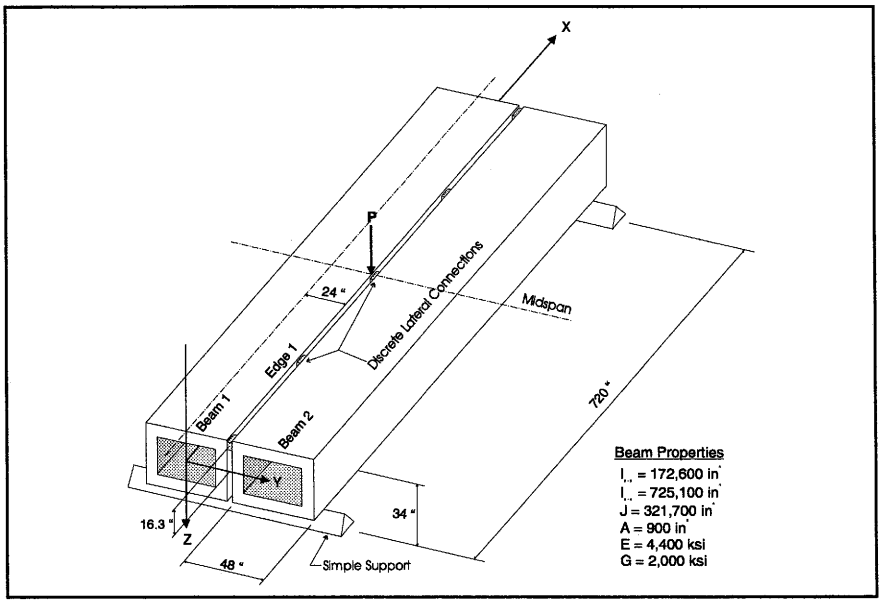

Figure 3.5. Two Beam Model Used for Analysis.

The discrete connection at each end of the beam would have a stiffness equal to half these values because they represent a length of continuous connection that is half that associated with each of the three interior connections. Analysis of the structure with program MBBA yields the four force components shown in Figure 3.4 at each of the five connections. To have quantities directly comparable to the joint force per unit length coming from the AMBB model, it is necessary to take the force components at a discrete connection and divide them by the characteristic joint segment length (180 in. in this discussion) to obtain an "average" joint force per unit length in the discrete model. The discretization described above was repeated using 11 and then 21 equally spaced discrete connections and the structure analyzed for each of these cases.

The results of this exercise are displayed in Figures 3.6 through 3.11. Figure 3.6 shows the variation of the vertical component of joint force f_z (see Figure 3.3) along the span when the concentrated force P=25 kips shown in Figure 3.5 is positioned at L/10, as predicted by the

continuous connection program AMBB. Also shown are three additional curves representing discrete connections spaced at S=L/4, L/10, and L/20 along the edge. Note that when spaced at S=L/20 (21 evenly spaced discrete connections), the vertical shear f_z along the joint predicted by MBBA is indistinguishable from the continuously connected structure analyzed with AMBB. Figures 3.7 and 3.8 show the same trend when the concentrated load P is positioned at quarter span and mid-span, respectively. Figures 3.9 through 3.11 display the same information for the transverse moment component of joint force m_c.

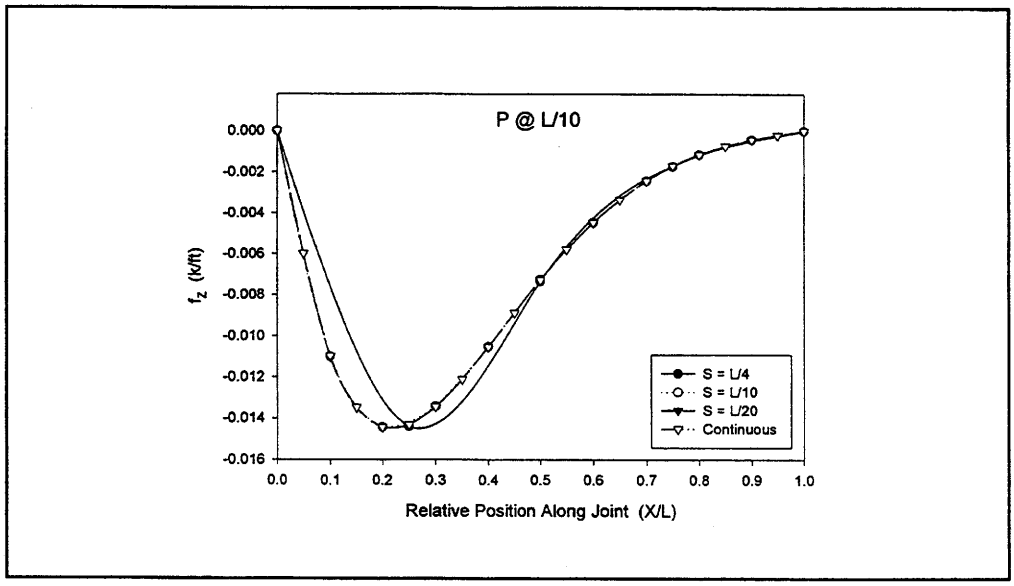

Figure 3.6. Vertical Shear Along Hinge Line for Load at Tenth Span.

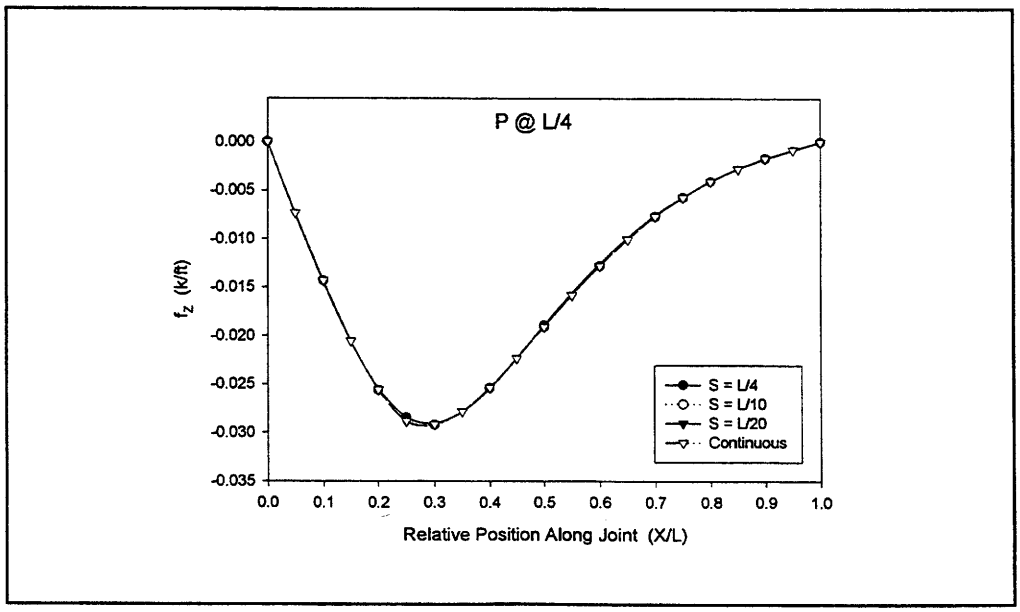

Figure 3.7. Vertical Shear Along Hinge Line for Load at Quarter Span.

These plots demonstrate the aforementioned convergence of joint forces to the continuous (AMBB) solution. Additional experimentation with larger spring stiffnesses than those used in Figures 3.6 through 3.11 displayed similar convergence properties as the number of discrete connections used reached 21. However, while the transverse moment m_c closed uniformly, the vertical shear component f_z behaved more erratically because of the large gradient occurring adjacent to the applied load P. In view of the good convergence on transverse moment, 21 equally spaced connections were chosen as a satisfactory discretization of the continuous connection between adjacent beams.

As a second comparison of the analysis results from AMBB with those of MBBA, the eight-beam structure shown in Figure 3.12 was analyzed. A single concentrated force at mid-span positioned on the right edge of beam 2 was used for loading. Figures 3.13 and 3.14 compare transverse moment m_c as predicted by the continuous (AMBB) and discrete (MBBA) models along the joint between beams 1 and 2 and between beams 2 and 3. Bending moment and shear force in each of the eight beams predicted by the AMBB and MBBA models were essentially identical.

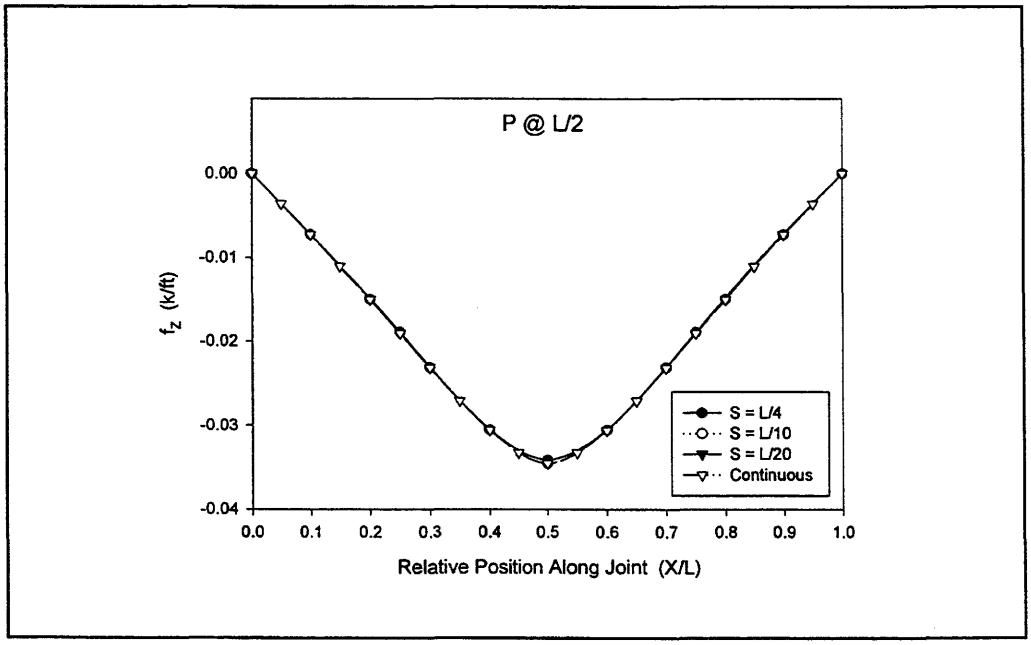

Figure 3.8. Vertical Shear Along Hinge Line for Load at Mid-Span.

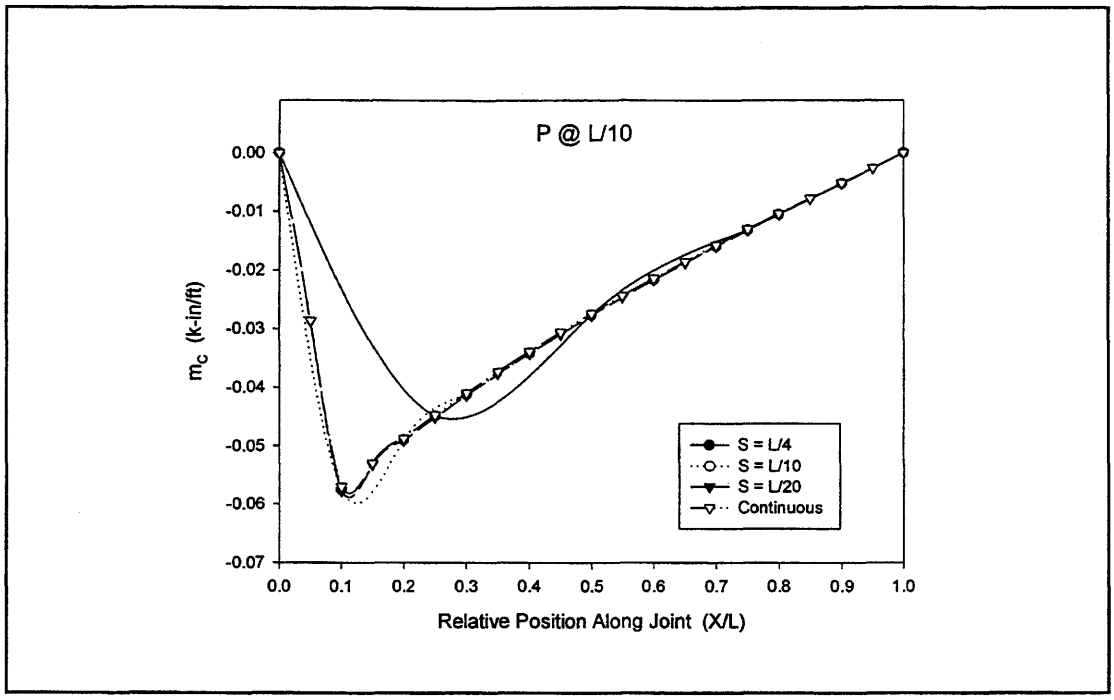

Figure 3.9. Transverse Moment Along Hinge Line for Load at Tenth Span.

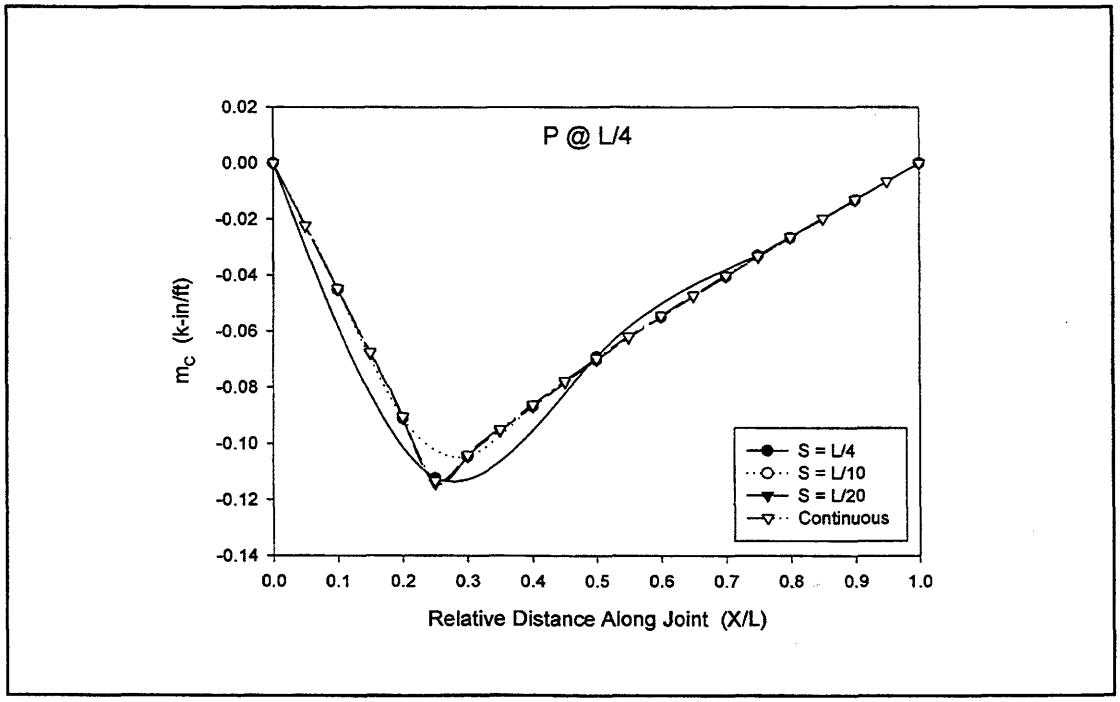

Figure 3.10. Transverse Moment Along Hinge Line for Load at Quarter Span.

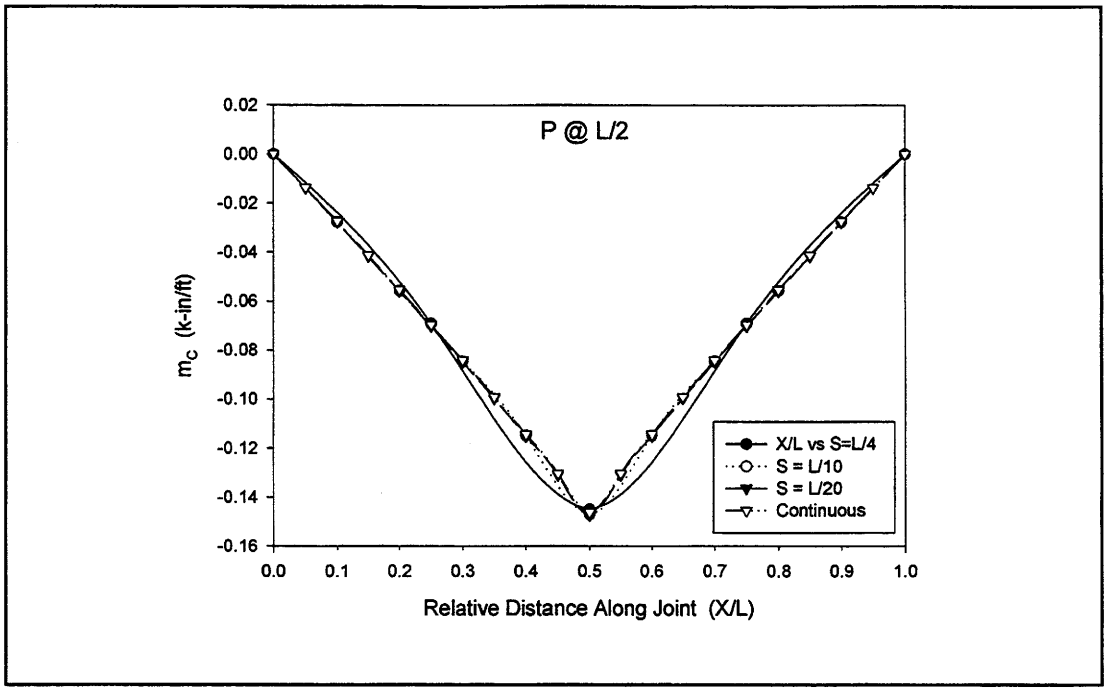

Figure 3.11. Transverse Moment Along Hinge Line for Load at Mid-Span.

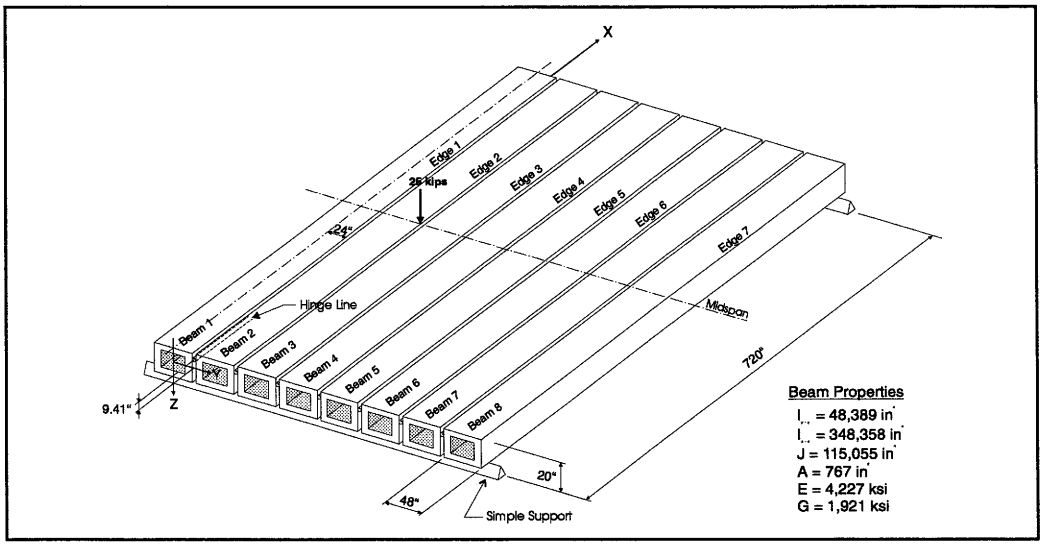

Figure 3.12. Eight Beam Model Used for Analysis.

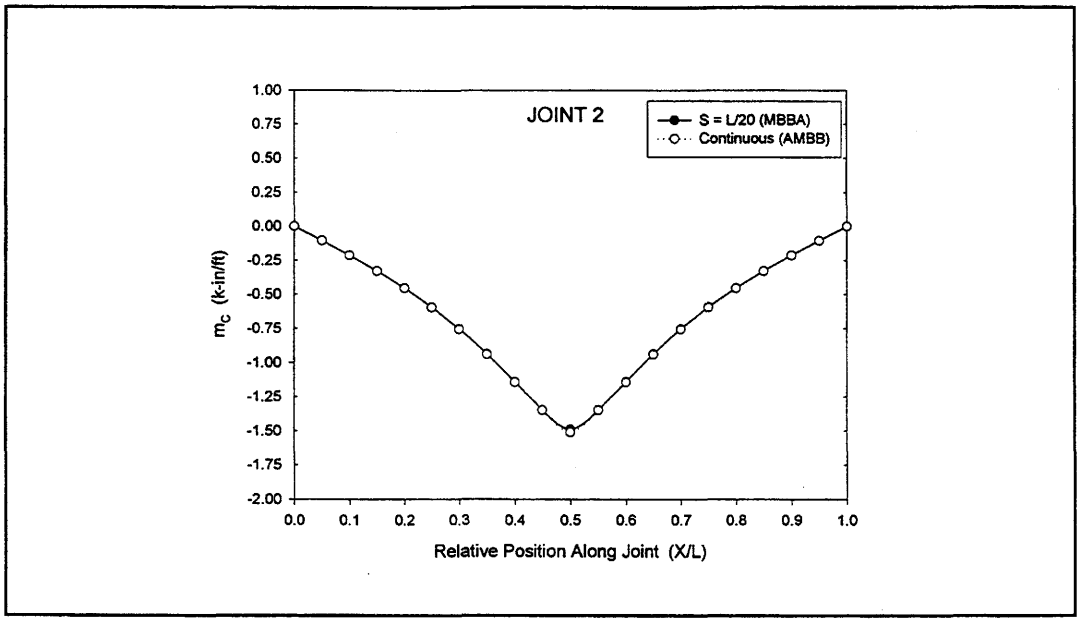

Figure 3.13. Transverse Moment Along Joint 2 in. 9 Beam Model.

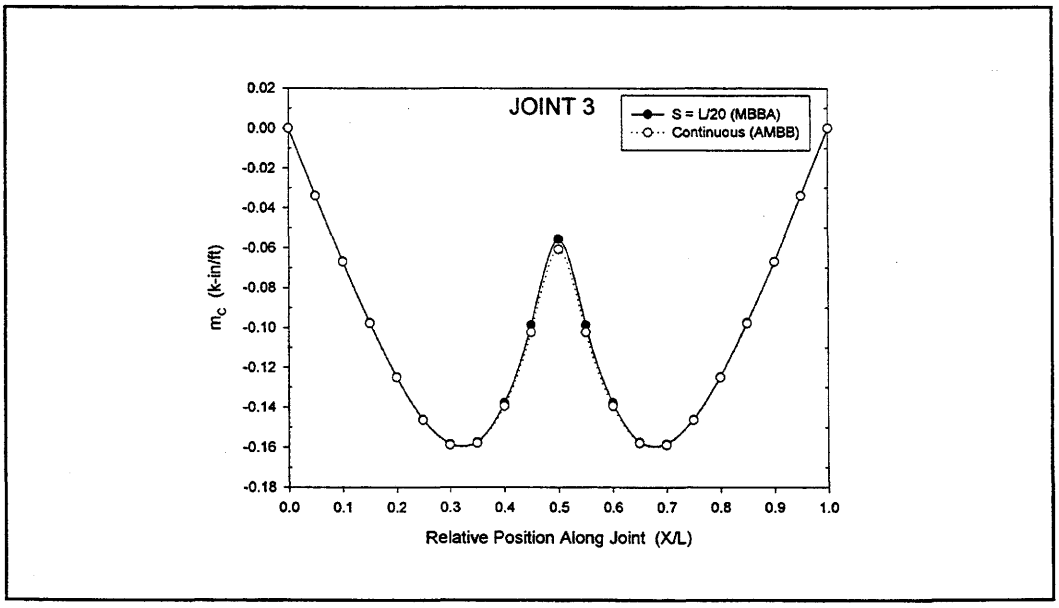

Figure 3.14. Transverse Moment Along Joint 3 in. 8 Beam Model.

Additional comparisons between the analysis results of programs AMBB and MBBA were made. They involved spans ranging from 40 ft to 115 ft, box beam section properties consistent with those of standard TxDOT boxes, and bridges with four to 10 boxes. When 10 discrete connections were used to represent the continuous connection between beams, agreement between beam forces predicted by programs AMBB and MBBA was consistently within 1 percent and connection spring

forces within 5 percent. When 20 discrete connections were used, results from the two programs were indistinguishable.

Based on these comparisons, the program MBBA was accepted as a valid implementation of the beam and hinge model. Additionally, the use of a minimum of 10 discrete connections to represent the truly continuous connection between adjacent beams created by the deck slab provides sufficient accurate results. Most of the analyses used in the parameter studies of Chapters Four and Five were conducted using 20 discrete connections.

Modeling of Composite Deck Multi-Box Beam Bridges

Programs AMBB and MBBA use a set of four springs to simulate the joining of adjacent beams. In the case of box beams with composite deck, that connection is in fact accomplished through the deck slab. In order to apply the two models, it is necessary to have a means of computing spring constants from the properties of the slab. This is accomplished by taking a strip of slab perpendicular to the span of the beams and extending the length of the void between the tops of adjacent boxes. For TxDOT box beams, this void is a minimum of 4 3/4 in. The strip has a width of unity and thickness t, as depicted in Figure 3.15. Taking in turn each of the four possible modes of deformation of this slab strip (Figures 3.16a through d), expressions based on elementary mechanics can be derived between the force component and the deformations. Thus, for example, in Figure 3.16a, the force f_y acts to cause the simple axial extension Δ. The two are related by $\Delta = f_y \cdot \ell / t \cdot E$. From this relationship, the spring constant k_y is found to be $E \cdot t / \ell$. Using this same approach, the stiffnesses of each of the four springs are:

$$k_x = G \cdot t / \ell \qquad \text{Eq. (3.1)}$$

$$k_y = E \cdot t / \ell \qquad \text{Eq. (3.2)}$$

$$k_z = E \cdot t^3 / \ell^3 \qquad \text{Eq. (3.3)}$$

$$k_\Phi = E \cdot t^3 / 12 \cdot \ell \qquad \text{Eq. (3.4)}$$

Each of the stiffnesses in Eqs. (3.1) through (3.4) are per unit length in the sense of the continuous springs of Figure 3.2. When modeling the deck slab, the hinge line in Figure 3.2 is positioned at mid-depth of the slab as shown in Figure 3.17.

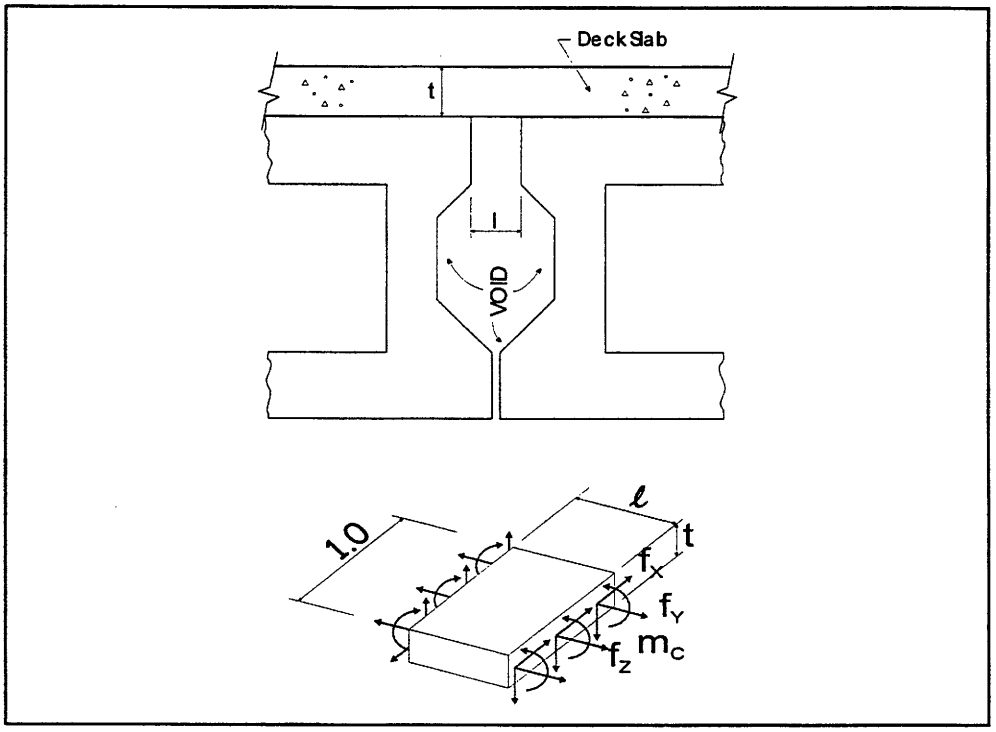

Figure 3.15. Forces Along Hinge Line Located in Deck Slab.

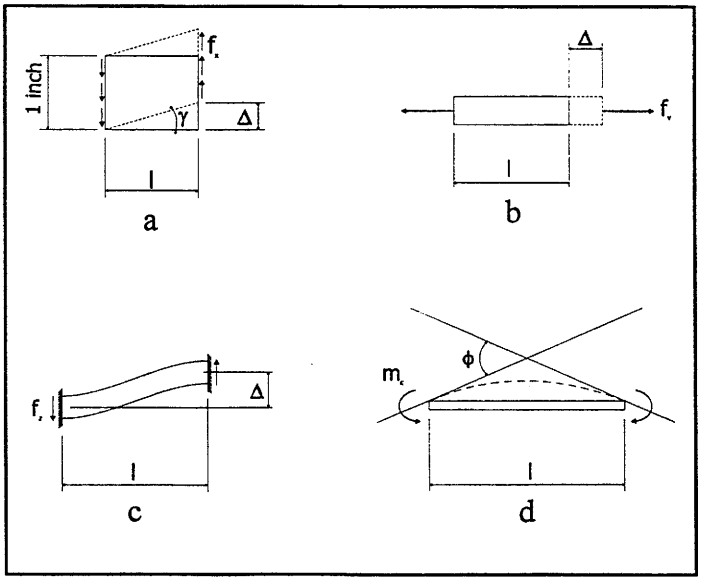

Figure 3.16. Stiffnesses for Springs in Deck Slab.

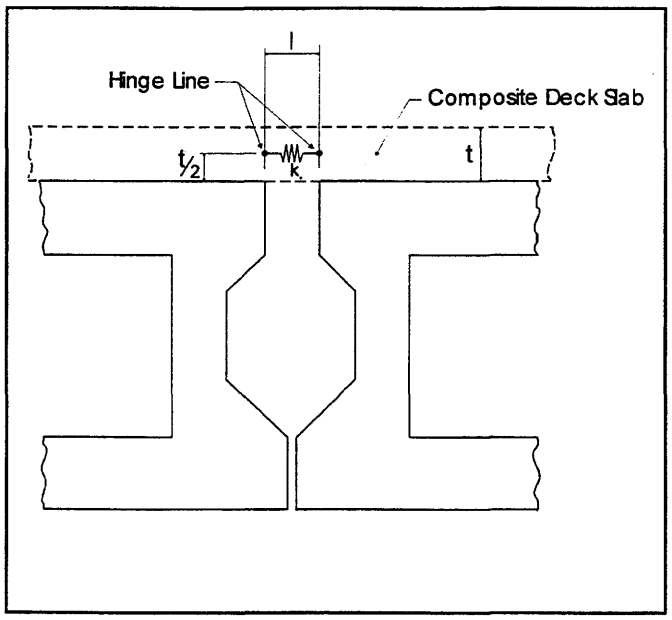

Figure 3.17. Location of Springs in Deck Slab.

FINITE ELEMENT MODEL FOR LIVE LOAD EFFECTS

A third, more elaborate model of the two-beam bridge in Figure 3.5 was created using the commercial finite element code SAP2000. This model was undertaken to provide verification that the beam and hinge models of AMBB and MBBA, with spring stiffnesses defined by means of Eqs. (3.1) through (3.4) to represent the composite deck slab, would indeed provide accurate predictions of transverse moment m_c in the deck as well as shear and moment in the individual beams. The SAP2000 model offered the advantage of being able to represent the composite deck slab with plate elements, generally considered to be the most appropriate numerical representation of a slab. In this model the box beams were represented with conventional beam elements, positioned at the centroid of each box. Figure 3.18 shows the element representation of the two-beam bridge model analyzed previously. The plate elements are located at the mid-depth position in the actual deck, and the beam elements representing the box beams are visible below. A useful feature of the SAP2000 program is its ability to lock displacements of various nodes together. When appropriate, this feature can lead to a significant reduction in the number of degrees of freedom needed to represent a structure. In this model, the "plane sections remain plane" assumption was made, and all nodes in a vertical plane

of a single beam (i.e., one perpendicular to the longitudinal axis of the beam) were constrained to remain in that plane as they displaced. At any station along the beam, the plane under discussion would contain a line of nodes in the deck slab and a single node at the box beam centroid. This simplification reduced the number of degrees of freedom by over 60 percent.

Comparison of Finite Element Model with AMBB and MBBA

The two beam bridge of Figure 3.5 was analyzed using a 4 in. grid spacing for plate elements. The beams have the same properties as those in Figure 3.5. This dimension provided a convenient means of modeling the gap existing at the top of adjacent beams. As before, a 25 kip concentrated force was used for loading. This load was applied to the left beam at L/4 from its end and laterally on its right edge. Figure 3.19 shows a comparison of transverse moment in the slab midway between beams as predicted by the SAP2000 finite element model with values from AMBB and MBBA. These results indicate that transverse slab moment from the simpler beam and hinge models, with spring stiffnesses defined through Eqs. (3.1) through (3.4), agrees very closely with the fundamentally more accurate but more complex finite element model. Mid-span beam moments and shears from the finite element model were within 1 percent of the values predicted by AMBB and MBBA.

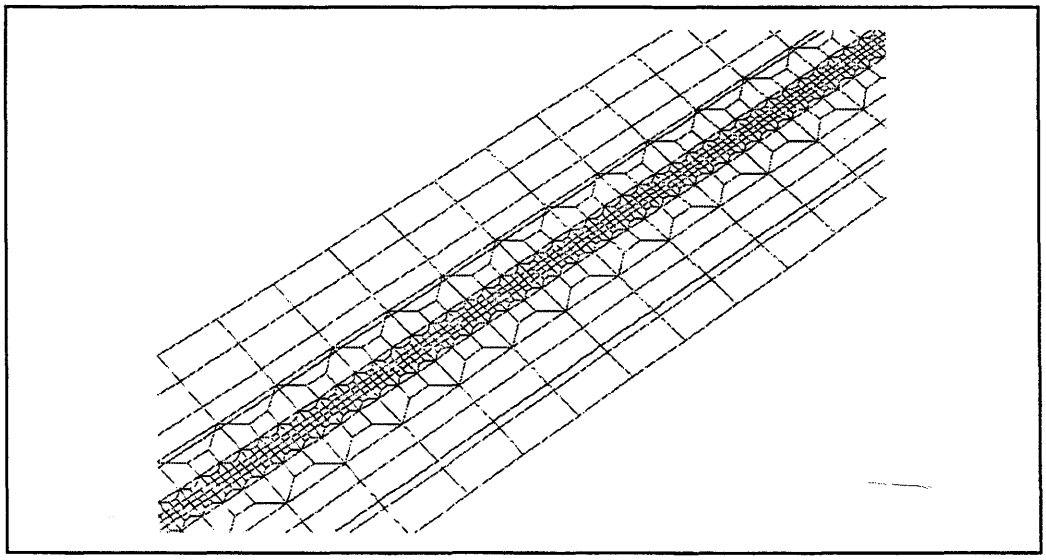

Figure 3.18. FEM Grid Used SAP2000 Analysis of Bridge.

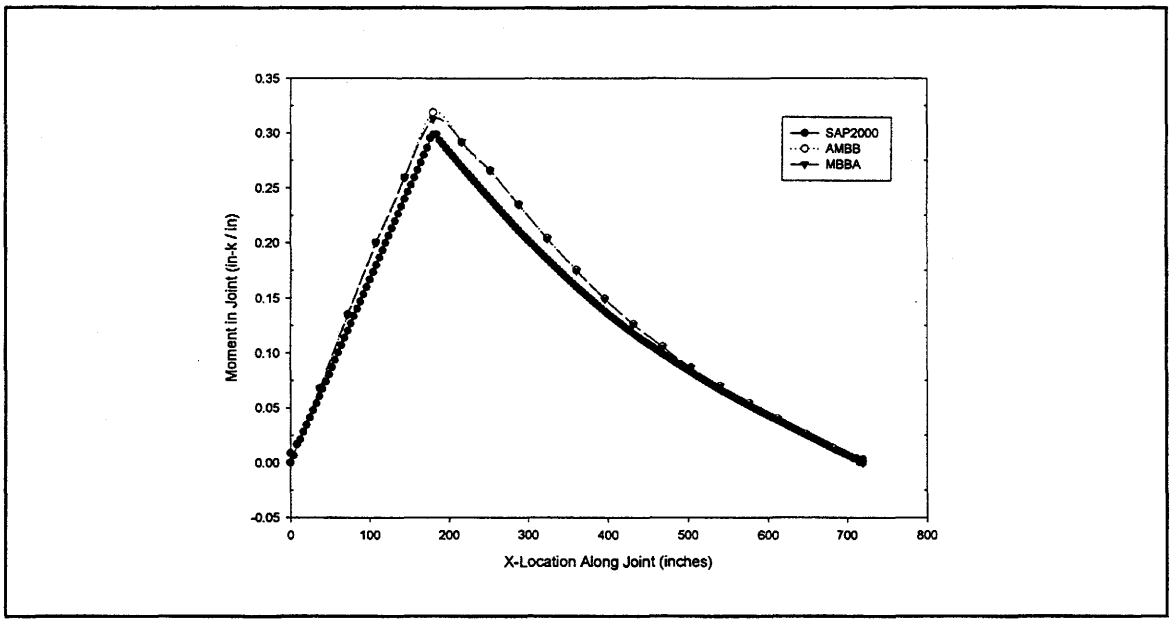

Figure 3.19. Comparison of Transverse Slab Moment Predicted by Three Analyses.

BEAM PROPERTIES FOR PROGRAM MBBA

The beam and hinge model MBBA requires input of the moment of inertia about horizontal and vertical axes, a cross-sectional area, and torsional stiffness of each longitudinal beam in the structure. To properly reflect the effect of the deck slab on beam response, the properties of a cross section consisting of the precast concrete beam plus that portion of the slab in contact with its top flange are needed. While computation of the inertia and area of this composite section is straightforward, the torsional stiffness J cannot be determined accurately with simple formulas for such irregularly shaped sections. AASHTO [1994, 1996] each contain a formula for the approximate calculation of J. Both formulas are derived from closed-form solutions for hollow rectangular sections with vertical sides having the same thickness and likewise for the two horizontal sides. TxDOT standard boxes are not perfectly rectangular in that the vertical sides are somewhat irregular. While the AASHTO formulas provide a conservative estimate of J in the presence of these irregularities, the addition of an upper horizontal side to the rectangle, which may be more than twice the thickness of the lower side, makes the use of these approximate formulas questionable.

The finite element code SAP2000 provides a convenient method of computing a much more exact value of the torsional stiffness of the section. The method is based on the principle that an elastic bar of length L fixed at one end and twisted with a torque T at the other undergoes an angle of twist φ given by

$$\varphi = \frac{TL}{GJ} \qquad \text{Eq. (3.5)}$$

where G is the shear modulus of the material. An eight-node solid element in SAP2000 was used to construct a bar with convenient length L and the desired cross-sectional shape. A unit torque T was then applied to its end as the loading, and the angle of rotation φ taken from program output. Equation (3.5) was then used to solve for J. This approach was tried on a solid rectangular shape and a hollow rectangle for which exact values of J were available, in order to determine approximately how fine an element mesh was needed to obtain results accurate to within 5 percent. Using a mesh established in this way, the various TxDOT box sections with 4, 6, and 8 in. composite deck slabs were analyzed. Figure 3.20 shows a typical element model. Tables 3.1 through 3.4 list the computed torsional stiffness and moment of inertia for TxDOT boxes with various thickness of composite deck slab which were used in this project.

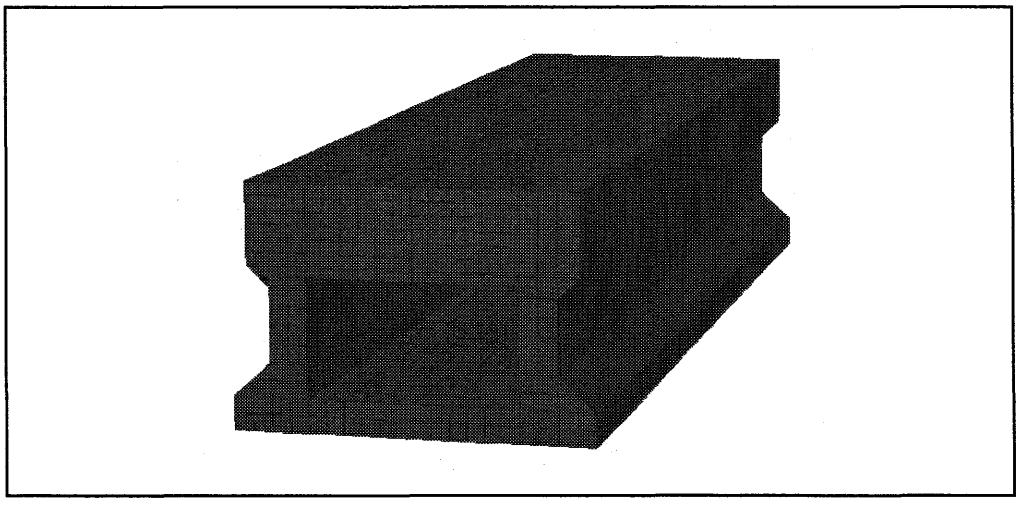

Figure 3.20. FEM Grid Used in SAP2000 Model for Torsional Stiffness.

Table 3.1. Properties of TxDOT Boxes.

TxDOT Box	I (in^4)	J (in^4)
4B20	28,085	70,735
5B20	35,235	99,680
4B28	68,745	126,980
5B28	85,370	187,070
4B34	115,540	198,190
5B34	142,040	293,410
4B40	176,555	284,690
5B40	215,245	425,350

Table 3.2. Properties of TxDOT Boxes with 4 in. Composite Deck Slab.

TxDOT Box	I (in^4)	J (in^4)
4B20	48,390	108,565
5B20	60,525	156,515
4B28	106,310	174,890
5B28	131,835	263,240
4B34	172,610	258,875
5B34	212,050	392,450
4B40	256,580	360,015
5B40	313,250	552,560

Table 3.3. Properties of TxDOT Boxes with 6 in. Composite Deck Slab.

TxDOT Box	I (in^4)	J (in^4)
4B20	60,510	129,885
5B20	75,515	188,730
4B28	126,710	199,850
5B28	156,765	303,475
4B34	202,600	295,620
5B34	248,270	439,790
4B40	297,870	394,490
5B40	362,890	608,805

Table 3.4. Properties of TxDOT Boxes with 8 in. Composite Deck Slab.

TxDOT Box	I (in^4)	J (in^4)
4B20	74,240	153,045
5B20	92,460	223,870
4B28	148,625	226,060
5B28	183,430	343,780
4B34	234,080	318,275
5B34	286,050	487,865
4B40	340,600	428,415
5B40	413,860	663,760

COMPARISON OF ANALYTICAL AND LOAD TEST RESULTS

Strain gage data taken during load tests on the FM 730 overpass on US 81 were given in Chapter Two. These results were compared to those predicted by the MBBA program using beam properties in Table 3.2, lateral connection stiffnesses computed from Eqs. (3.1) through (3.4) with E=5,100,000 psi, and the truck loads shown in Figure 2.16. The design strength of the beam concrete was 6,850 psi and actual strength estimated at about 8,000 psi, which by American Concrete Institute (ACI) formula yields the value of modulus given above. The computed and measured values of strain for each of the five loadings are compared in Tables 3.5 and 3.6.

Table 3.5. Comparison of Measured and Predicted Beam Strains.

Load No.	Beam No. 1			Beam No. 2			Beam No. 3			Beam No. 4		
	Meas.	Pred.	Ratio	Meas.	Pred.	Ratio	Meas.	Pred.	Ratio	Meas.	Pred.	Ratio
1	+36	+36	1.00	+28	+34	0.82	+24	+31	0.77	+22	+28	0.79
2	+17	+29	0.59	+16	+30	0.53	+18	+29	0.62	+21	+28	0.75
3	+21	+29	0.72	+20	+30	0.67	+18	+29	0.62	+19	+28	0.68
4	+43	+36	1.19	+35	+34	1.03	+32	+21	1.03	+32	+28	1.14
5	+7	+15	0.46	+7	+17	0.41	+5	+19	0.26	+9	+22	0.41

Load No.	Beam No. 5			Beam No. 6			Beam No. 7			Beam No. 8		
	Meas.	Pred.	Ratio	Meas.	Pred.	Ratio	Meas.	Pred.	Ratio	Meas.	Pred.	Ratio
1	+16	+25	0.64	+20	+21	0.95	+7	+18	0.39	+7	+16	0.44
2	+8	+27	0.30	+12	+26	0.46	+17	+24	0.71	+18	+22	0.82
3	+13	+27	0.48	+16	+26	0.61	+11	+24	0.46	+9	+22	0.41
4	+24	+25	0.96	+25	+21	1.19	+19	+18	1.06	+19	+16	1.19
5	+20	+26	0.77	+30	+29	1.03	+20	+29	0.69	+19	+26	0.73

Table 3.6. Comparison of Measured and Predicted Slab Strains.

Load No.	Slab Point No. 1			Slab Point No. 2			Slab Point No. 3		
	Meas.	Pred.	Ratio	Meas.	Pred.	Ratio	Meas.	Pred.	Ratio
1	-7	28	-0.25	-2	+27	-0.07	-10	+17	-0.58
2	-30	-19	1.58	+12	+14	0.86	+4	+16	0.25
3	-22	-19	1.16	+5	+14	0.36	-9	+16	-0.56
4	+1	+28	0.04	+7	+27	.026	+9	+17	-0.53
5	+30	-37	-0.81	-2	-82	0.02	-6	-90	0.07

The ratio values in each table are the measured value divided by the value predicted with program MBBA. A value of +1.00 represents perfect agreement between measured and predicted values. Generally speaking, the agreement between measured and predicted strains is better for the beams (Table 3.5) than for the slab. The larger differences found in Table 3.6 for the slab are due in part to the greater sensitivity of moment (and hence strain) in the slab to position of wheel loads on the structure. In retrospect, the position of the truck on the bridge was not measured with sufficient accuracy in light of this sensitivity. Another obvious factor in assessing the accuracy of the measured strains is their size. Small strains are more difficult to measure accurately in the presence of fluctuating temperature, which definitely was the case here.

The purpose for performing these load tests was to provide additional confirmation that the analytical model MBBA could predict the forces present in this type bridge. They were only partially successful in doing that in light of ratios in the tables, which in some cases deviate from 1.0 by significant amounts.

CHAPTER FOUR ■ RECOMMENDATIONS FOR CONTROL OF DECK CRACKING

This chapter addresses the causes of longitudinal cracking of the concrete deck slab in TxDOT multi-box beam bridges. Inspections of existing bridges and reports from related research studies strongly suggest that drying shrinkage is the primary initiator of this type of cracking. Transverse bending moment in the slab, however, caused by vehicular traffic acting on these cracks provides the mechanism to enlarge and deepen them over time, possibly causing them to grow to objectionable size. An extensive analytical study was performed, using computer program MBBA described and documented in the previous chapter, with the objective of providing the data needed to create design equations for predicting slab transverse bending moment that could be used by designers to proportion a deck slab and its reinforcement. This effort is documented in subsequent sections of this chapter.

With regard to simple equations or procedures to predict the transverse slab moment, the AASHTO code provisions do not address transverse slab moment in this type structure, nor could any predictive equations be found in published research findings. Consequently, it was necessary to develop suitable functions to relate the parameters known to influence transverse slab bending moment to the extreme values for these moments in a specific structure, and then use large numbers of computer analyses and least squares fitting to evaluate the parameters in these functions.

As explained in what follows, the accuracy of equations in predicting peak transverse slab moment was found to decrease as more causal factors were introduced into the equation. For example, it was found that an equation with maximum error of 5 percent and an average error under 3 percent could be constructed to predict the peak slab moment in any one of the common TxDOT bridges listed in Table 4.2 with a given slab thickness and specified transverse distance between adjacent beams. However, an equation which treated these latter two factors as independent variables typically had an average error on the order of 10-15 percent and maximum error of 50 percent or more in isolated cases. Analysis of these errors indicated that they consistently occurred in predicting small values of moment, and that the accuracy for moments which would control the design of a slab were still predicted within the 10-15 percent range. Thus, the equations for

transverse slab moment presented later in this chapter are approximate but provide values suitable for design of the deck slab and its reinforcing for specific bridge configurations.

This chapter also explores the effects of post tensioning as a device for controlling transverse deck cracking. Finally, the use of auxiliary means of laterally connecting adjacent boxes is briefly discussed and some typical data derived to demonstrate the benefits this approach holds if practical means of forming such connections can be found.

LIVE LOAD INDUCED DECK STRESSES

The presence of transverse tensile stresses in the deck slab caused by vehicular loads increases the severity of longitudinal cracking initiated by drying shrinkage and other non-vehicular load sources. The deck slab forces caused by trucks that are of interest are the lateral in-plane component f_y and the transverse moment component m_c, both shown in Figure 3.15. The component m_c causes bending normal stress in the transverse direction of the deck, directly above the void between adjacent beams, as shown in Figure 4.1. A positive moment m_c produces tensile

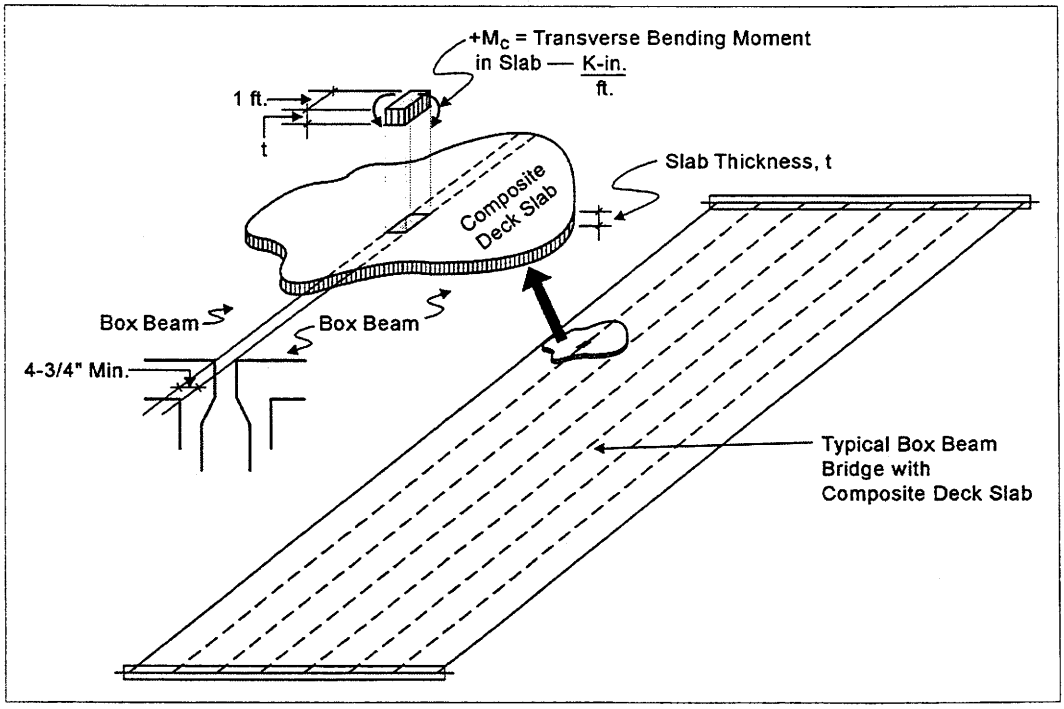

Figure 4.1. Transverse Bending Moment in Composite Deck Slab Caused by Truck Loads. Positive M_c Causes Tension in the Top of the Slab.

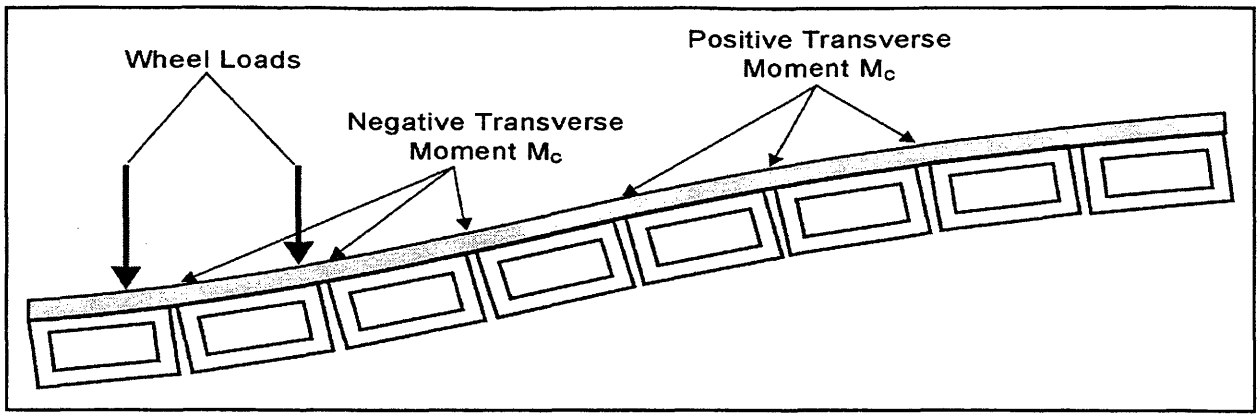

Figure 4.2. Typical Transverse Section of Loaded Bridge Showing Locations of Positive and Negative Transverse Moment in Slab. Scale Exaggerated. Positive M_c Causes Tension Stress in the Top of the Slab.

stress in the top of the deck, while a negative value produces tension in its underside, and both occur in a typical bridge deck as indicated in Figure 4.2. The transverse in-plane component f_y in Figure 3.15 creates normal stress which adds or subtracts directly to bending normal stress. In the absence of very substantial transverse post-tensioning force, the component f_y is quite small. Hence, the transverse moment m_c has the most significant influence on the development and growth of longitudinal cracks in the deck slab.

Figure 4.3 shows the variation of transverse moment m_c at the juncture between adjacent beams (referred to here as an "edge" - see Figure 3.1) in a typical bridge, obtained using the beam and hinge model program MBBA described and documented in the previous chapter. Edge 1 in the figure is along the juncture between the left outside beam and the first interior beam, edge 2 between beam two and beam three, and so forth. The structure has a 28 ft wide roadway constructed from six 5B34 TxDOT boxes, with a 4 in. deck slab, 92 ft span and is unskewed. A single AASHTO HS-20 truck is positioned on the left edge of the roadway so that the first wheel line is 2 ft from the railing and the two 32 kip axles are equally spaced on either side of mid-span. The rather smooth buildup of transverse moment m_c toward a maximum in the region between the two heavy axles is typical of results found for all unskewed bridges. If the truck is moved longitudinally forward or backward from the mid-span position, it tends to reduce the peak transverse moment values that occur between the two heavy axles. Positioning the truck as close to the railing as possible will

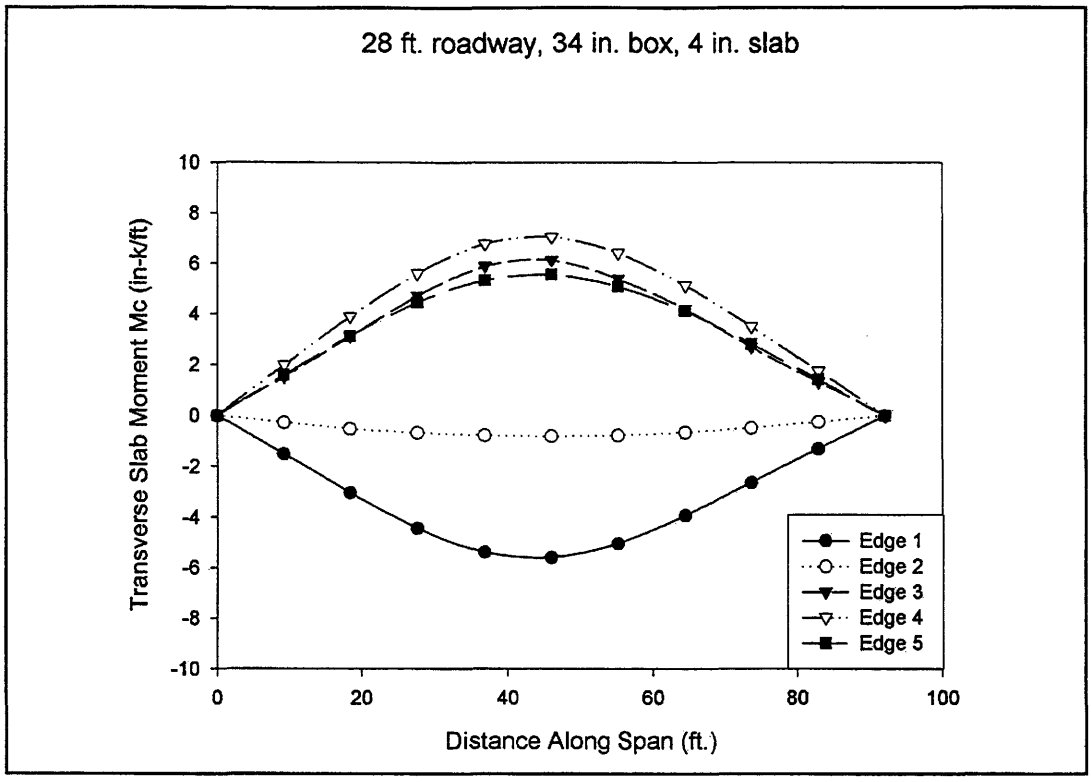

Figure 4.3. Variation of Transverse Slab Moment.

produce the largest value of positive transverse moment (moment causing tensile stress on top) in the deck slab, usually at an edge near the opposite side of the bridge. When loading to obtain the largest positive value of transverse moment, adding a second vehicle only causes a reduction in the maximum positive moment value. Maximum negative values of transverse moment tend to occur at an edge near the center of the bridge cross section and with as many trucks on the structure as design lanes permit.

Figure 4.4 shows the variation of transverse moments for the same structure with a 45 degree skew. Comparison of the two figures demonstrates the typical effects of skew on slab transverse moment. The largest positive moment value tends to decrease somewhat while the largest negative moment is increased.

Analyses were also carried out using the AASHTO Design Tandem consisting of two 25 kip axles spaced 4 ft apart. In every case, however, this loading produced somewhat smaller transverse slab moment values than the HS-20 truck with a 14 ft spacing between rear axles.

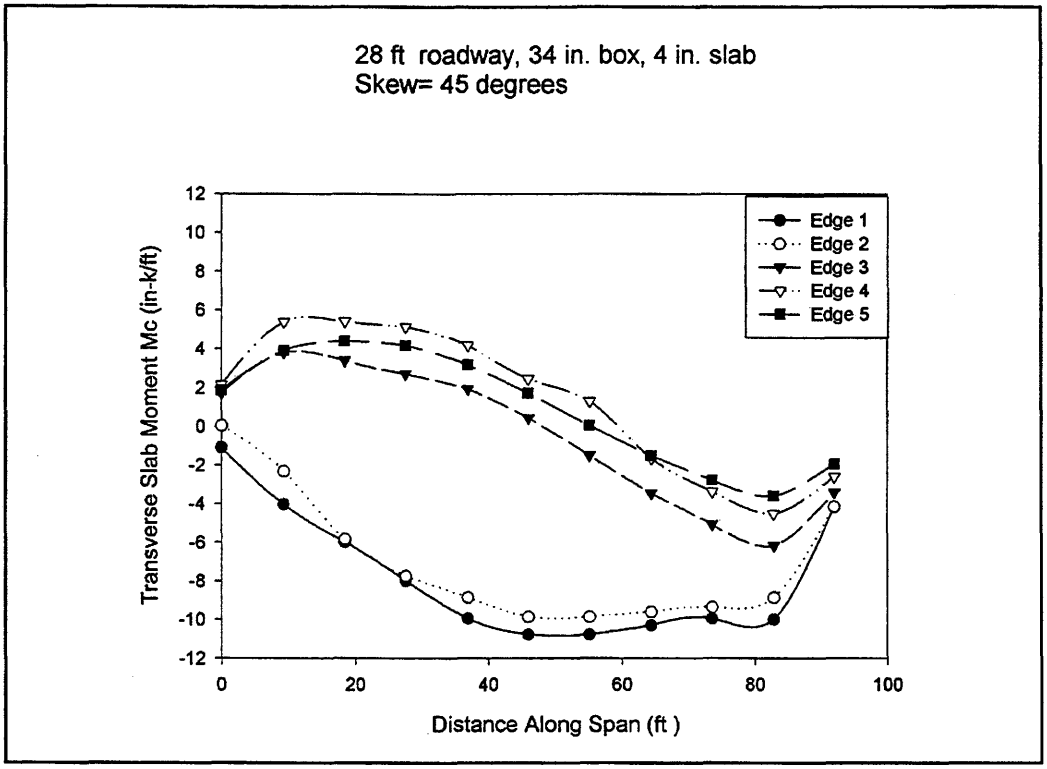

Figure 4.4. Variation of Transverse Slab Moment (Skewed Bridge).

BASIC PARAMETER STUDY

In order to develop some sense of the maximum transverse moment m_c produced in the deck slab of typical TxDOT bridges by truck traffic, a parameter study was conducted in which a variety of common TxDOT multi-beam bridge configurations were analyzed for the effects of AASHTO HS-20 truck loadings (without impact or multi-presence factors). The parameter study examined roadway widths (and their accompanying arrangement of beams shown in Table 4.2) of 28, 30, 34, 38, 40, 42, and 44 ft, using 20, 28, 34, and 40 in. deep TxDOT boxes with 4, 6, and 8 in. composite deck slabs. Three typical span lengths (a short, medium, and long span), which are listed in Table 4.1, were examined for each box size, giving a total of 252 different bridges analyzed. In addition, the effect on m_c of variations in the lateral distance between adjacent boxes was also incorporated in the study. Table 4.2 describes the beam arrangement for each of the roadway widths, which were taken from TxDOT designs. The modulus of elasticity for all beams was based on an assumed

concrete compressive strength of 5,500 psi, while for computing the modulus of the deck slab concrete, a compressive strength of 4,000 psi was used.

The clear distance between adjacent beam top flanges ℓ (see Figure 3.15) was varied between 5 and 14 in. The 5 in. dimension represents what is by far the most common condition in TxDOT bridges, corresponding to a gap of 3/4 to 1 in. between the bottom flanges of adjacent beams as they rest on the bent caps. Larger gaps have correspondingly larger ℓ values. The use of a sheet metal strip to eliminate the shear key causes a condition in which ℓ is not well defined, but under which it is clearly larger than the gap between top flanges. This issue is addressed in more detail in a subsequent section of this chapter.

Table 4.1. Common TxDOT Multi-Box Beam Bridge Spans.

Box	Span Range		
Depth	Short	Medium	Long
20 in.	39 ft	49 ft	59 ft
28 in.	39 ft	59 ft	79 ft
34 in.	65 ft	78.5 ft	92 ft
40 in.	79 ft	92 ft	105 ft

Table 4.2. Common TxDOT Multi-Box Beam Bridge Configurations.

Roadway Width	Number of Boxes	Box Arrangement
28 ft	6	6[5Bxx]
30 ft	8	8[4Bxx]
34 ft	8	2[5Bxx] + 4[4Bxx] + 2[5Bxx]
38 ft	8	8[5Bxx]
40 ft	10	5Bxx + 8[4Bxx] + 5Bxx
42 ft	10	2[5Bxx] + 6[4Bxx] + 2[5Bxx]
44 ft	10	3[5Bxx] + 4[4Bxx[+ 3[5bxx]

Roughly speaking, the process followed in computing the largest positive and largest negative values for transverse slab bending moment m_c using program MBBA was as follows. First, the bridge was divided into either two or three AASHTO design lanes, according to the width of the bridge. A single HS-20 truck was then situated longitudinally on the bridge so the two heavy axles were an equal distance on either side of the bridge mid-span. The truck was then positioned laterally at the left edge of the left most design lane (observing the required 2 ft offset from lane edge to wheel line) and an analysis of the structure performed. The moment component of connection force at each of 20 discrete connections (see Figure 3.4) along each of the edges between adjacent beams was recorded. The truck was then moved laterally to the right 6 in. and the next analysis was performed. This process continued until the truck had traversed the width of the lane. Next, the truck was moved to the second lane, and analyses were run for each of the lateral truck positions in that lane. When all lanes had been analyzed, the results from each lane were then combined so as to produce the largest positive and largest negative value of connection moment at a specific connection. Finally, the largest of these maximums among all the discrete connections in the bridge was identified and taken as the extreme values (one positive and one negative). The values were then divided by the discrete connection spacing and multiplied by 12 to obtain extreme slab moment in units of in.-kips per foot width of slab. This process was, of course, automated by inserting additional coding in the basic analysis program MBBA to carry out these steps.

The results of the parameter study were a single maximum value of positive transverse slab moment and maximum negative transverse slab moment for each bridge analyzed. A review of these many results made the following clear:

(1) Extreme values of slab moment m_c for a given arrangement of boxes and box depth are sensitive to both slab thickness and slab span ℓ. For example, in several cases the difference in maximum m_c between two structures identical in every respect except for slab thicknesses of 4 in. versus 8 in. had slab moments which differed by more than 70 percent. In all cases, the thicker the slab, the greater the slab moment. Sensitivity to slab span was not as pronounced, but it was clear it was a factor which could not be completely ignored. In general, the shorter the slab span ℓ, the larger the moment.

(2) Extreme values of slab moment m_c are affected by box depth. For two bridges identical in all respects except for box depth, m_c values were found to vary by 30 percent or more.

(3) The single most important factor affecting extreme values of slab moment m_c appears to be the bridge span. As span increases, so does m_c.

(4) The arrangement of boxes within the cross section of the bridge has significant impact on m_c. While there seemed to be general, but different, trends in changes in positive and negative m_c with increasing width of bridge, the effect of having a mixture of box widths within the cross section produced erratic variations. That is, no obvious relationship between bridge cross section and extreme values of slab moment exists, or at least none could be determined.

SLAB TRANSVERSE MOMENT PREDICTION FOR SPECIFIC CONFIGURATIONS

The first effort at extracting some relationship between maximum transverse moment in a bridge's deck slab and the various parameters known to influence it was based on plotting the maximum positive m_c value against span length for various combinations of slab thickness (4, 6, and 8 in.) and box size (20, 28, 34, and 40 in.), as seen in Figure 4.5 for a 28 ft roadway. The plot suggests that, in general, the thicker the slab, the larger the maximum moment it must resist. Beyond this, however, the scattering of points indicates that slab moment is dependent on at least the slab stiffness, beam stiffness, and bridge span. With some experimentation it was found that the function,

$$m_c = c_1 J^{c_2} I^{c_3} L^{c_4} \qquad \text{Eq. (4.1)}$$

where c1,...,c4 are constants, gave reasonably accurate predictions of m_c for a specific bridge geometry, slab thickness, and slab span ℓ. In Eq. (4.1), L is the span length, I the moment of inertia, and J the torsional stiffness of the beams. I and J as used in the equation are computed for the beam alone—that is, for the non-composite section. When the bridge contains a mixture of box sizes, the I and J are the weighted average of the property based on the number of each type box present. Experimentation led to the conclusion that using composite section properties did not enhance the predictive powers of the equation and so the simpler non-composite properties were used instead.

As an example, Table 4.3 lists the 12 cases used in a regression to compute the constants c1,...,c4 for a 28 ft roadway (see Table 4.2), 4 in. thick deck slab, with a slab span ℓ of 5 in. The constants were found to be c1=835.6, c2=-0.781, c3=0.181, and c4=0.693, giving the equation

$$m_c = 835.5 J^{-0.781} I^{0.181} L^{0.693}$$

in which I and J have units of in.^{4} and L is in feet. In all cases the exact values of m_c shown were obtained using program MBBA and the process described above for obtaining extreme values of slab moment and represent the largest positive and largest negative transverse bending moments occurring anywhere in the deck slab. From Table 4.3 it can be seen that the maximum absolute value of error is 6.6 percent, and the average error is 2.4 percent.

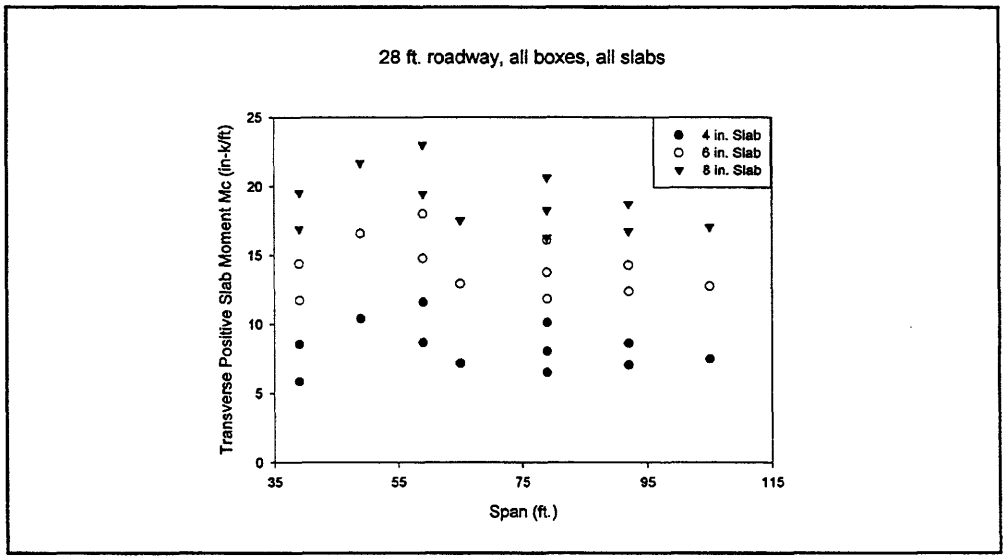

Figure 4.5. Transverse Positive Slab Moment.

These results suggested that Eq. (4.1) involved the proper factors for a given bridge configuration and could form the basis for bridge-specific slab design. Next, the efforts were expanded in an attempt to generalize Eq. (4.1) to reflect the effects of slab thickness and slab span but once again for a specific bridge cross section. It was recognized that the stiffness factor k_Φ (see Eq. 3.4) used in the MBBA model was the primary way through which both slab thickness and slab span were reflected, and that by including the factor in Eq. (4.1), both effects might possibly be accounted for. Toward this end, the following equation was posed:

$$m_c = b_1 (k_s)^{b_2} J^{b_3} I^{b_4} L^{b_5} \qquad \text{Eq. (4.2)}$$

where k_s is the slab stiffness given by

$$k_s = \frac{E_s t^3}{3{,}600\ell}$$

E_s is the modulus of elasticity of the slab concrete in ksi units, t is the slab thickness in inches, and ℓ is the slab span in inches. In the equation, the bridge span L is in feet, and the section properties I and J are those for the beam without composite slab expressed in units of in.^{4} (see Table 3.1). In cases where there is a mixture of box sizes in the bridge, the I and J are the weighted average of those properties for the beams in the bridge. For example, the 42 ft roadway in Table 4.1 shows four 5 ft and six 4 ft wide boxes in the section. Using the section properties from Table 3.1 for a 34 in. deep box, one would have

$$I = \frac{6(115{,}540) + 4(142{,}040)}{10} = 126{,}140 \ in.^4$$

The weighted average for J would be computed in the same manner.

Table 4.3. Twelve Bridges Used to Compute Regression Constants.

Roadway Width ft	Slab Thickness in.	Box Size	Span ft	I in.^4	J in.^4	Exact +Mc in.-kips/ft	Predicted +Mc in.-kips/ft	% Error
28	4	20 in.	39	35,235	99,680	8.6	8.8	-1.9
28	4	20 in.	49	35,235	99,680	10.4	10.3	1.7
28	4	20 in.	59	35,235	99,680	11.6	11.7	-0.3
28	4	28 in.	39	85,370	187,070	5.9	6.3	-6.6
28	4	28 in.	59	85,370	187,070	8.7	8.4	3.9
28	4	28 in.	79	85,370	187,070	10.1	10.2	-1.3
28	4	34 in.	65	142,040	293,410	7.2	6.9	4.0
28	4	34 in.	78.5	142,040	293,410	8.1	7.9	1.8
28	4	34 in.	92	142,040	293,410	8.7	8.8	-1.6
28	4	40 in.	79	215,245	425,350	6.5	6.4	2.1
28	4	40 in.	92	215,245	425,350	7.1	7.1	0.1
28	4	40 in.	105	215,245	425,350	7.5	7.8	-3.4

Eq. (4.2) was applied to the 28 ft roadway structure listed in Table 4.2 by running a regression on 108 different combinations of box size (20, 28, 34, and 40 in.), slab thickness (4, 6, and 8 in.), span lengths (see Table 4.1), and slab span (5, 7.4, and 14 in.) to determine the value of the constants b1,..,b5. For positive m_c, the average (in absolute value) percent error over the 108

cases was 7.1 percent. Although on average the error in predicting positive m_c is small, the percent error in isolated cases was quite large; up to 72 percent in the worst case. There is, however, a consistent pattern to the errors in the sense that the large errors occur in predicting the smallest values of m_c. For example, the 72 percent error occurred for a 39 ft span using 28 in. boxes, a 4 in. slab with a 1 in. space between the bottom flanges (a 5 in. slab span). In this case, the maximum positive m_c in the bridge was 2.54 k-in./ft, while the value predicted by Eq. (4.2) is 4.37. It seems unlikely in such a bridge that such a small transverse moment would be troublesome since it is almost an order of magnitude less than the slab cracking moment. On the other hand, this same bridge constructed with 8 in. rather than 4 in. slab experiences a peak transverse moment of 16.9 k-in./ft, which is predicted by the equation to be 16.1 k-in./ft, a 5 percent error.

SLAB TRANSVERSE MOMENT PREDICTION - ATTEMPTS AT MORE GENERAL RESULTS

With the success of Eq. (4.2) to predict m_c for a variety of slab thicknesses and slab spans, and knowing that it had been arrived at by generalizing Eq. (4.1), it seemed likely that one more pass at generalizing Eq. (4.2) to include the effects of various arrangements of boxes within the cross section of the bridge would provide the ultimate goal of a single equation suitable for predicting m_c for any bridge constructed with standard TxDOT boxes. This conjecture turned out to be at best overly ambitious and certainly more than a bit naive.

Although to some degree the arrangement of boxes within a bridge section is reflected in the weighted average of I and J used in Eqs. (4.1) and (4.2), it quickly proved incapable of fully accounting for variations in m_c between say the 34 and 38 ft roadway bridges in Table 4.2. Both have eight boxes in the cross section, but one contains only 5 ft boxes while the other is a mixture of the two box widths. Results of the 108 analyses described earlier and made on each of these two bridges showed differences in m_c for essentially identical structures (same bridge span, slab thickness, box depth, and slab span) ran to 40 percent and more—differences due solely to which two box widths were used and how they were arranged within the bridge. A regression was run on Eq. (4.2) using the 108 data for each of these two bridges to evaluate the constants $b_1,...,b_5$. The results were disappointing, but not unexpected. The equation proved incapable of consistently predicting m_c within the target accuracy of 5-10 percent for *either* bridge.

An inspection of m_c values among the seven bridges in Table 4.2 indicated a general trend of increasing value with an increase in bridge width, raising the hope that perhaps adding a bridge width term to Eq. (4.2) might provide the elusive "general" equation. Equation (4.2) was altered to read

$$M_c = b_1 W^{b_2} (k_s)^{b_3} J^{b_4} I^{b_5} L^{b_6} \qquad \text{Eq. (4.3)}$$

The 108 data for each of the seven bridge configurations in Table 4.2 were used in a regression to determine the constants. The results proved to be quite unreliable. On average, the error in predicting m_c (either positive or negative value) was unacceptably large for any one of the bridges and far in excess of the errors yielded by Eq. (4.2) for a single bridge of specified box arrangement. At this point the quest for a "general" formula was abandoned, and focus returned to adapting Eq. (4.2) to the various bridge configurations used by TxDOT.

RECOMMENDED SLAB DESIGN MOMENT EQUATION FOR TxDOT BRIDGES

The bridges described in Table 4.2 were selected for study because they occur with good frequency among existing bridges in the state. In addition, discussions with TxDOT personnel indicated a move toward standardization of designs for these type bridges was under way in an effort to utilize the most economical bridge cross section for a specified roadway width. This turns out to be that cross section with the most 5 ft boxes consistent with the roadway width and lateral spacing between adjacent beams desired. Problems have sometimes been encountered during construction with sweep of the boxes, suggesting the need to revisit the lateral spacing usually left between bottom flanges of adjacent beams. The new proposed standard bridge configurations are listed in Table 4.4 and include roadway widths from 24 to 52 ft.

Equation (4.2), listed again below for reference, was applied to each of the bridge configurations

$$M_c = b_1 (k_s)^{b_2} J^{b_3} I^{b_4} L^{b_5}$$

$$k_s = \frac{E_s t^3}{3{,}600\ell}$$

in Table 4.2 and Table 4.4 and a regression run to determine the constants $b_1,...,b_5$. For each such bridge, a total of 108 combinations of beam span, box depth, slab thickness, and slab span ℓ described earlier was used in the regression. The results are listed in Tables 4.5 (for predicting $+m_c$) and 4.6 (for predicting $-m_c$) for the common bridge configurations of Table 4.2 and in Tables 4.7 and 4.8 for the new proposed standard configurations of Table 4.4. They are applicable to unskewed bridges. A subsequent section of this chapter presents a method to account for the effects of skew on slab moment.

Table 4.4 Proposed New TxDOT Multi-Box Beam Bridge Configurations.

Roadway Width	Number of Boxes	Box Arrangement
24 ft	6	5Bxx + 4[4Bxx] + 5Bxx
26 ft	6	4Bxx + 4[5Bxx] + 4Bxx
28 ft	6	6[5Bxx]
30 ft	7	2[5Bxx] + 3[4Bxx] + 2[5Bxx]
32 ft	8	4[4Bxx] + 5Bxx + 3[4Bxx]
34 ft	8	2[4Bxx] + 3[5Bxx] + 3[4Bxx]
36 ft	8	2[5Bxx] + 3[4Bxx] + 3[5Bxx]
38 ft	8	8[5Bxx]
40 ft	9	2[4Bxx] + 5[5Bxx] + 2[4Bxx]
42 ft	9	4Bxx + 7[5Bxx] + 4Bxx
44 ft	9	9[5Bxx]
46 ft	10	3[5Bxx] + 3[4Bxx] + 4[5Bxx]
48 ft	10	4[5Bxx] + 4Bxx + 5[5Bxx]
50 ft	11	2[4Bxx] + 7[5Bxx] +2[4Bxx]
52 ft	11	4Bxx + 9[5Bxx] + 4Bxx

Table 4.5. Constants in Eq. (4.2) to Predict Positive Slab Transverse Slab Moment M_c in Bridges from Table 4.2.

Roadway Width	Box Arrangement	Constants				
		b_1	b_2	b_3	b_4	b_5
28 ft	6[5Bxx]	53.95	0.42	-0.45	0.05	0.45
30 ft	8[4Bxx]	64.932	0.478	-0.607	0.129	0.590
34 ft	2[5Bxx] + 4[4Bxx]+ 2[5Bxx]	81.423	0.559	-0.727	0.185	0.739
38 ft	8[5Bxx]	83.884	0.614	-0.717	0.125	0.864
40 ft	5Bxx + 8[4Bxx] + 5Bxx	56.813	0.638	-0.721	0.108	0.938
42 ft	2[5Bxx] + 6[4Bxx] + 2[5Bxx]	35.805	0.648	-0.614	0.022	0.977
44 ft	3[5Bxx] + 4[4Bxx] + 3[5Bxx]	86.498	0.639	-0.868	0.220	0.980

Table 4.6. Constants in Eq. (4.2) to Predict Negative Slab Transverse Slab Moment M_c in Bridges from Table 4.2.

Roadway Width	Box Arrangement	Constants				
		b_1	b_2	b_3	b_4	b_5
28 ft	6[5Bxx]	41.53	0.42	-0.36	-0.09	0.71
30 ft	8[4Bxx]	64.530	0.485	-0.578	0.090	0.677
34 ft	2[5Bxx] + 4[4Bxx]+ 2[5Bxx]	94.019	0.512	-0.725	0.177	0.789
38 ft	8[5Bxx]	87.902	0.592	-0.767	0.169	0.916
40 ft	5Bxx + 8[4Bxx] + 5Bxx	116.250	0.525	-0.771	0.209	0.779
42 ft	2[5Bxx] + 6[4Bxx] + 2[5Bxx]	57.280	0.578	-0.674	0.099	0.943
44 ft	3[5Bxx] + 4[4Bxx] + 3[5Bxx]	0.582	0.599	0.699	-0.977	0.976

Equation (4.2) together with the constants in Tables 4.4 through 4.8 can be used to compute positive and negative slab design moments for any of the bridge configurations of Tables 4.2 and 4.4. To use the equation, one must specify a slab stiffness k_s which in turn requires a slab span ℓ. As introduced in Chapter Three, Figure 3.15, the slab span is the length of slab transverse to adjacent

Table 4.7. Constants in Eq. (4.2) to Predict Positive Slab Transverse Slab Moment M_c in Bridges from Table 4.4.

Roadway Width	Box Arrangement	Constants				
		b_1	b_2	b_3	b_4	b_5
24 ft	5Bxx + 4[4Bxx] + 5Bxx	35.173	0.440	-0.546	0.118	0.574
26 ft	4Bxx + 4[5Bxx] + 4Bxx	3.049	0.402	0.447	-0.605	0.323
28 ft	6[5Bxx]	70.843	0.452	-0.553	0.109	0.536
30 ft	2[5Bxx] + 3[4Bxx] + 2[5Bxx]	36.312	0.470	-0.492	0.034	0.676
32 ft	4[4Bxx] + 5Bxx + 3[4Bxx]	87.530	0.542	-0.668	0.129	0.705
34 ft	2[4Bxx] + 3[5Bxx] + 3[4Bxx]	27.795	0.579	-0.319	-0.165	0.771
36 ft	2[5Bxx] + 3[4Bxx] + 3[5Bxx]	84.733	0.590	-0.773	0.189	0.845
38 ft	8[5Bxx]	85.305	0.614	-0.721	0.128	0.864
40 ft	2[4Bxx] + 5[5Bxx] + 2[4Bxx]	124.260	0.638	-0.856	0.199	0.936
42 ft	4Bxx + 7[5Bxx] + 4Bxx	87.925	0.633	-0.766	0.141	0.968
44 ft	9[5Bxx]	151.123	0.656	-0.973	0.287	0.999
46 ft	3[5Bxx] + 3[4Bxx] + 4[5Bxx]	171.321	0.626	-1.014	0.339	0.941
48 ft	4[5Bxx] + 4Bxx + 5[5Bxx]	207.306	0.637	-1.061	0.371	0.957
50 ft	2[4Bxx] + 7[5Bxx] + 2[4Bxx]	9.150	0.635	0.019	-0.521	0.997
52 ft	4Bxx +9[5Bxx] + 4Bxx	203.110	0.644	-1.053	0.349	0.991

beams which transfers forces. When a shear key is used and, hence, no metal sheet is present to break bond between slab and box concrete, the slab span is equal to the clear distance between top beam flanges. When a shear key is omitted by placing the sheet metal strip (see Figure 4.6), the slab span is affected. For negative transverse moment m_c which causes tension stress on the underside of the slab, the slab tends to curl upward, lifting off the unbonded metal surface and producing a longer slab span. The upper limit of ℓ in this case would be the width of the metal sheet, as shown in the figure. The actual effective slab span for negative m_c, lies somewhere between the clear distance between flanges and the width of the sheet. While it is not possible to be more precise

Table 4.8. Constants in Eq. (4.2) to Predict Negative Slab Transverse Slab Moment M_c in Bridges from Table 4.4.

Roadway Width	Box Arrangement	Constants				
		b_1	b_2	b_3	b_4	b_5
24 ft	5Bxx + 4[4Bxx] + 5Bxx	47.198	0.451	-0.496	0.058	0.605
26 ft	4Bxx + 4[5Bxx] + 4Bxx	0.00484	0.496	2.399	-2.284	0.751
28 ft	6[5Bxx]	95.704	0.516	-0.739	0.186	0.756
30 ft	2[5Bxx] + 3[4Bxx] + 2[5Bxx]	58.144	0.480	-0.511	0.030	0.699
32 ft	4[4Bxx] + 5Bxx + 3[4Bxx]	89.787	0.559	-0.758	0.187	0.801
34 ft	2[4Bxx] + 3[5Bxx] + 3[4Bxx]	92.563	0.588	-0.759	0.174	0.838
36 ft	2[5Bxx] + 3[4Bxx] + 3[5Bxx]	61.977	0.531	-0.680	0.138	0.861
38 ft	8[5Bxx]	88.590	0.592	-0.768	0.170	0.917
40 ft	2[4Bxx] + 5[5Bxx] + 2[4Bxx]	108.363	0.568	-0.778	0.194	0.832
42 ft	4Bxx + 7[5Bxx] + 4Bxx	27.998	0.586	-0.423	-0.099	0.940
44 ft	9[5Bxx]	103.929	0.610	-0.838	0.212	0.970
46 ft	3[5Bxx] + 3[4Bxx] + 4[5Bxx]	112.183	0.580	-0.863	0.249	0.946
48 ft	4[5Bxx] + 4Bxx + 5[5Bxx]	99.604	0.610	-0.827	0.197	1.009
50 ft	2[4Bxx] + 7[5Bxx] + 2[4Bxx]	15.755	0.631	-0.294	-0.227	1.022
52 ft	4Bxx +9[5Bxx] + 4Bxx	95.931	0.631	-0.827	0.182	1.036

about slab span, the analyses run for the parameter study clearly show that taking the shorter value (i.e., the clear distance between flanges) leads to conservative results—that is, predicts larger values of transverse moment. Therefore, it is recommended that this distance be used for the slab span in applying Eq. (4.2).

Eq. (4.2) and the constants of Tables 4.5 through 4.8 were used, along with the slab span recommended above, to develop slab design moments for the various bridge configurations of Tables 4.2 and 4.4 with span lengths from 30 to 110 ft and deck thicknesses of 4, 6, and 8 in. In all cases

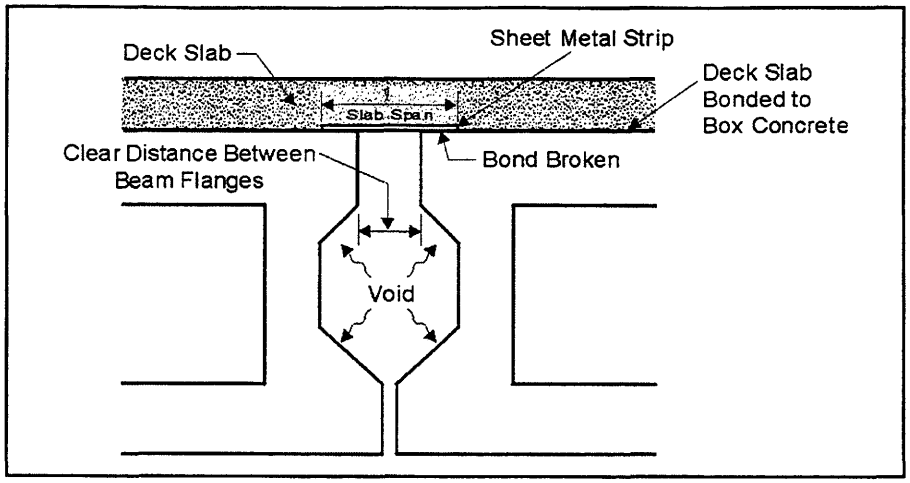

Figure 4.6. Slab Span.

the clear distance between top flanges of adjacent beams was taken conservatively to be 5 in. These tables of design moments are located in Appendices A and B.

SKEW EFFECTS ON SLAB TRANSVERSE MOMENT

Skew angle does affect extreme values of slab transverse moment m_c; that is, the values of slab design moment in Appendix A are, strictly speaking, incorrect for those same bridges with skew. The extent of this effect was first explored by re-running analyses of selected bridges from Tables 4.2 and 4.4 using skew angles between 15 and 45 degrees. Those results indicated that for skew angles up to approximately 25 degrees, *significant* slab design moments actually decrease slightly in practically all cases. Significant in this context refers to those cases where the slab transverse moment m_c in the unskewed bridge (see Appendix A) was roughly as large as the slab cracking moment. For skew angles greater than 25 degrees, negative slab design moments typically begin to increase beyond those in Appendix A for non-skewed bridges, while positive slab design moments increased slowly, rarely exceeding 10 percent over the non-skewed values. In many cases positive m_c values actually decreased and rather dramatically in some instances. In summary, one can safely use the values of positive slab transverse moment for unskewed bridges listed in Appendix A for bridges with skews up to 45 degrees, although they may be quite conservative in some instances. Negative slab transverse moments from Appendix A can be seriously in error on the unconservative side for skew angles beyond about 25 degrees.

Study of the analysis results also indicated that how m_c changed with skew angle was quite dependent upon the particulars of the bridge. For some combinations of slab thickness, box size, and span, the changes in m_c with skew angle were less than 10 percent, while for others it exceeded 100 percent and, in general, there appeared to be no consistent pattern to the change. This circumstance made it clear that any formula for a multiplier to be applied to non-skewed m_c values in order to account for skew effects with reasonable accuracy would be specific to a particular bridge structure.

Numerical experimentation leads to the following formula for the transverse slab moment m_c in skewed bridges:

$$m_{c_\theta} = m_{c_0}(1 + a_1\theta + a_2\theta^2) \qquad \text{Eq. (4.3)}$$

where m_{c_θ} is the value of the transverse moment m_c for a bridge with skew angle θ (in radians), and m_{c_0} is the moment in the same bridge without skew. A regression was run on each of the bridge configurations in Tables 4.2 and 4.4 to determine the values of the constants a_1 and a_2, which are listed in Tables 4.9 through 4.12.

Table 4.9. Constants in Eq. (4.3) to Predict Positive Slab Transverse Slab Moment M_c in Skewed Bridges from Table 4.2.

Roadway Width	Box Arrangement	Constants	
		a_1	a_2
28 ft	6[5Bxx]	-0.526	0.840
30 ft	8[4Bxx]	-0.162	0.075
34 ft	2[5Bxx] + 4[4Bxx] + 2[5Bxx]	-0.794	0.620
38 ft	8[5Bxx]	-0.800	0.626
40 ft	5Bxx + 8[4Bxx] + 5Bxx	-0.666	0.430
42 ft	2[5Bxx] + 6[4Bxx] + 2[5Bxx]	-0.663	0.500
44 ft	3[5Bxx] + 4[4Bxx] + 3[5Bxx]	-0.718	0.606

Table 4.10. Constants in Eq. (4.3) to Predict Negative Slab Transverse Slab Moment M_c in Skewed Bridges from Table 4.2.

Roadway Width	Box Arrangement	Constants	
		a_1	a_2
28 ft	6[5Bxx]	-0.103	1.615
30 ft	8[4Bxx]	0.834	-0.154
34 ft	2[5Bxx] + 4[4Bxx] + 2[5Bxx]	0.007	1.000
38 ft	8[5Bxx]	0.065	1.108
40 ft	5Bxx + 8[4Bxx] + 5Bxx	0.007	0.916
42 ft	2[5Bxx] + 6[4Bxx] + 2[5Bxx]	0.013	0.746
44 ft	3[5Bxx] + 4[4Bxx] + 3[5Bxx]	0.110	0.600

Table 4.11. Constants in Eq. (4.3) to Predict Positive Slab Transverse Slab Moment M_c in Skewed Bridges from Table 4.4.

Roadway Width	Box Arrangement	Constants	
		a_1	a_2
24 ft	5Bxx + 4[4Bxx] + 5Bxx	-0.244	0.256
26 ft	4Bxx + 4[5Bxx] + 4Bxx	-0.635	0.806
28 ft	6[5Bxx]	-0.862	0.981
30 ft	2[5Bxx] + 3[4Bxx] + 2[5Bxx]	-0.486	0.628
32 ft	4[4Bxx] + 5Bxx + 3[4Bxx]	-0.675	0.502
34 ft	2[4Bxx] + 3[5Bxx] + 3[4Bxx]	-0.651	0.452
36 ft	2[5Bxx] + 3[4Bxx] + 3[5Bxx]	-0.688	0.533
38 ft	8[5Bxx]	-0.811	0.638
40 ft	2[4Bxx] + 5[5Bxx] + 2[4Bxx]	-0.677	0.433
42 ft	4Bxx + 7[5Bxx] + 4Bxx	-1.112	0.889
44 ft	9[5Bxx]	-0.739	0.546
46 ft	3[5Bxx] + 3[4Bxx] + 4[5Bxx]	-0.650	0.532
48 ft	4[5Bxx] + 4Bxx + 5[5Bxx]	-0.712	0.583
50 ft	2[4Bxx] + 7[5Bxx] + 2[4Bxx]	-0.827	0.651

Table 4.12. Constants in Eq. (4.3) to Predict Negative Slab Transverse Slab Moment M_c in Skewed Bridges from Table 4.4.

Roadway Width	Box Arrangement	Constants	
		a_1	a_2
24 ft	5Bxx + 4[4Bxx] + 5Bxx	-0.306	1.730
26 ft	4Bxx + 4[5Bxx] + 4Bxx	0.107	1.653
28 ft	6[5Bxx]	0.562	1.220
30 ft	2[5Bxx] + 3[4Bxx] + 2[5Bxx]	-0.011	1.236
32 ft	4[4Bxx] + 5Bxx + 3[4Bxx]	0.014	1.067
34 ft	2[4Bxx] + 3[5Bxx] + 3[4Bxx]	0.006	0.984
36 ft	2[5Bxx] + 3[4Bxx] + 3[5Bxx]	-0.034	1.173
38 ft	8[5Bxx]	0.035	1.092
40 ft	2[4Bxx] + 5[5Bxx] + 2[4Bxx]	0.032	0.888
42 ft	4Bxx + 7[5Bxx] + 4Bxx	0.062	0.767
44 ft	9[5Bxx]	0.046	0.780
46 ft	3[5Bxx] + 3[4Bxx] + 4[5Bxx]	0.040	0.705
48 ft	4[5Bxx] + 4Bxx + 5[5Bxx]	0.022	0.692
50 ft	2[4Bxx] + 7[5Bxx] + 2[4Bxx]	0.022	0.713
52 ft	4Bxx + 9[5Bxx] + 4Bxx	0.008	0.692

MECHANISMS FOR CONTROLLING DECK STRESSES

One obvious means of controlling longitudinal tensile cracking in the deck would be the addition of transverse post tensioning to the deck slab. The maximum slab moment a deck must resist can be computed from information presented above, and a tendon layout determined from it to reduce the peak tensile stress to an acceptable level. This likely would not be a cheap solution.

Transverse post tensioning of the bridge, more or less like that used in the past on TxDOT bridges, does little to reduce transverse tensile stresses in the deck slab. In fact, this approach is only workable with a shear key to provide a bearing surface between beams. Without it, post-tensioning forces would induce substantial transverse bending moment in the slab, offsetting the gains of direct compression stresses from the post tensioning. Analyses on typical bridge configurations with full

depth shear keys confirmed these problems. In order to generate enough force to effectively counteract the transverse slab moments from truck loads, an absurd amount of post tensioning is required (on the order of a 29 kip strand every 18 in. or less). In short, conventional transverse post tensioning in composite deck slab bridges contributes very little to the performance of the slab.

One factor which would work towards reducing longitudinal cracking in the deck slab is to return to the use of a shear key. While the precise effect on transverse tensile stresses is difficult to quantify, the presence of a deeper section of concrete at the location where transverse moment acts can only improve the situation. This fact is supported to some degree by the bridge inspection results cited in Chapter Two. There, the bridges with shear keys tended to be less severely cracked, although the span lengths and level of traffic varied considerably among them, making direct comparisons impossible.

Multi-box beam bridges with composite deck slab and no shear key share vehicular loads through action of the slab between adjacent beams. This turns out to be a somewhat inefficient mechanism. In Figure 4.2 the cross section of a typical bridge is shown supporting wheel loads. The cross section does not deflect downward uniformly, and as a result two things happen: the box beams tend to rotate relative to one another as depicted in the figure, and transverse moment in the deck slab is induced as a result of these beam rotations. The mode of deformation suggests that if this more or less independent rotation among boxes could be curtailed, it would reduce the transverse bending moment in the slab. The efficacy of this approach was examined analytically for several typical bridges in Table 4.2. In each structure, auxiliary connections were added at the bottom of each box, tying it to its neighbors as shown in Figure 4.7. With adequate stiffness, these connections dramatically reduced the transverse moment in the slab—typically to less than 2 in.-kips/ft.

On an intuitive basis, the mechanics of this effect are shown in Figure 4.8. Without auxiliary connection at the bottom of the beams, the slab carries a transverse moment m_c. The presence of this connection creates a couple with force F acting through a moment arm of d, which essentially replaces the slab moment, reducing it to a small or zero value. This suggests that an estimate of the connection force F could be made from

$$\alpha dF = m_c \qquad \text{Eq. (4.4)}$$

where m_c is the slab moment that exists without the auxiliary connection, computed as described earlier in this chapter, and α is a factor to approximately account for the imperfect theory. Selected bridges from Tables 4.2 and 4.4 were analyzed with auxiliary connections centered 3 in. above the bottom of the beams. The stiffness k_y (see Figure 3.2 and Eqs. (3.1) through (3.4)) was taken equal to that of the slab and the other stiffnesses set to zero. This would simulate a uniaxial force, such as that which would exist in a bolt, connecting adjacent beams. For each bridge analyzed, its slab moment was taken from Appendix A, and a value of the parameter α computed from Eq. (4.4). The results of these analyses were rather scattered, indicating that Eq. (4.4) is a pretty crude approximation. Coefficient α values were found to range from about 0.2 to about 0.5, with an average value of about 0.28. Note that in applying Eq. (4.4), the force F will be the force per unit length along the beam and have kip/ft units when the moment m_c has in.-kip/ft units as those in Appendices A and B.

Auxiliary connections offer perhaps the structurally most efficient means for controlling the transverse slab moment which leads to longitudinal cracking of the deck. Exactly how these connections can be made is not obvious. One suggestion which has been offered is the use of an epoxy joint. This could be formed by installing a backer strip at the bottom of the juncture between the bottom beam flanges and then pouring the epoxy from above before the deck is cast. The depth of the joint would be dictated by the need to limit the tensile stresses at the epoxy/concrete interface.

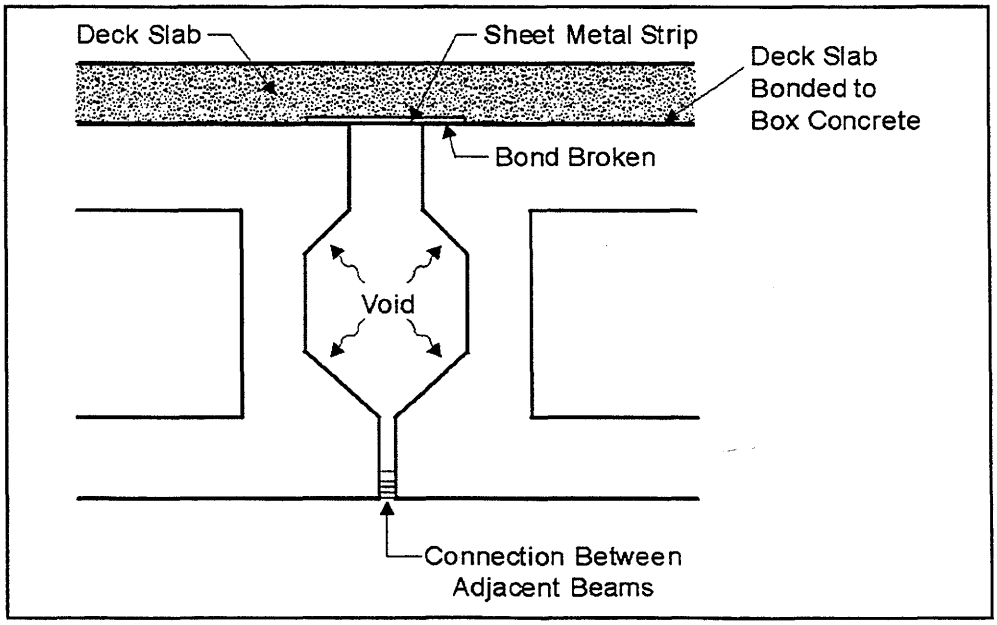

Figure 4.7. Beam-to-Beam Lateral Connection.

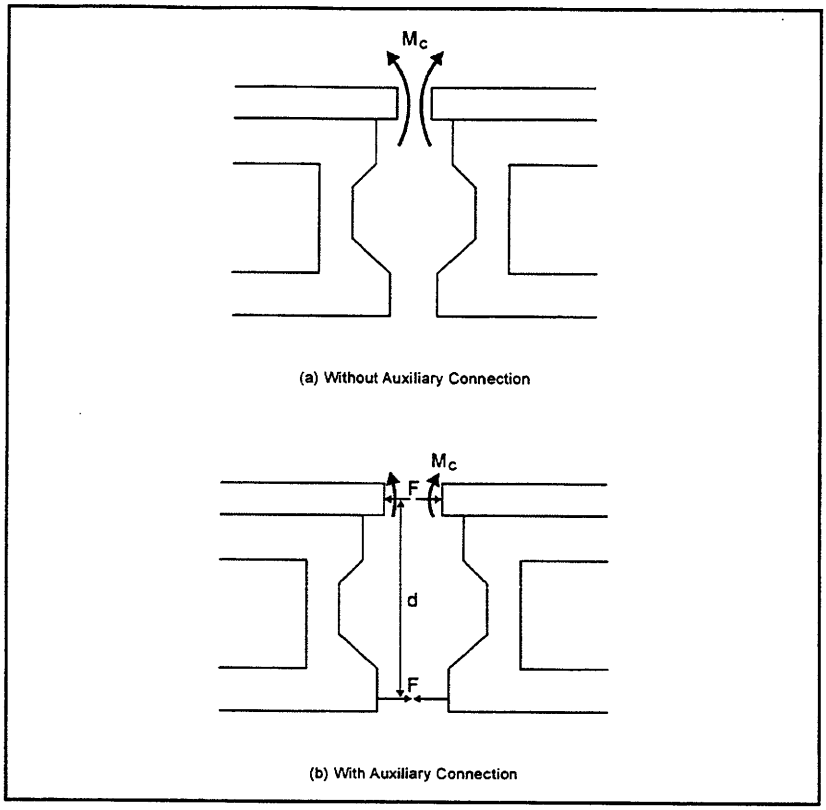

Figure 4.8. Forces in System with Lateral Connections.

CHAPTER FIVE ■ LIVE LOAD LATERAL DISTRIBUTION FACTORS

The AASHTO *Design Specifications for Bridges* has for years contained approximate formulas for computing the fraction of bending moment and shear force produced by trucks to be resisted by a single beam in a multi-beam bridge. The two most current formulas are AASHTO [1996]

$$LF=(S/D) \qquad \text{Eq. (5.1)}$$

where LF is the fraction of the effect produced by a single *truck* and S= width of the precast member,

$$D=(11.5-N_L)+1.4N_L(1-0.2C)^4;C\leq 5 \qquad \text{Eq. (5.2)}$$

$$D=(5.75-0.5N_L);C>5$$

N_L = number of traffic lanes,

C = $K(W/L)$,

W = overall width of bridge,

L = span length, and

$$K=\sqrt{(1+\mu)(I/J)} \qquad \text{Eq. (5.3)}$$

and AASHTO [1994] (the "LRFD" formula)

$$LF=k(b/305)^{0.6}(b/12L)^{0.2}(I/J)^{0.06} \qquad \text{Eq. (5.4)}$$

where

k = $2.5N_b^{-0.2} \geq 1.5$,

b = width of member,

N_b = number of beams in the bridge,

L = span length,

I = moment of inertia of the beam about a horizontal axis, and

J = polar moment of inertia.

In the context of this chapter, the term "live load lateral distribution factor" (abbreviated LLDF in this report) and the quantity LF in Eqs. (5.1) and (5.4) are synonymous. When a bridge contains more than two design lanes, the load fraction LF given by Eq. (5.1) may be reduced by a multi-

presence factor (e.g., 0.9 for three lanes). According to AASHTO [1994], the value from Eq. (5.4) should not be modified with a multi-presence factor because it was included in the development of the formula.

The AASHTO formulas are approximations, intended to encompass multi-beam bridges having a variety of different techniques by which adjacent beams are made to act as a unit in sharing truck loads, as well as beams having various cross-sectional shapes and properties. On the other hand, the analysis model MBBA described and documented in Chapter Three can be used to compute an "exact" LLDF for a given bridge. In this chapter, exact LLDFs are presented for interior beam bending moment in beams from the seven common TxDOT bridge configurations introduced in Table 4.2 and the proposed new configurations of Table 4.4 in Chapter Four. The effect of skew on the LLDF for these common designs is also accounted for by means of an AASHTO-like modification factor.

A general formula for LLDF, similar in character to AASHTO Eqs. (5.1) or (5.4) above, and capable of giving accurate values for such diverse situations as may arise in future TxDOT designs, simply could not be established. As a compromise, quite accurate approximate equations were developed for the specific bridge geometries common to most existing TxDOT multi-box beam bridges and were then used to generate tables of LLDFs for various span conditions.

BASIC PARAMETER STUDY

In order to develop data on LLDFs for the seven common TxDOT bridge geometries of Table 4.2, a parameter study was performed in which exact LLDFs were computed using program MBBA. Roughly speaking, the process followed in computing an "exact" LLDF for beam bending moment using program MBBA was as follows. First, the bridge was divided into either two or three AASHTO design lanes according to the width of the bridge. A single HS-20 truck was then situated longitudinally on the bridge so as to produce absolute maximum bending moment, which occurs beneath the 32 kip axle closest to mid-span. The truck was then positioned laterally at the left edge of the design lane (observing the required 2 ft offset from lane edge to wheel line), and an analysis of the structure performed, and the maximum bending moment in each beam recorded. The truck was then moved laterally to the right 6 in. and the next analysis performed. This process was

continued until the truck had traversed the width of the lane. Next, the truck was moved to the second lane, and analyses run for each of the lateral positions in that lane. When all lanes had been analyzed, the results from each lane loading were then combined so as to produce the maximum bending moment in a particular beam. Finally, the largest of these maximums among interior beams was identified. These moments were then divided by the total static moment produced on the span by the HS-20 truck to obtain the interior live load lateral distribution factors. In cases where the bridge contained a mixture of box widths, separate LLDFs were tracked for the two different box widths. This process was, of course, automated by inserting additional coding in the basic analysis program MBBA to carry out these steps.

Using the above process for obtaining a lateral distribution factor for beam bending moment, a parameter study was undertaken to examine the variation in distribution factors for a range of typical TxDOT bridge designs. As before, seven bridge widths (see Table 4.2), each with three different span lengths (Table 4.1), four different box sizes (20, 28, 34, and 40 in. depths), and all of these with composite deck thicknesses of 4, 6, and 8 in. were included in the study for a total 252 different bridge configurations. In this initial effort, only non-skewed structures were considered. The effects of skew are examined later in this chapter.

AASHTO LLDFs VERSUS EXACT VALUES

Preliminary examination of the parameter study analyses revealed one unexpected result: for a given bridge geometry, the LLDF is essentially independent of all factors except span length. This implies that for say a 34 ft roadway with boxes arranged as 2[5Bxx]+4[4Bxx]+2[5Bxx], the LLDF is essentially the same whether the bridge is built with 20 in. (xx=20) or 28, 34, or even 40 in. deep boxes. Furthermore, the slab thickness has negligible influence on the LLDF. This is somewhat surprising since it dramatically affects the stiffness of the connection between adjacent beams, but nevertheless was found to hold in all cases. A closer examination of the two AASHTO equations makes it less surprising that box size does not affect the factor since both equations are insensitive to changes in the I/J ratio. For example, this ratio is 0.398 for a 4B20 box and 0.583 for the 4B34, yet it effects less than a 3 percent change in the value of LLDF predicted by Eq. (5.4).

This fact suggested that a productive way to organize the many analysis results and to compare them to values predicted by the two AASHTO equations would be by bridge width. This was done, creating the plots of LLDF versus span length shown in Figures 5.1 through 5.7. Each of the plots contains, for the given bridge width, results for four different box sizes (20, 28, 34, and 40 in.) each with three span lengths and three slab thicknesses, giving a total of 36 bridge conditions represented. In each plot, the LLDF obtained from Eq. (5.1) and (5.4) are shown along with values from the MBBA parameter study. In applying the two AASHTO equations, the composite I and J properties from Tables 3.2 through 3.4 were used. In bridges containing a mixture of 4 ft and 5 ft box widths, a weighted average of the properties of the two box types was used. Values obtained via Eq. (5.1) are shown as open circles and labeled as "16th Edition," referring to AASHTO [1996]. Values from Eq. (5.4) are shown as filled circles and labeled as "LRFD," while the values plotted as triangles are from MBBA analysis. No multi-presence factors nor impact factors were applied to the values before plotting. However, for bridge widths of 36 ft or wider which will accommodate three design lanes, the LRFD values from Eq. (5.4) have a built-in multi-presence factor, presumably 0.9.

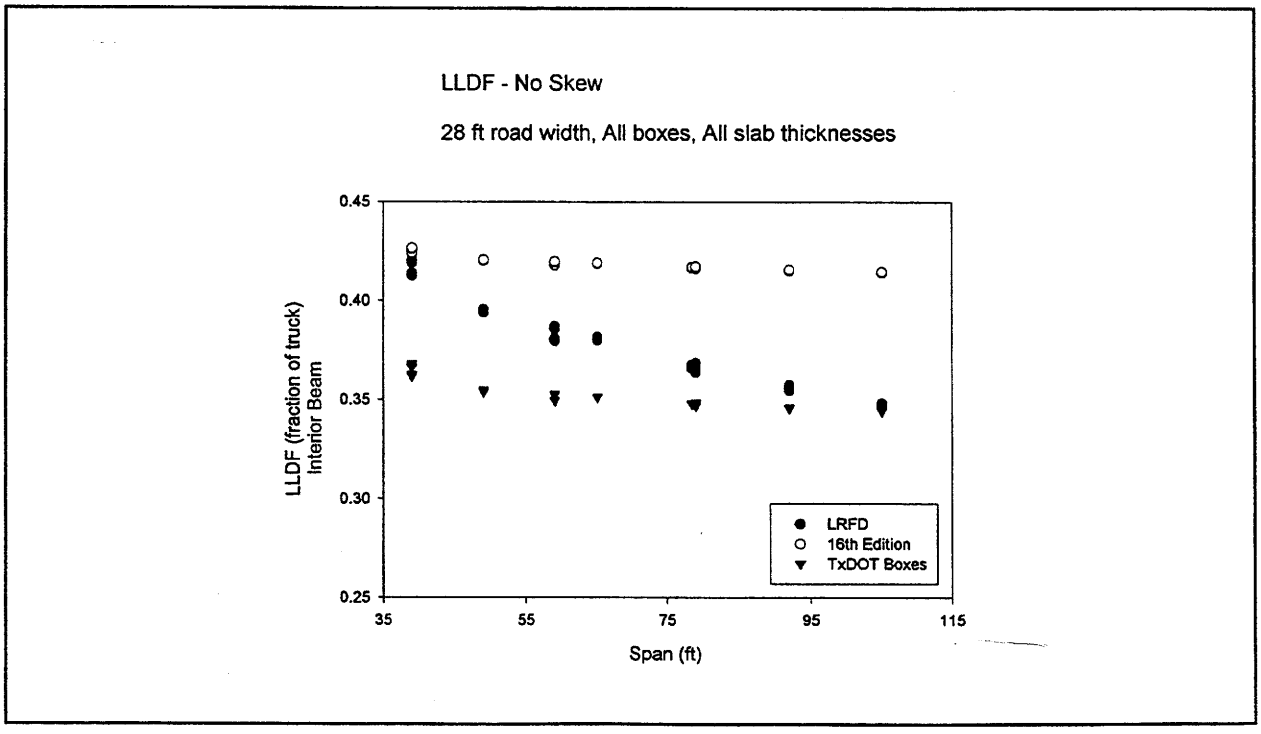

Figure 5.1. Live Load Distribution Factors - 28 ft Roadway.

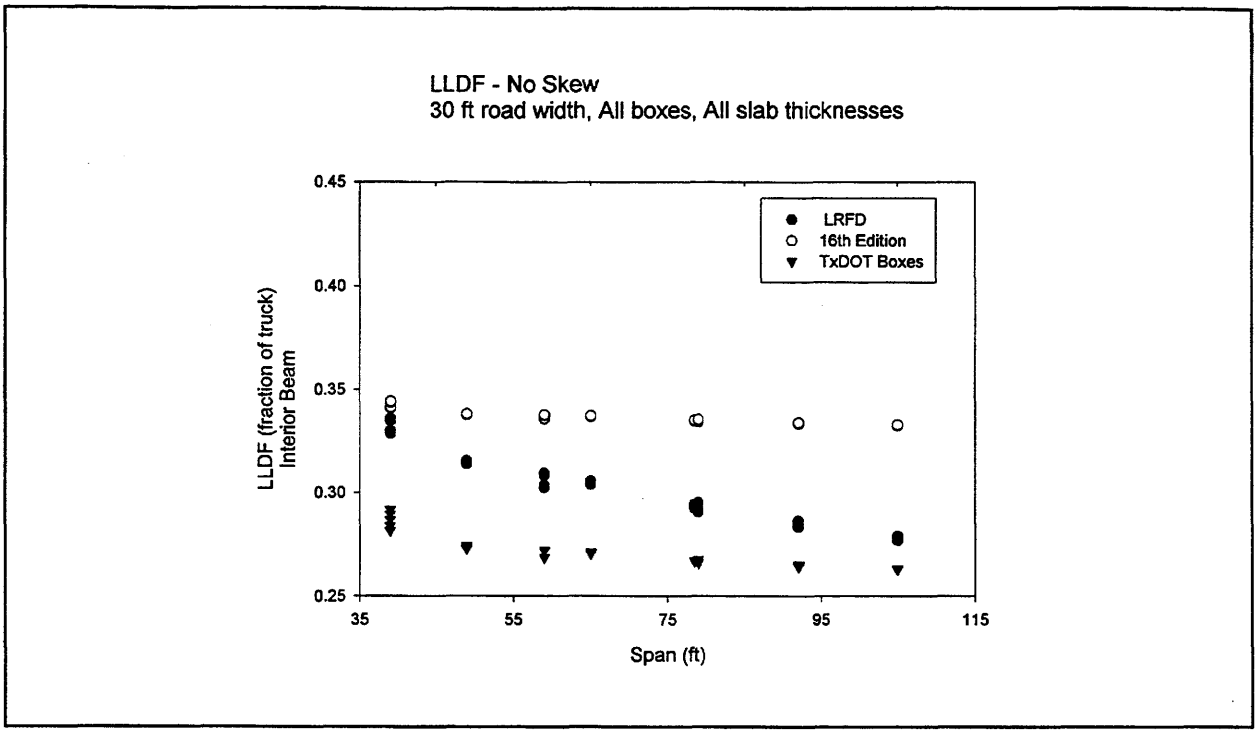

Figure 5.2. Live Load Distribution Factors - 30 ft Roadway.

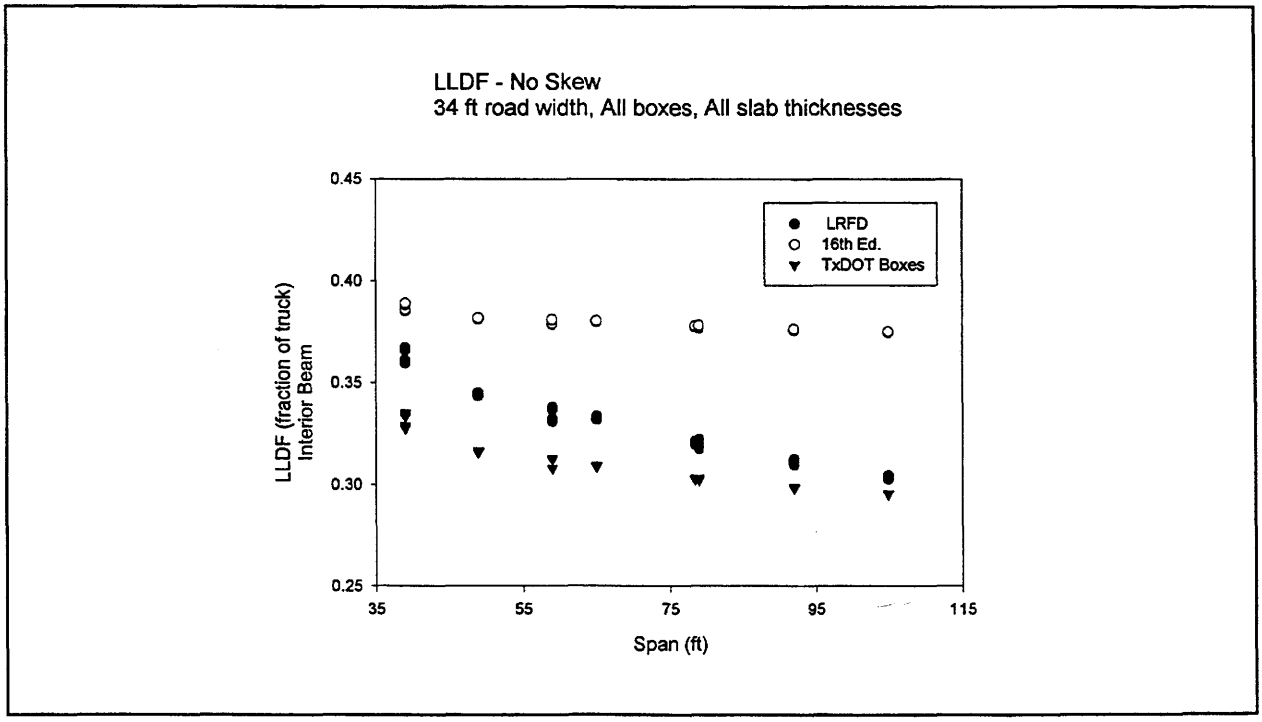

Figure 5.3. Live Load Distribution Factors - 34 ft Roadway.

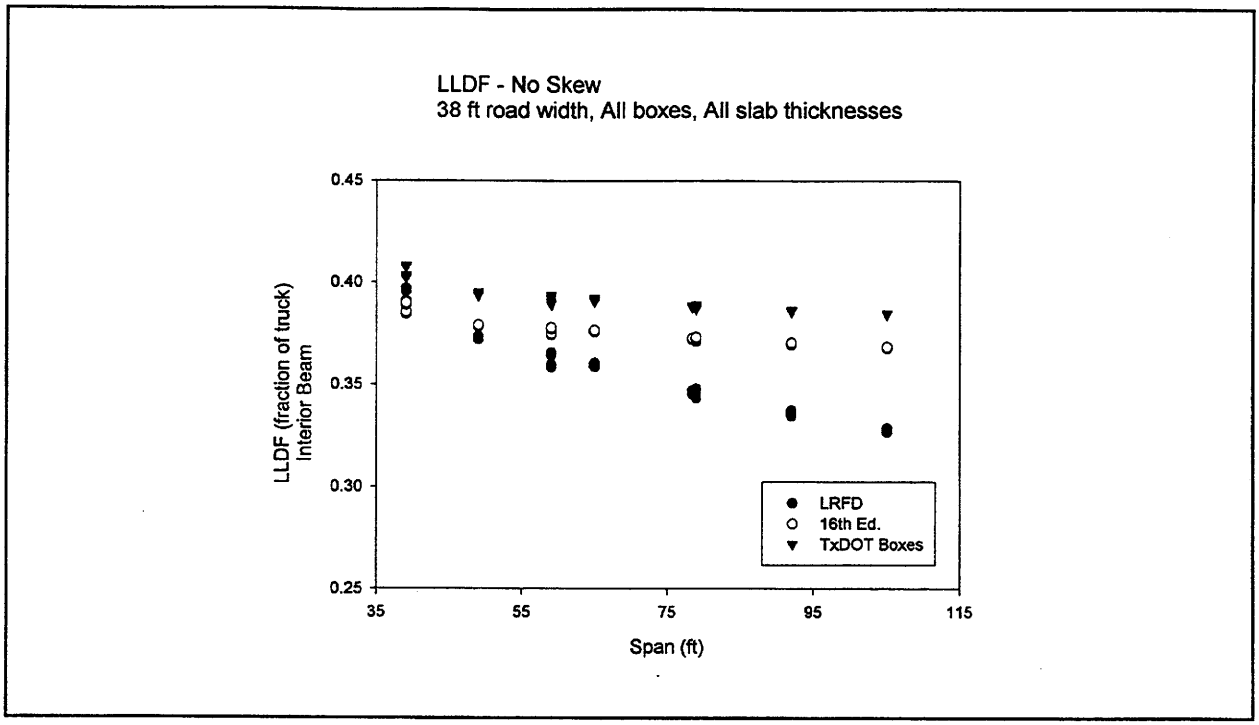

Figure 5.4. Live Load Distribution Factors - 38 ft Roadway.

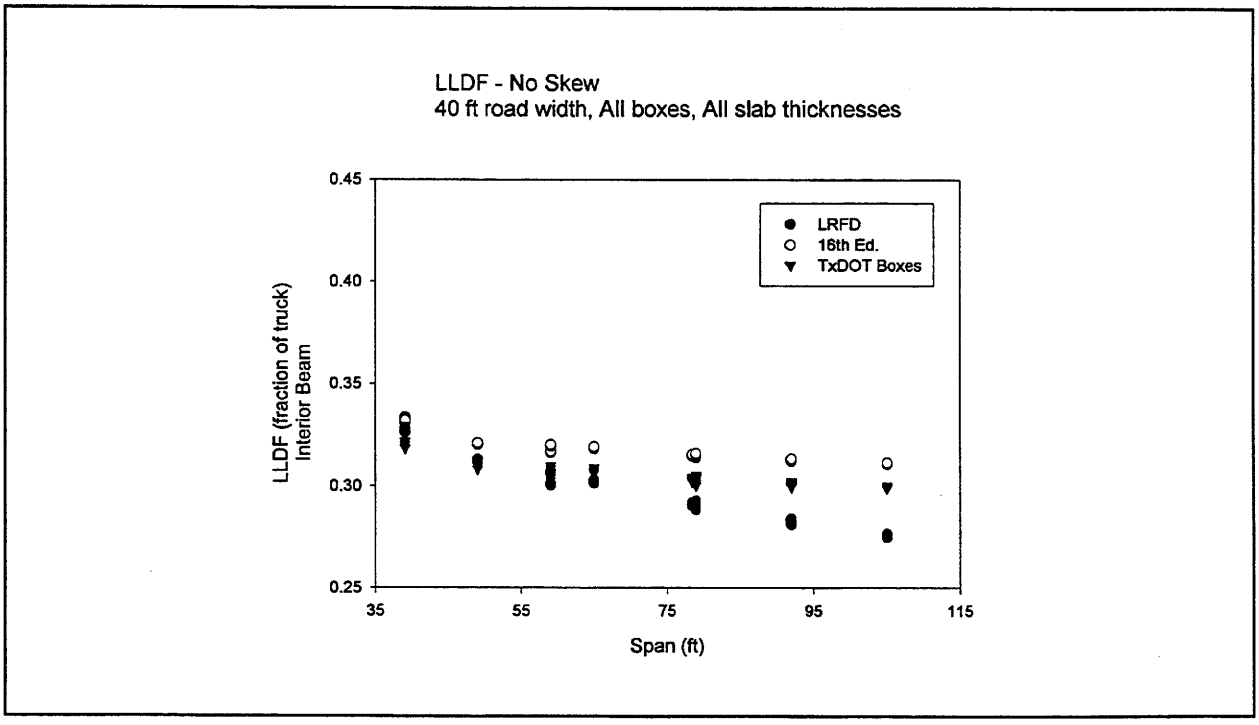

Figure 5.5. Live Load Distribution Factors - 40 ft Roadway.

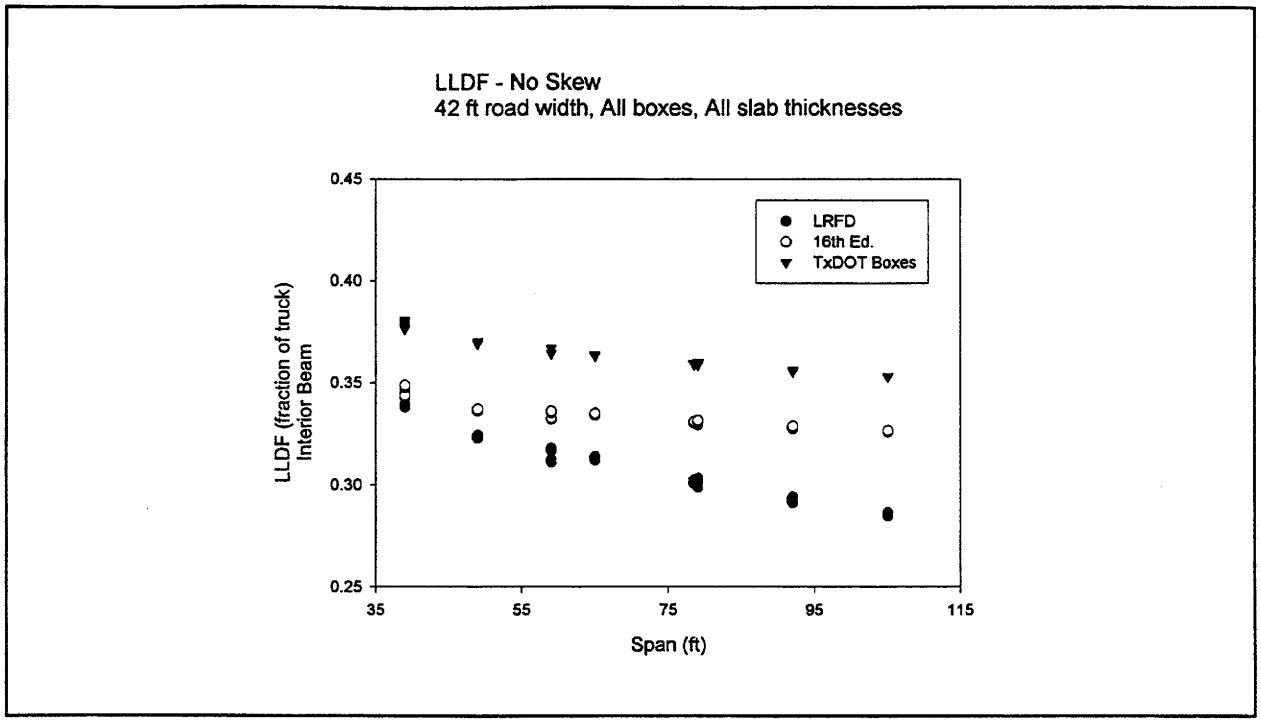

Figure 5.6. Live Load Distribution Factors - 42 ft Roadway.

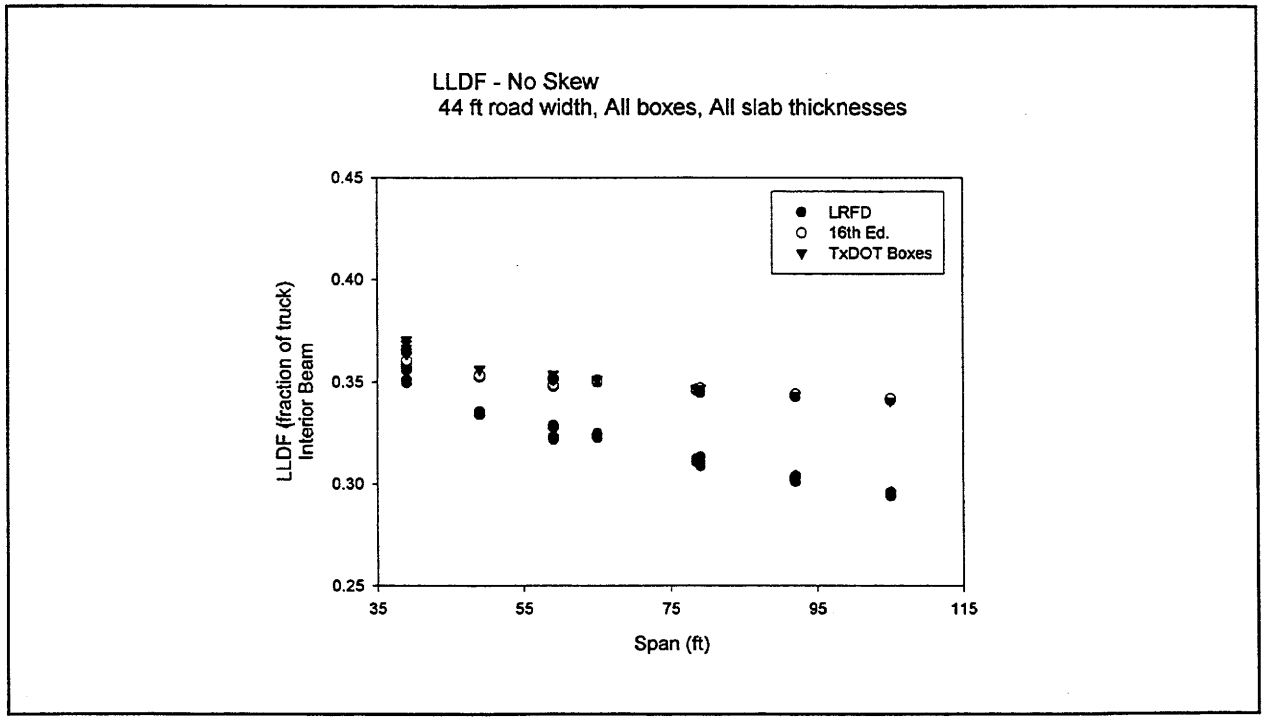

Figure 5.7. Live Load Distribution Factors - 44 ft Roadway.

From the figures, it is apparent that the "exact" values of LLDF for TxDOT bridges tend to be smaller than those predicted by either AASHTO formula for bridges carrying only two traffic lanes. For bridges wide enough to accommodate three lanes, the reverse tends to be true. For these structures, the "LRFD" formula tends to underestimate the load fraction for beams, particularly for longer spans. Generally speaking, the "LRFD" formula tended to display a sensitivity to span length not reflected in the values from exact analysis. For the unskewed bridges considered, the exact LLDF ranged between a minimum of slightly less than 0.3 to a maximum of about 0.4.

Another important consideration not evident in the data plots of Figures 5.1 through 5.7 is the LLDF variation between boxes of 4 ft and 5 ft width when mixed in the same structure. In those plots, it turned out that the controlling LLDF always corresponded to the larger 5 ft box whenever they occurred as an interior beam. This is not unexpected and is consistent with the notion that the stiffer the beam, the more moment it tends to attract. As indicated in Table 4.2, bridges with roadway widths of 34 ft, 40 ft, 42 ft, and 44 ft all have mixtures of box sizes. The 40 ft roadway, however, has only two of the larger boxes, and they are the exterior beams. The difference between the LLDF for the two box sizes exceeded 25 percent in some cases, making it obvious that separate factors needed to be reported for use in mixed box situations. Interestingly, neither of the ASSHTO formulas directly addresses the possible use of mixtures of different beam sizes within the same bridge.

DEVELOPMENT OF TxDOT LLDFs - UNSKEWED BRIDGES

The 252 TxDOT bridge configurations analyzed in the parameter study were organized by bridge width and LLDFs recorded separately for 4 ft and 5 ft boxes in each case. These results were then plotted as Figures 5.8 through 5.14. Each plot addresses a particular roadway width and its inherent arrangement of boxes, which are noted in the plot's legend. Otherwise, a plot is applicable for any of the four standard TxDOT box depths and slab thicknesses from 4 to 8 in. When there are a mixture of box widths in the structure, the LLDF for 4 ft and 5 ft wide boxes are plotted separately.

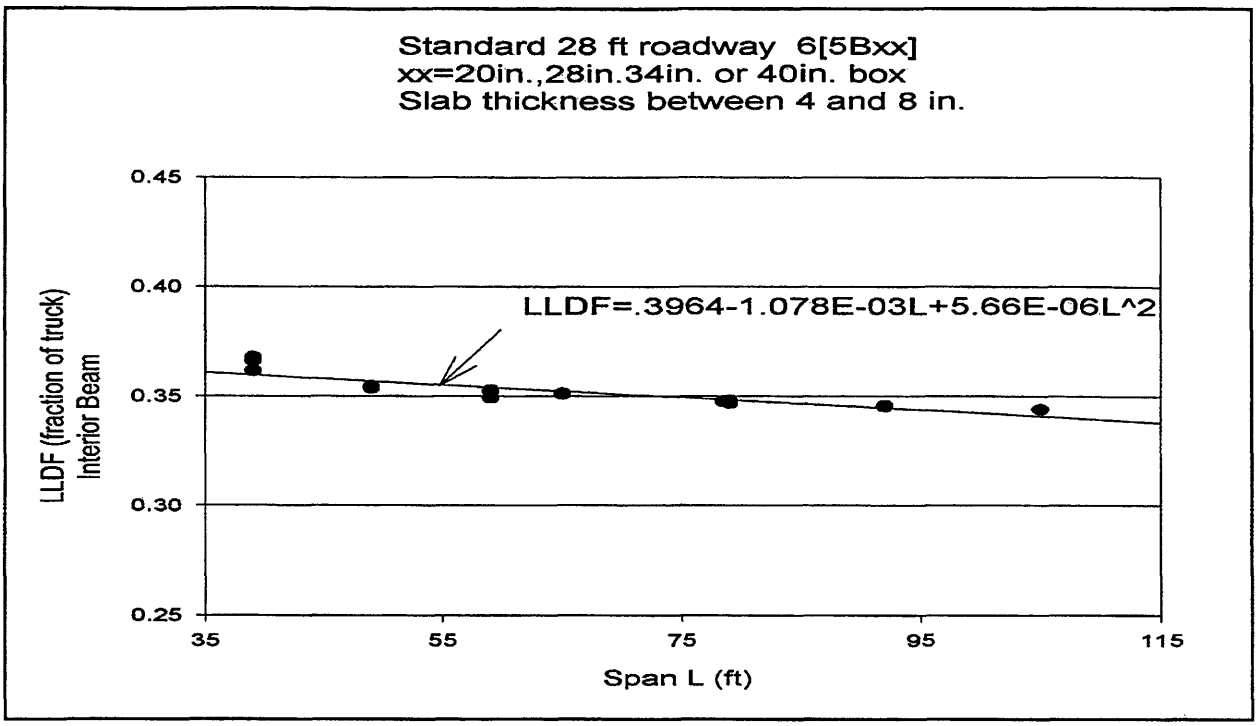

Figure 5.8. Exact Live Load Distribution Factor - 28 ft Roadway.

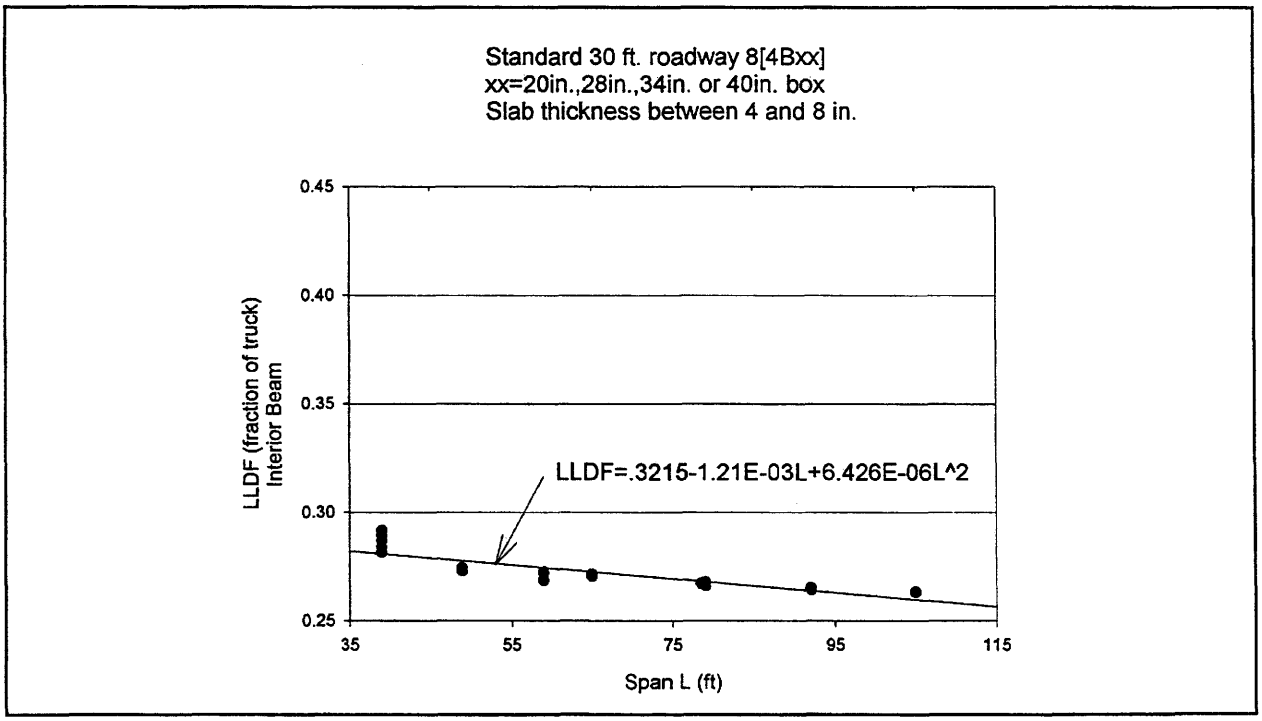

Figure 5.9. Exact Live Load Distribution Factor - 30 ft Roadway.

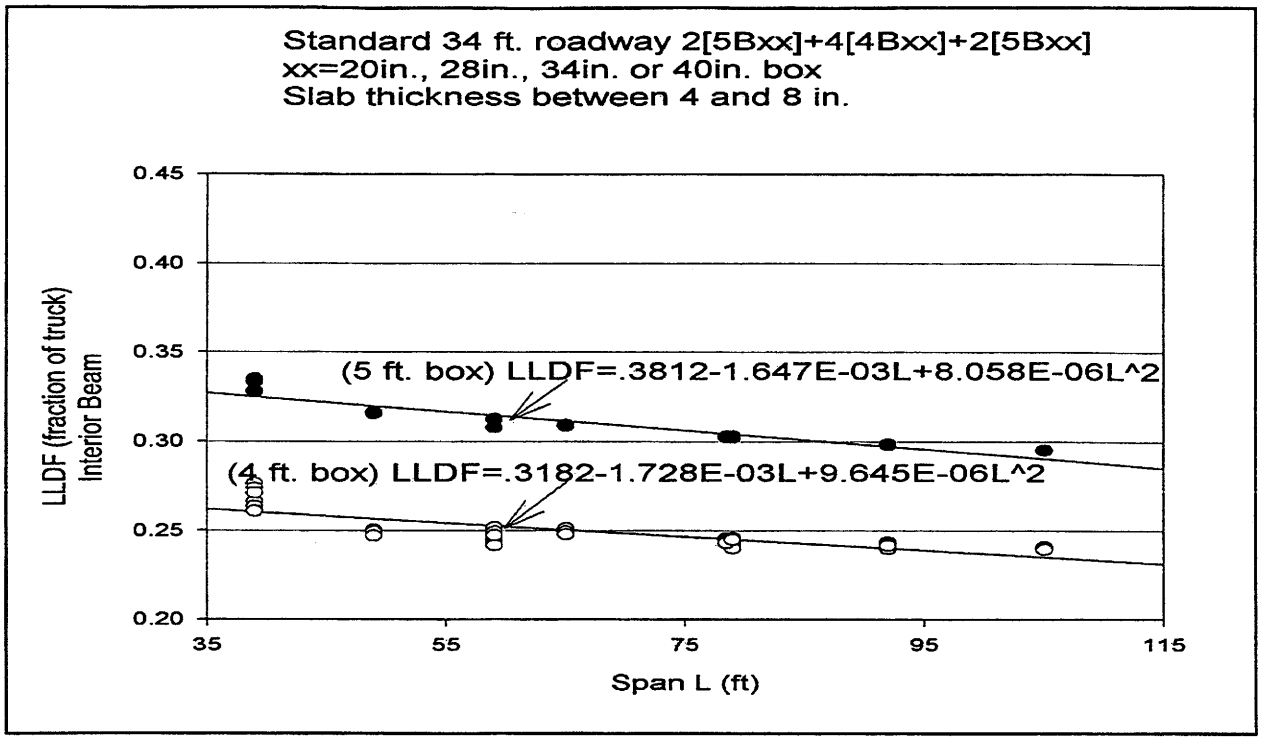

Figure 5.10. Exact Live Load Distribution Factor - 34 ft Roadway.

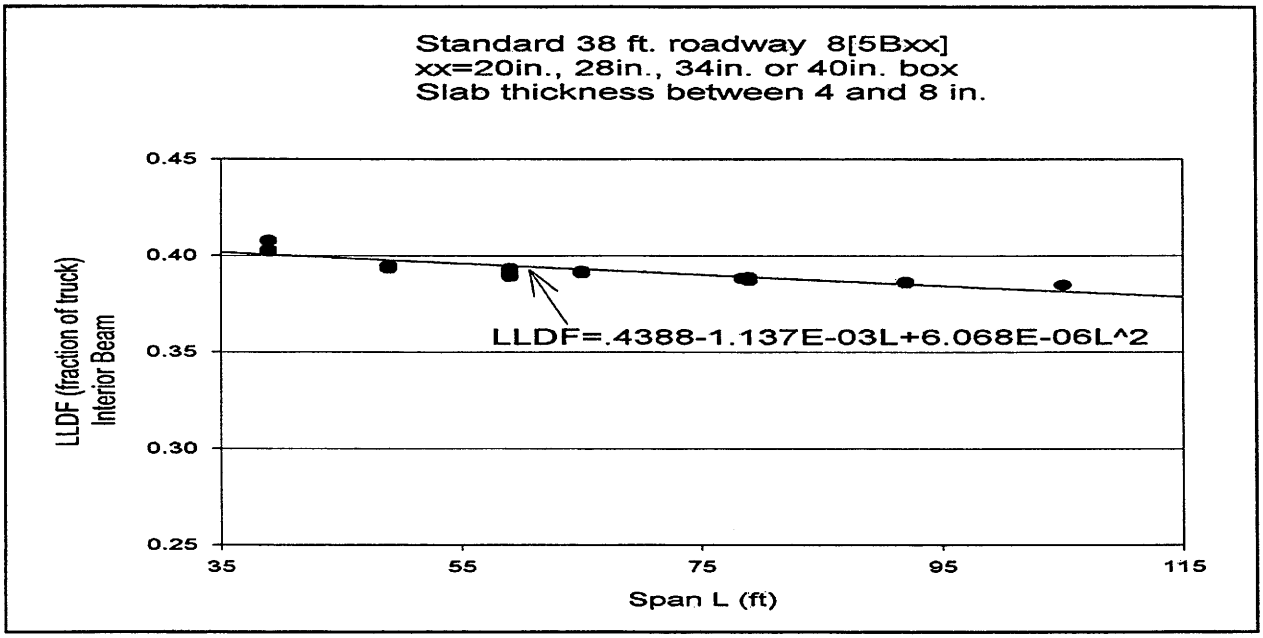

Figure 5.11. Exact Live Load Distribution Factor - 38 ft Roadway.

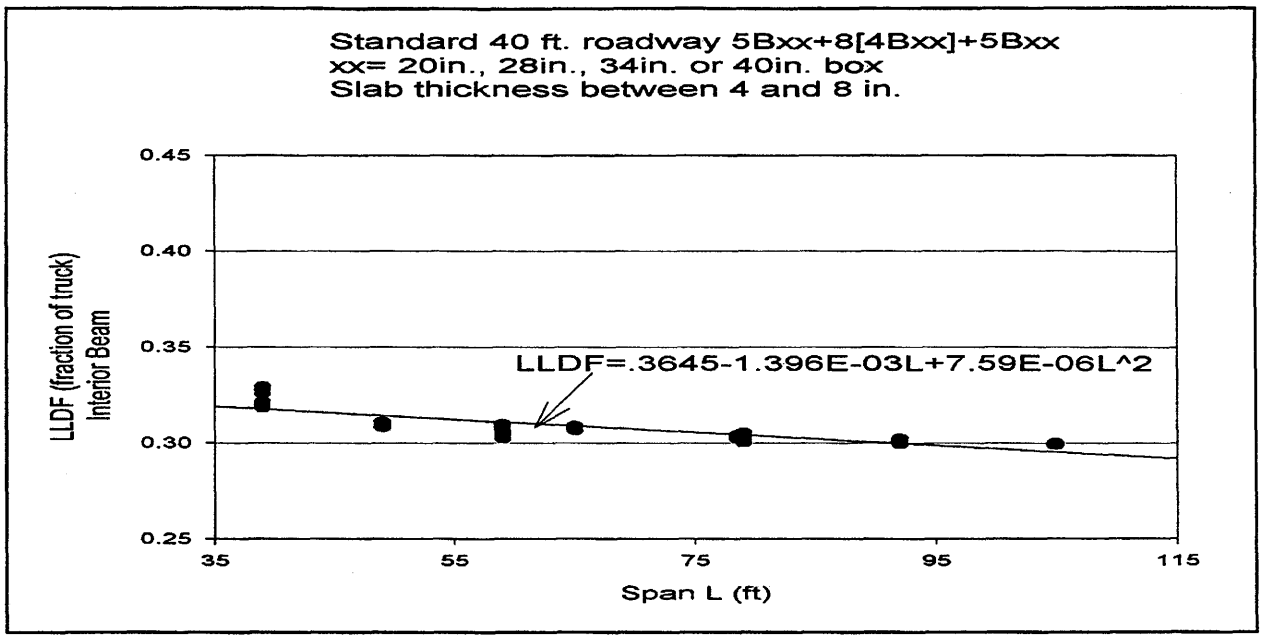

Figure 5.12. Exact Live Load Distribution Factor - 40 ft Roadway.

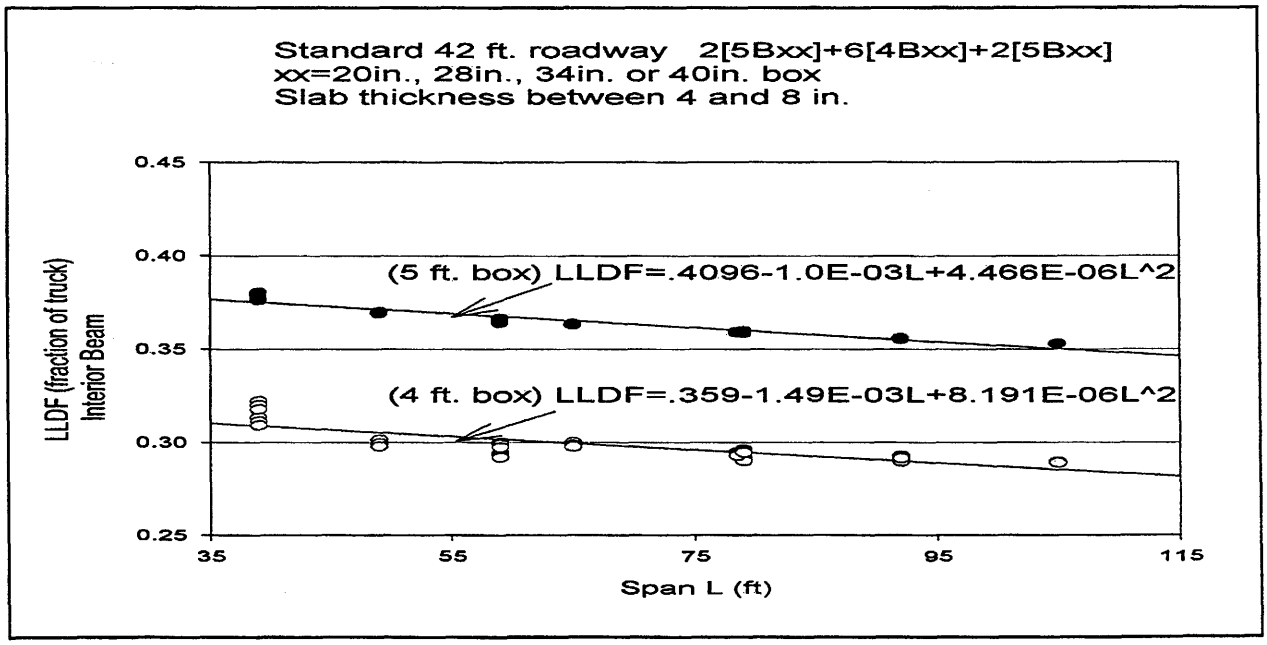

Figure 5.13. Exact Live Load Distribution Factor - 42 ft Roadway.

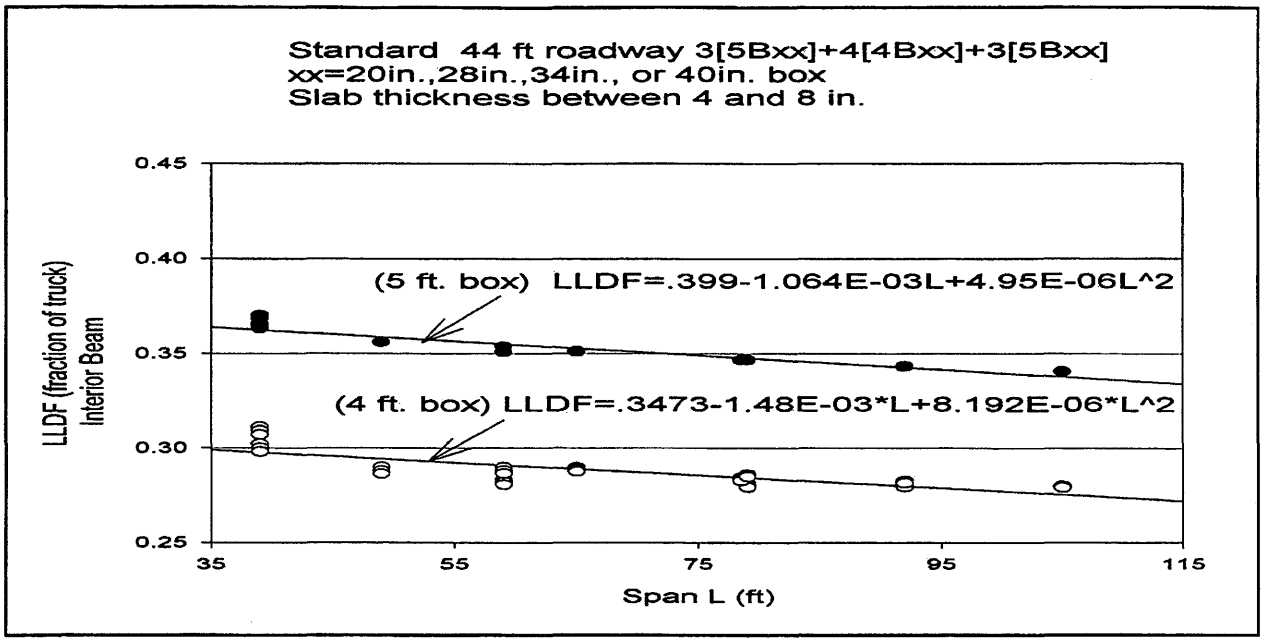

Figure 5.14. Exact Live Load Distribution Factor - 44 ft Roadway.

Also shown on each plot is a second order polynomial equation for the LLDF as a function of span length obtained by regression and which can be used in lieu of graphically extracting values from the plot. Over the 36 different combinations of slab thickness and box types represented in a particular plot, the maximum difference between the exact LLDF value and that computed from the equation was typically under 4 percent. Note that these plots apply to unskewed structures and give the LLDF for interior beams.

TOWARD A GENERAL EQUATION FOR LLDF

The efforts documented in the previous section illustrate that an accurate LLDF formula can be developed for a specific bridge geometry; i.e., for a specified number and arrangement of boxes within the bridge cross section. One obvious shortcoming of results in this form is that they do not address the LLDF in bridges with arrangements of boxes, which differs from those listed in Table 4.2. Therefore, an effort to generate a general formula for predicting interior beam moment LLDF in unskewed bridges with an arbitrary arrangement of boxes was undertaken but with rather disappointing results.

The AASHTO LLDF Eq. (5.4) was first studied to see if it could be adapted by changing the values of the constants and powers of the existing equation. This effort was not successful. The resulting equation produced errors in LLDF values as high as 45 percent. Inspection of those results suggested that part of the inadequacy could be attributed to the mixture of two different box widths in the same structure. As an attempt to remedy this shortcoming, a number of variations on the basic form of Eq. (5.4) were tried, each incorporating additional parameters to reflect the presence of different box widths. The most successful of these was an equation of the form:

$$LLDF=c_1(N/N_b)^{c_2}(b/bAvg)^{c_3}N_b^{c_4}(bAvg/305)^{c_5}(bAvg/12L)^{c_6}(I/J)Avg^{c_7} \qquad \text{Eq. (5.5)}$$

A regression was then run using all 252 bridges in the basic parameter study in the fit, in order to establish the values of the constants. This resulted in

$$LLDF=2.529(N/N_b)^{0.170}(b/bAvg)^{0.926}N_b^{0.453}(bAvg/305)^{1.541}(bAvg/12L)^{0.0983}(I/J)Avg^{0.0684} \qquad \text{Eq. (5.6)}$$

In this equation $bAvg$ and $(I/J)Avg$ are the weighted average beam width and weighted average (I/J) ratio for the non-composite section. For example, according to Table 4.1, a 42 ft roadway configuration utilizes four 5 ft wide and six 4 ft wide boxes. Assuming a 28 in. box and taking values from Table 3.1, one obtains I/J ratios of 0.541 for the 4 ft box and 0.456 for the 5 ft box. Then the values would be

$$(I/J)Avg=\frac{6(0.541)+4(0.456)}{10}=0.507$$

$$bAvg=\frac{6(48)+4(60)}{10}=52.8$$

In the equation, N is the number of boxes in the bridge of the width b whose LLDF is being computed. As an example, in computing the LLDF for the 4 ft box in a 42 ft wide bridge, b would be 48 in. and N would be 6, while in computing the factor for the 5 ft box in the same structure, b=60 in. and N would be 4. The terms N_b and L are the total number of beams in the cross section and the span length, respectively.

The maximum error over the 252 data sets between the exact LLDF and the value predicted by Eq. (5.6) above was 7.9 percent while the average error was 3.2 percent. Eq. (5.6) is somewhat

less accurate than the equations cited in the previous section and given in Figures 5.8 through 5.14, but no doubt would suffice when used on the bridges in Table 4.2. However, this equation still lacks the ability to properly account for mixtures of boxes. This became evident when a variation on the 28 ft roadway structure in Table 4.2 was analyzed. The bridge considered consisted of 3[4B20]+5B20+3[4B20]. For spans of 39, 49, and 59 ft the exact LLDF values were (0.2971, 0.3955), (0.2894, 0.3774), and (0.2879, 0.3717), where the first number in parenthesis is the factor for the 4 ft box and the second is for the 5 ft box. Applying Eq. (5.6) gave values of (0.2398, 0.2645), (0.2345, 0.2586), and (0.2302, 0.2539). These results are indicative of the dangers inherent in extrapolating a purely empirical equation beyond the range of conditions for which it was developed, and made it apparent that a general equation covering any arrangement of boxes is simply not feasible.

RECOMMENDED LLDFs FOR CURRENT AND PROPOSED TxDOT BOX ARRANGEMENTS

Since a general formula is not feasible, it was felt that a compilation of factors should be developed for the more common current TxDOT bridge designs as well as for proposed new configurations currently under development. Toward this end, information was obtained on the 15 proposed new standard designs shown in Table 4.4 for roadway widths ranging from 24 ft through 52 ft. Analyses were then run on these new designs for unskewed structures using the same span ranges as before (see Table 4.1) in combination with the four standard box depths and slab thicknesses from 4 to 8 in.

As expected, the LLDFs for these new geometries were found to be equally insensitive to slab thickness and box depths as the common TxDOT designs of Table 4.1, so that LLDF reduces to a function of span length. Furthermore, a review of the earlier results of Figures 5.8 through 5.14 indicates the dependence on span length is not strong—typically effecting less than a 5 percent variation over the range of span lengths a specific box can sustain. Therefore, in order to arrange the information in as simple a format as possible consistent with the accuracy involved, a single LLDF is given for each of the standard four box depths. For clarity, the range of spans used in the analyses to extract the listed factor is included, although the many analyses performed suggest that the factors listed are still sufficiently accurate for spans somewhat outside the listed range.

The recommended LLDFs for interior beams in unskewed bridges are found in Tables 5.1 (current common designs) and 5.2 (proposed new designs), while factors for exterior beams are listed in Tables 5.3 and 5.4. Where a bridge contains a mixture of box widths, the factor to be used for each box width is listed and represents the largest moment seen by any interior box of that width in the bridge. Furthermore, the values in the table are for the *specific* arrangement of boxes shown in the second column of the tables.

RECOMMENDED LLDFs FOR SKEWED TxDOT BRIDGES

The effect of skew on LLDF was examined by re-analyzing common (Table 5.1) and proposed new (Table 5.2) TxDOT bridge configurations for skews of 15, 30, and 45 degrees. AASHTO [1994] gives the following relationship for computing the LLDF for a skewed structure

$$LLDF_\theta = LLDF_0[1.05 - 0.25\tan(\theta)] \qquad \text{Eq. (5.7)}$$

$LLDF_\theta$ is the distribution factor for the bridge with skew angle θ, and $LLDF_0$ is the factor computed for the same structure with no skew. This equation implies that only the angle θ affects the distribution. To test this idea, a series of analyses were carried out on one of the common TxDOT bridge configurations. Using a 28 ft roadway structure, analyses were performed on four box sizes, three different span lengths for each box size, each with three slab thicknesses. Each one of these 36 different bridges was then analyzed for skew angles of 0, 15, 30, and 45 degrees. For each bridge, the LLDF at 15, 30, and 45 degrees was then divided by the LLDF at 0 degrees for that structure. These normalized factors were then plotted in Figure 5.15. Also shown are the AASHTO equation values at each of the three angles. If the data was correctly described by the AASHTO equation, there would only be one plotting point visible at each angle, and it would coincide with the square symbol. Clearly, this is not the case. Although the AASHTO equation is conservative (predicts a larger LLDF than is actually present), it would appear to be overly so for larger angles of skew. At 45 degrees, for example, the equation predicts a factor of 0.80 while the actual factor may be as low as 0.57 according to Figure 5.15. This is a 40 percent relative error. For a particular value of skew, the scatter of values in the plot are an indication that the correct relationship involves factors other than just skew angle. As a baseline for later comparison, a regression was run on the

Table 5.1. Interior Live Load Lateral Distribution Factors for Current TxDOT Designs.

Roadway Width (ft)	Box Arrangement	Box Depth (in.)	Span Range (ft)	Recommended LLDF[1]	
				4 ft Box	5 ft Box
28	6[5Bxx]	20	39-59		0.35
		28	39-79		0.35
		34	65-92		0.35
		40	79-105		0.35
30	8[4Bxx]	20	39-59	0.27	
		28	39-79	0.27	
		34	65-92	0.27	
		40	79-105	0.26	
34	2[5Bxx] + 4[4Bxx] + 2[5Bxx]	20	39-59	0.25	0.32
		28	39-79	0.25	0.31
		34	65-92	0.25	0.30
		40	79-105	0.24	0.30
38	8[5Bxx]	20	39-59		0.40
		28	39-79		0.39
		34	65-92		0.39
		40	79-105		0.39
40	5Bxx + 8[4Bxx] + 5Bxx	20	39-59	0.31	
		28	39-79	0.31	
		34	65-92	0.30	
		40	79-105	0.30	
42	2[5Bxx] + 6[4Bxx] + 2[5Bxx]	20	39-59	0.30	0.37
		28	39-79	0.30	0.37
		34	65-92	0.29	0.36
		40	79-105	0.29	0.36
44	3[5Bxx] + 4[4Bxx] + 3[5Bxx]	20	39-59	0.29	0.36
		28	39-79	0.29	0.35
		34	65-92	0.28	0.35
		40	79-105	0.28	0.34

[1]LLDF = Live load lateral distribution factor-fraction of truck.
For interior beams of unskewed structures. No multi-presence or impact factors included.
NOTE: Arrangement of mixed sizes of boxes is significant. Factors shown apply only to box arrangement listed.

Table 5.2. Interior Live Load Lateral Distribution Factors for Proposed TxDOT Designs.

Roadway Width (ft)	Box Arrangement	Box Depth (in.)	Span Range (ft)	Recommended LLDF[1]	
				4 ft Box	5 ft Box
24	5Bxx + 4[4Bxx] + 5Bxx	20	39-59	0.33	
		28	39-79	0.33	
		34	65-92	0.32	
		40	79-105	0.32	
26	4Bxx + 4[5Bxx] + 4Bxx	20	39-59		0.37
		28	39-79		0.37
		34	65-92		0.36
		40	79-105		0.36
28	6[5Bxx]	20	39-59		0.36
		28	39-79		0.35
		34	65-92		0.35
		40	79-105		0.35
30	2[5Bxx] + 3[4Bxx] + 2[5Bxx]	20	39-59	0.31	0.35
		28	39-79	0.31	0.35
		34	65-92	0.31	0.34
		40	79-105	0.30	0.34
32	4[4Bxx] + 5Bxx + 3[4Bxx]	20	39-59	0.29	0.35
		28	39-79	0.30	0.36
		34	65-92	0.28	0.33
		40	79-105	0.27	0.32
34	2[4Bxx] + 3[5Bxx] + 3[4Bxx]	20	39-59	0.30	0.34
		28	39-79	0.31	0.34
		34	65-92	0.30	0.34
		40	79-105	0.29	0.33
36	2[5Bxx] + 3[4Bxx] + 3[5Bxx]	20	39-59	0.34	0.43
		28	39-79	0.34	0.44
		34	65-92	0.34	0.42
		40	79-105	0.34	0.42
38	8[5Bxx]	20	39-59		0.40
		28	39-79		0.39
		34	65-92		0.39
		40	79-105		0.39

Table 5.2. Interior Live Load Lateral Distribution Factors for Proposed TxDOT Designs (cont.).

Roadway Width (ft)	Box Arrangement	Box Depth (in.)	Span Range (ft)	Recommended LLDF[1]	
				4 ft Box	5 ft Box
40	2[4Bxx[+ 5[5Bxx] + 2[4Bxx]	20	39-59	0.33	0.40
		28	39-79	0.33	0.40
		34	65-92	0.32	0.39
		40	79-105	0.32	0.38
42	4Bxx + 7[5Bxx] + 4Bxx	20	39-59		0.40
		28	39-79		0.40
		34	65-92		0.40
		40	79-105		0.39
44	9[5Bxx]	20	39-59		0.37
		28	39-79		0.37
		34	65-92		0.36
		40	79-105		0.36
46	3[5Bxx] + 3[4Bxx] + 4[5Bxx]	20	39-59	0.36	0.46
		28	39-79	0.36	0.45
		34	65-92	0.35	0.45
		40	79-105	0.35	0.45
48	4[5Bxx] + 4Bxx + 5[5Bxx]	20	39-59	0.35	0.44
		28	39-79	0.35	0.43
		34	65-92	0.34	0.42
		40	79-105	0.34	0.42
50	2[4Bxx] + 7[5Bxx] + 2[4Bxx]	20	39-59	0.33	0.42
		28	39-79	0.33	0.42
		34	65-92	0.32	0.41
		40	79-105	0.32	0.41
52	4Bxx + 9[5Bxx] + 4Bxx	20	39-59		0.41
		28	39-79		0.41
		34	65-92		0.40
		40	79-105		0.40

[1]LLDF = Live load lateral distribution factor-fraction of truck.
For interior beams of unskewed structures. No multi-presence or impact factors included.
NOTE: Arrangement of mixed sizes of boxes is significant. Factors shown apply only to box arrangement listed.

Table 5.3. Exterior Live Load Lateral Distribution Factors for Current TxDOT Designs.

Roadway Width (ft.)	Box Arrangement	Box Depth (in.)	Span Range (ft.)	Recommended LLDF[1]	
				4 ft. Box	5 ft. Box
28	6[5Bxx]	20	39-59		0.36
		28	39-79		0.36
		34	65-92		0.36
		40	79-105		0.36
30	8[4Bxx]	20	39-59	0.28	
		28	39-79	0.28	
		34	65-92	0.28	
		40	79-105	0.28	
34	2[5Bxx] + 4[4Bxx] +2[5Bxx]	20	39-59		0.33
		28	39-79		0.33
		34	65-92		0.33
		40	79-105		0.33
38	8[5Bxx]	20	39-59		0.39
		28	39-79		0.39
		34	65-92		0.39
		40	79-105		0.39
40	5Bxx + 8[4Bxx] + 5Bxx	20	39-59		0.38
		28	39-79		0.38
		34	65-92		0.38
		40	79-105		0.38
42	2[5Bxx] + 6[4Bxx] + 2[5Bxx]	20	39-59		0.37
		28	39-79		0.37
		34	65-92		0.35
		40	79-105		0.35
44	3[5Bxx] + 4[4Bxx] + 3[5Bxx]	20	39-59		0.36
		28	39-79		0.36
		34	65-92		0.35
		40	79-105		0.35

[1]LLDF = Live load lateral distribution factor-fraction of truck.
For Exterior beams of unskewed structures. No multi-presence or impact factors included.
NOTE: Arrangement of mixed sizes of boxes is significant. Factors shown apply only to box arrangement listed.

Table 5.4. Exterior Live Load Lateral Distribution Factors for Proposed TxDOT Designs.

Roadway Width (ft.)	Box Arrangement	Box Depth (in.)	Span Range (ft.)	Recommended LLDF[1]	
				4 ft. Box	5 ft. Box
24	5Bxx + 4[4Bxx] + 5Bxx	20	39-59		0.39
		28	39-79		0.39
		34	65-92		0.38
		40	79-105		0.38
26	4Bxx + 4[5Bxx] + 4Bxx	20	39-59	0.28	
		28	39-79	0.28	
		34	65-92	0.28	
		40	79-105	0.28	
28	6[5Bxx]	20	39-59		0.36
		28	39-79		0.36
		34	65-92		0.35
		40	79-105		0.35
30	2[5Bxx] + 3[4Bxx] + 2[5Bxx]	20	39-59		0.35
		28	39-79		0.35
		34	65-92		0.34
		40	79-105		0.34
32	4[4Bxx] + 5Bxx + 3[4Bxx]	20	39-59	0.29	
		28	39-79	0.28	
		34	65-92	0.26	
		40	79-105	0.26	
34	2[4Bxx] + 3[5Bxx] + 3[4Bxx]	20	39-59	0.30	
		28	39-79	0.30	
		34	65-92	0.29	
		40	79-105	0.29	
36	2[5Bxx] + 3[4Bxx] + 3[5Bxx]	20	39-59		0.41
		28	39-79		0.40
		34	65-92		0.40
		40	79-105		0.40
38	8[5Bxx]	20	39-59		0.34
		28	39-79		0.34
		34	65-92		0.34
		40	79-105		0.34

Table 5.4. Exterior Live Load Lateral Distribution Factors for Proposed TxDOT Designs (cont.).

Roadway Width (ft.)	Box Arrangement	Box Depth (in.)	Span Range (ft.)	Recommended LLDF[1]	
				4 ft. Box	5 ft. Box
40	2[4Bxx[+ 5[5Bxx] + 2[4Bxx]	20	39-59	0.30	
		28	39-79	0.30	
		34	65-92	0.30	
		40	79-105	0.30	
42	4Bxx + 7[5Bxx] + 4Bxx	20	39-59	0.30	
		28	39-79	0.30	
		34	65-92	0.30	
		40	79-105	0.30	
44	9[5Bxx]	20	39-59		0.35
		28	39-79		0.35
		34	65-92		0.35
		40	79-105		0.35
46	3[5Bxx] + 3[4Bxx] + 4[5Bxx]	20	39-59		0.37
		28	39-79		0.37
		34	65-92		0.37
		40	79-105		0.37
48	4[5Bxx] + 4Bxx + 5[5Bxx]	20	39-59		0.41
		28	39-79		0.41
		34	65-92		0.40
		40	79-105		0.40
50	2[4Bxx] + 7[5Bxx] + 2[4Bxx]	20	39-59	0.32	
		28	39-79	0.32	
		34	65-92	0.32	
		40	79-105	0.32	
52	4Bxx + 9[5Bxx] + 4Bxx	20	39-59	0.31	
		28	39-79	0.31	
		34	65-92	0.31	
		40	79-105	0.31	

[1]LLDF = Live load lateral distribution factor-fraction of truck.
For exterior beams of unskewed structures. No multi-presence or impact factors included.
NOTE: Arrangement of mixed sizes of boxes is significant. Factors shown apply only to box arrangement listed.

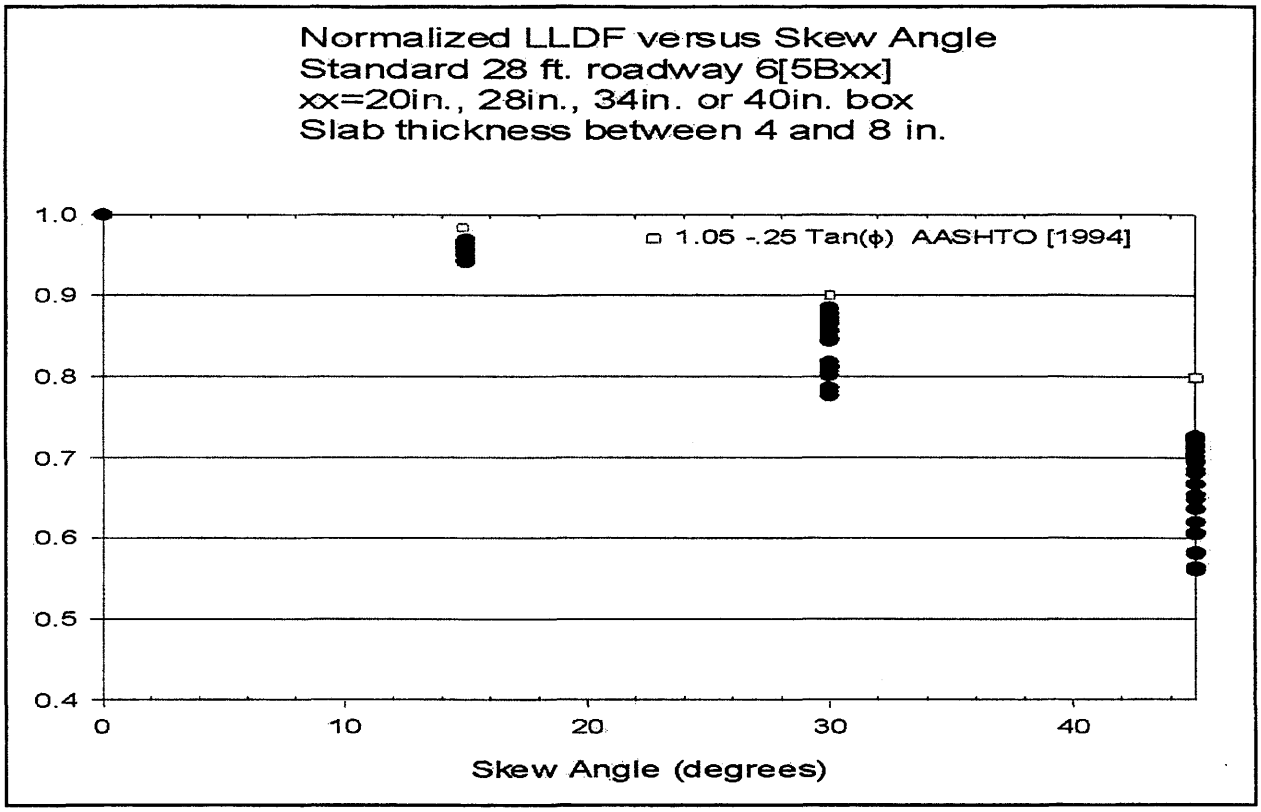

Figure 5.15. Normalized Live Load Distribution Factor.

data of Figure 5.15 against the AASHTO Eq. (5.7) to re-compute the constants. This yielded the equation

$$LLDF_{\theta}=LLDF_{0}[1.07-0.40\tan(\theta)] \qquad \text{Eq. (5.8)}$$

which for this data set reduces the maximum percent error from 40 percent down to 20 percent. However, this level of error is still unacceptable.

In an attempt to discern what factors besides skew angle might influence the LLDF, the data of Figure 5.15 was re-plotted as Figure 5.16. This plot explicitly accounts for the variation in span length, and thus scatter in the data comes from other sources. When the skew angle is zero, LLDF is essentially a function of span length, regardless of the box depth or slab thickness used, a fact that led to Figures 5.8 through 5.14. As the skew increases, the effects of different box sizes and slab thicknesses come into play, leading to the scattering of points for a particular value of span length. This effect is clearly more pronounced for shorter spans.

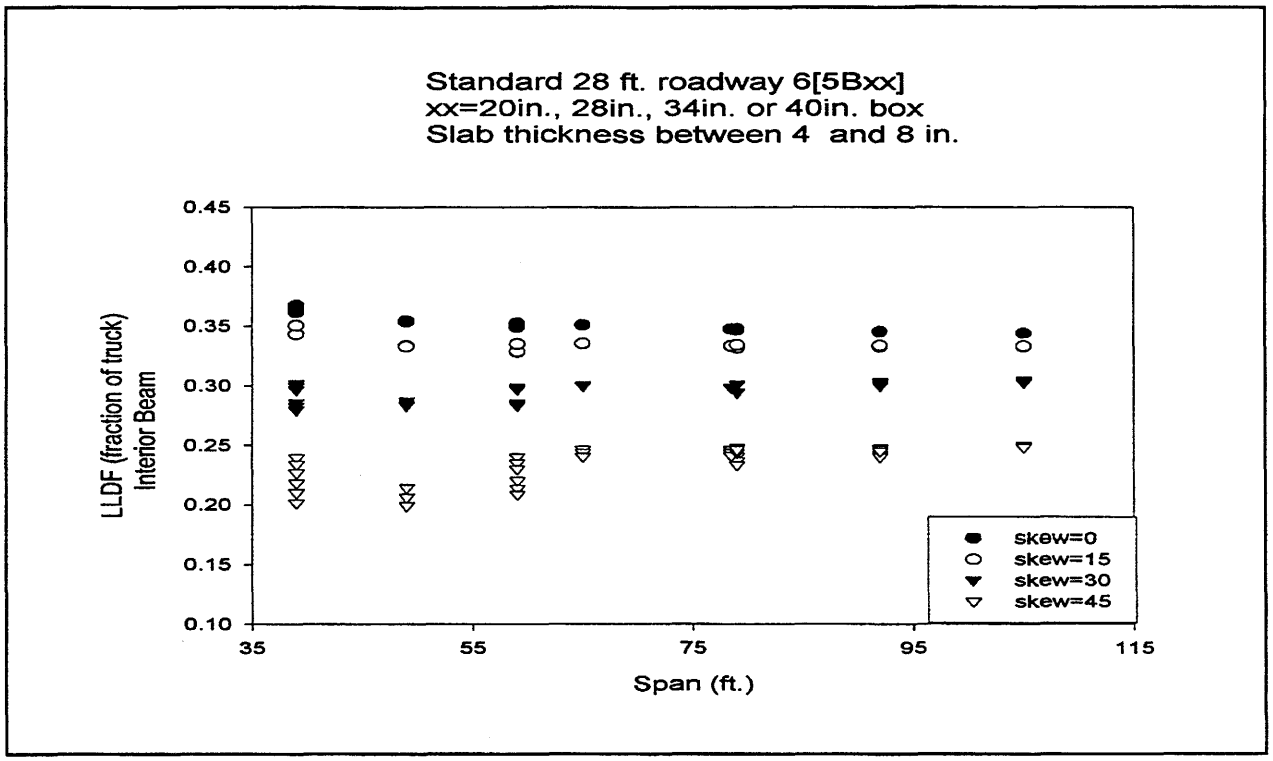

Figure 5.16. Effects of Skew on Live Load Distribution Factor.

Experimentation was conducted on several variations of Eq. (5.8) which added terms to account for factors other than skew angle. The most accurate was found to be

$$LLDF_{\theta}=LLDF_{0}(c_1+c_2L^{c_3}(I/J)^{c_4}\tan(\theta)) \qquad \text{Eq. (5.9)}$$

which is similar in form to the AASHTO equation, except the second term is a function of span length and I/J ratio as well as skew angle. Regressions were run on Eq. (5.9) to determine the best-fit values of constants c_1,c_2,c_3,c_4. Initially, the equation was fit to one standard roadway width configuration at a time. However, it was discovered that performing a regression using data from all seven common roadway widths and selected data sets form the proposed new standard designs simultaneously lead to an equation with accuracy comparable to that obtained for any one of the roadways alone. The final equation resulting from this effort and which is recommended for use in accounting for the effects of skew on the LLDF is:

$$LLDF_{\theta}=LLDF_{0}(1.06-1.13L^{(-0.284)}(I/J)^{(-0.184)}\tan(\theta)) \qquad \text{Eq. (5.10)}$$

In Eq. (5.10), $LLDF_0$ is the LLDF for the beam in question (either interior or exterior) with skew angle of zero, and the I/J ratio is for the composite beam section (see Tables 3.2 through 3.4). When the bridge cross section contains a mixture of boxes, the I/J ratio should be the weighted average as demonstrated with Eq. (5.6). This equation has an average prediction error of approximately 2 percent across all data sets. The maximum error was 14.5 percent, which consistently occurred in configurations with a mixture of box widths, shortest spans (39 ft), and 8 in. thick decks. Among all the other cases, the maximum error in prediction was generally under 5 percent, with a few cases reaching 8 percent.

REFERENCES

AASHTO LRFD Bridge Design Specifications (with Customary US Units), American Association of State Highway and Transportation Officials, 1st edition, 1994.

AASHTO LRFD Standard Specifications for Highway Bridges, American Association of State Highway and Transportation Officials, 16th edition, 1996.

Annamalai, G., and Brown, R., "Shear Strength of Post-Tensioned Grouted Keyed Connections," *PCI Journal,* May-June 1990.

Arockiasamy, M., and Reddy, D., "Static and Fatigue Behavior of Longitudinal Joints in Multi-Box Beam Prestressed Concrete Bridges," Department of Ocean Engineering, Florida Atlantic University, Boca Raton, Florida, March 1992.

Arya, A., Khachaturian, N., and Siess, C., "Lateral Distribution of Concentrated Loads on Multibeam Bridges," Structural Research Series 213, Department of Civil Engineering, University of Illinois, Urbana, Illinois, May 1961.

Cusens, A., and Pama, R., "Design of Concrete Multibeam Bridge Decks," *Journal of the Structural Division,* American Society of Civil Engineers, October 1965.

Duberg, J. E., Khachaturian, N., and Fradinger, R. E., "Method for Analysis of Multibeam Bridges," *Journal of the Structural Division*, American Society of Civil Engineers, July 1960.

Dunker, K., and Rabbat, B., "Performance of Prestressed Concrete Highway Bridges in the United States—The First 40 Years," *PCI Journal,* Prestressed Concrete Institute, May-June 1992.

El-Remaily, A., Tadros, M., Yamane, T., and Krause, G., "Transverse Design of Adjacent Precast Prestressed Concrete Box Girder Bridges," *PCI Journal,* Prestressed Concrete Institute, July-August 1996.

Gulyas, R., Wirthlin, G., and Champa, J., "Evaluation of Keyway Grout Test Methods for Precast Concrete Bridges," *PCI Journal,* January-February 1995.

Hlavacs, G., Long, T., Miller, R., and Baseheart, T., "Nondestructive Determination of Response of Shear Keys to Environmental and Structural Cyclic Loading," Transportation Research Record No. 1574, Materials and Construction, Transportation Research Board, Washington, D.C., 1997.

Huckelbridge, A., El-Esnawi, H., and Moses, F., "An Investigation of Load Transfer in Multi-Beam Prestressed Box Girder Bridges," Report No. FHWA/OH-94/002, Department of Civil Engineering, Case and Western Reserve University, Cleveland, Ohio, September 1993.

Huckelbridge, A., El-Esnawi, H., and Moses, F., "Shear Key Performance in Multibeam Box Girder Bridges," *Journal of Constructed Facilities,* American Society of Civil Engineers, November 1995.

Jones, H. L., James, M. E., and Cline, T. W., "Automated Design of Prestressed Concrete Box Girders," Report 194-1F, State Department of Highways and Public Transportation, 1975.

Jones, H. L., and Boaz, I. B., "Skewed Discretely Connected Multi-Beam Bridges," *Journal of Structural Engineering,* American Society of Civil Engineers, February 1986.

Kaneko, Y., Connor, J., Triantafillou, T., and Leung, C., "Fracture Mechanics Approach for Failure of Concrete Shear Key. I: Theory," *Journal of Engineering Mechanics,* American Society of Civil Engineers, April 1993.

Kaneko, Y., Connor, J., Triantafillou, T., and Leung, C., "Fracture Mechanics Approach for Failure of Concrete Shear Key. II: Verification," *Journal of Engineering Mechanics,* American Society of Civil Engineers, April 1993.

Koseki, K., and Breen, J., "Exploratory Study of Shear Strength of Joints for Precast Segmental Bridges," Research Report No. 248-1, Center for Transportation Research, University of Texas, Austin, Texas, 1983.

Krauss, P., and Rogalla, E., "Transverse Cracking in Newly Constructed Bridge Decks," NCHRP Report 380, Transportation Research Board, Washington D.C., 1996.

PCI Bridge Technical Committee, "Reflective Cracking in Adjacent Box Beam Bridge Superstructures - 2nd Draft," Subcommittee on Adjacent Box Beam Bridges, Prestressed Concrete Institute, October 1995.

Pool, R., "An Investigation of Joint Forces in Multibeam Bridges," Ph.D. Dissertation, Department of Civil Engineering, University of Illinois, Urbana, Illinois, 1963.

Powell, G. H., Ghose, A., and Buckle, I. G., "Analysis of Multibeam Bridges," *Journal of the Structural Division,* American Society of Civil Engineers, September 1969.

Yamane, T., Tadros, M., and Arumugasaamy, P., "Short to Medium Span Precast Prestressed Concrete Bridges in Japan," *PCI Journal,* Prestressed Concrete Institute, March-April 1994.

Ybanez, L., *Bridge Design Guide,* Texas Department of Highways and Public Transportation, 1st edition, 1990.

Walther, R., "Investigation of Multibeam Bridges," *Journal of the American Concrete Institute,* December 1957.

Zokaie, T., Mish, K., and Imbsen, R., "Distribution of Wheel Loads on Highway Bridges," Phase III, NCHRP Study 12-26/2, Transportation Research Board, Washington, D.C., December 1993.

APPENDIX A

RECOMMENDED SLAB TRANSVERSE DESIGN MOMENTS FOR COMMON TXDOT BRIDGE CONFIGURATIONS

Table A.1P. Maximum Positive Slab Moment in (in.-kips/ft) for 28 ft Roadway on 6[5Bxx].

Box Depth	Slab Thickness	Bridge Span (ft)																
		30	35	40	45	50	55	60	65	70	75	80	85	90	95	100	105	110
(in.)	(in.)																	
	4	7.5	8.0	8.5	9.0	9.4	9.8											
20	6	12.4	13.3	14.2	14.9	15.7	16.4											
	8	17.8	19.1	20.3	21.4	22.5	23.5											
	4		6.3	6.7	7.1	7.4	7.8	8.1	8.4	8.7	9.0	9.2	9.5					
28	6		10.5	11.2	11.8	12.4	12.9	13.5	14.0	14.4	14.9	15.3	15.8					
	8		15.1	16.1	17.0	17.8	18.6	19.3	20.0	20.7	21.4	22.0	22.6					
	4					6.3	6.5	6.8	7.0	7.3	7.5	7.7	8.0	8.2	8.4			
34	6					10.4	10.9	11.3	11.7	12.1	12.5	12.9	13.2	13.6	13.9			
	8					15.0	15.6	16.2	16.8	17.4	18.0	18.5	19.0	19.5	20.0			
	4							5.9	6.1	6.3	6.5	6.7	6.9	7.1	7.3	7.4	7.6	7.7
40	6							9.8	10.2	10.5	10.8	11.2	11.5	11.8	12.1	12.4	12.6	12.9
	8							14.1	14.6	15.1	15.6	16.0	16.5	16.9	17.3	17.7	18.1	18.5

Note: Positive Moment Causes Tension on Top of Slab

Table A.1N. Maximum Negative Slab Moment in (in.-kips/ft) for 28 ft Roadway on 6[5Bxx].

Box Depth	Slab Thickness	Bridge Span (ft)																
		30	35	40	45	50	55	60	65	70	75	80	85	90	95	100	105	110
(in.)	(in.)																	
	4	8.6	9.6	10.6	11.5	12.4	13.3											
20	6	14.5	16.2	17.8	19.3	20.8	22.3											
	8	20.9	23.3	25.6	27.9	30.1	32.2											
	4		7.1	7.8	8.5	9.2	9.8	10.4	11.1	11.7	12.2	12.8	13.4					
28	6		11.9	13.1	14.3	15.4	16.5	17.5	18.5	19.5	20.5	21.5	22.4					
	8		17.2	18.9	20.6	22.2	23.7	25.3	26.7	28.2	29.6	31.0	32.4					
	4					7.5	8.0	8.5	9.0	9.5	10.0	10.4	10.9	11.3	11.8			
34	6					12.5	13.4	14.2	15.1	15.9	16.7	17.5	18.2	19.0	19.8			
	8					18.0	19.3	20.5	21.7	22.9	24.1	25.2	26.3	27.4	28.5			
	4							7.2	7.6	8.0	8.4	8.8	9.2	9.6	9.9	10.3	10.7	11.0
40	6							12.0	12.7	13.4	14.1	14.7	15.4	16.0	16.7	17.3	17.9	18.5
	8							17.3	18.3	19.3	20.3	21.3	22.2	23.1	24.0	24.9	25.8	26.7

Note: Negative Moment Causes Tension on Bottom of Slab

Table A.2P. Maximum Positive Slab Moment in (in.-kips/ft) for 30 ft Roadway on 8[4Bxx].

Box Depth	Slab Thickness	Bridge Span (ft)																
		30	35	40	45	50	55	60	65	70	75	80	85	90	95	100	105	110
(in.)	(in.)																	
	4	7.0	7.7	8.3	8.9	9.4	10.0											
20	6	12.5	13.7	14.8	15.9	16.9	17.9											
	8	18.9	20.7	22.4	24.0	25.5	27.0											
	4		6.0	6.5	7.0	7.4	7.9	8.3	8.7	9.1	9.4	9.8	10.2					
28	6		10.8	11.7	12.5	13.3	14.1	14.8	15.5	16.2	16.9	17.6	18.2					
	8		16.3	17.6	18.9	20.1	21.3	22.4	23.5	24.5	25.5	26.5	27.5					
	4					6.1	6.4	6.8	7.1	7.4	7.7	8.0	8.3	8.6	8.9			
34	6					10.9	11.5	12.1	12.7	13.2	13.8	14.3	14.8	15.4	15.9			
	8					16.4	17.3	18.3	19.1	20.0	20.8	21.6	22.4	23.2	23.9			
	4							5.7	6.0	6.3	6.5	6.8	7.0	7.3	7.5	7.7	8.0	8.2
40	6							10.2	10.7	11.2	11.7	12.1	12.6	13.0	13.4	13.9	14.3	14.7
	8							15.5	16.2	17.0	17.7	18.3	19.0	19.7	20.3	20.9	21.5	22.1

Note: Positive Moment Causes Tension on Top of Slab

Table A.2N. Maximum Negative Slab Moment in (in.-kips/ft) for 30 ft Roadway on 8[4Bxx].

Box Depth	Slab Thickness	Bridge Span (ft)																
		30	35	40	45	50	55	60	65	70	75	80	85	90	95	100	105	110
(in.)	(in.)																	
	4	8.8	9.7	10.6	11.5	12.4	13.2											
20	6	15.8	17.5	19.2	20.8	22.3	23.8											
	8	24.0	26.7	29.2	31.6	33.9	36.2											
	4		7.5	8.2	8.9	9.6	10.2	10.8	11.4	12.0	12.6	13.2	13.7					
28	6		13.6	14.8	16.1	17.3	18.4	19.5	20.6	21.7	22.7	23.7	24.7					
	8		20.6	22.5	24.4	26.2	28.0	29.7	31.3	32.9	34.5	36.0	37.6					
	4					7.8	8.3	8.8	9.3	9.7	10.2	10.7	11.1	11.5	12.0			
34	6					14.0	14.9	15.8	16.7	17.6	18.4	19.2	20.0	20.8	21.6			
	8					21.2	22.7	24.0	25.4	26.7	27.9	29.2	30.4	31.6	32.8			
	4							7.4	7.8	8.2	8.6	9.0	9.4	9.7	10.1	10.4	10.8	11.1
40	6							13.3	14.1	14.8	15.5	16.2	16.9	17.5	18.2	18.8	19.5	20.1
	8							20.2	21.4	22.5	23.5	24.6	25.6	26.6	27.6	28.6	29.6	30.5

Note: Negative Moment Causes Tension on Bottom of Slab

Table A.3P. Maximum Positive Slab Moment in (in.-kips/ft) for 34 ft Roadway on 2[5Bxx] + 4[4Bxx] + 2[5Bxx].

Box Depth	Slab Thickness	Bridge Span (ft)																
		30	35	40	45	50	55	60	65	70	75	80	85	90	95	100	105	110
(in.)	(in.)																	
	4	7.4	8.3	9.1	10.0	10.8	11.6											
20	6	14.6	16.4	18.1	19.7	21.3	22.8											
	8	23.7	26.5	29.3	31.9	34.5	37.0											
	4		6.3	6.9	7.5	8.1	8.7	9.3	9.9	10.4	11.0	11.5	12.1					
28	6		12.4	13.6	14.9	16.1	17.3	18.4	19.5	20.6	21.7	22.8	23.8					
	8		20.0	22.1	24.1	26.1	28.0	29.8	31.7	33.4	35.2	36.9	38.6					
	4					6.5	6.9	7.4	7.9	8.3	8.7	9.2	9.6	10.0	10.4			
34	6					12.8	13.7	14.6	15.5	16.4	17.2	18.1	18.9	19.7	20.5			
	8					20.7	22.2	23.7	25.1	26.5	27.9	29.3	30.6	32.0	33.3			
	4							6.1	6.5	6.9	7.2	7.6	7.9	8.3	8.6	8.9	9.3	9.6
40	6							12.1	12.8	13.5	14.3	15.0	15.6	16.3	17.0	17.6	18.3	18.9
	8							19.6	20.8	22.0	23.1	24.2	25.3	26.4	27.5	28.6	29.6	30.7

Note: Positive Moment Causes Tension on Top of Slab

Table A.3N. Maximum Negative Slab Moment in (in.-kips/ft) for 34 ft Roadway on 2[5Bxx] + 4[4Bxx] + 2[5Bxx].

Box Depth	Slab Thickness	Bridge Span (ft)																
		30	35	40	45	50	55	60	65	70	75	80	85	90	95	100	105	110
(in.)	(in.)																	
	4	8.5	9.6	10.6	11.7	12.7	13.7											
20	6	15.8	17.8	19.8	21.7	23.6	25.5											
	8	24.6	27.8	30.8	33.8	36.8	39.6											
	4		7.2	8.0	8.8	9.5	10.3	11.0	11.7	12.4	13.1	13.8	14.5					
28	6		13.4	14.9	16.3	17.8	19.1	20.5	21.8	23.2	24.4	25.7	27.0					
	8		20.9	23.2	25.4	27.6	29.8	31.9	34.0	36.0	38.0	40.0	42.0					
	4					7.5	8.1	8.7	9.3	9.8	10.4	10.9	11.4	12.0	12.5			
34	6					14.1	15.1	16.2	17.3	18.3	19.3	20.4	21.4	22.3	23.3			
	8					21.9	23.6	25.3	26.9	28.5	30.1	31.7	33.2	34.8	36.3			
	4							7.2	7.6	8.1	8.6	9.0	9.4	9.9	10.3	10.7	11.2	11.6
40	6							13.4	14.3	15.1	16.0	16.8	17.6	18.4	19.2	20.0	20.8	21.6
	8							20.8	22.2	23.5	24.8	26.1	27.4	28.7	29.9	31.2	32.4	33.6

Note: Negative Moment Causes Tension on Bottom of Slab

Table A.4P. Maximum Positive Slab Moment in (in.-kips/ft) for 38 ft Roadway on 8[5Bxx].

Box Depth	Slab Thickness	Bridge Span (ft)																
		30	35	40	45	50	55	60	65	70	75	80	85	90	95	100	105	110
(in.)	(in.)																	
	4	7.3	8.3	9.4	10.4	11.4	12.3											
20	6	15.4	17.6	19.8	21.9	24.0	26.0											
	8	26.2	29.9	33.6	37.1	40.7	44.2											
	4		5.9	6.7	7.4	8.1	8.8	9.5	10.1	10.8	11.5	12.1	12.8					
28	6		12.5	14.1	15.6	17.0	18.5	19.9	21.4	22.8	24.2	25.6	26.9					
	8		21.3	23.9	26.4	28.9	31.4	33.9	36.3	38.7	41.1	43.4	45.8					
	4					6.2	6.8	7.3	7.8	8.3	8.8	9.4	9.9	10.4	10.9			
34	6					13.2	14.3	15.4	16.5	17.6	18.7	19.7	20.8	21.9	22.9			
	8					22.3	24.2	26.1	28.0	29.9	31.7	33.5	35.3	37.1	38.9			
	4							5.9	6.3	6.7	7.1	7.6	8.0	8.4	8.8	9.2	9.6	9.9
40	6							12.4	13.3	14.2	15.1	15.9	16.8	17.6	18.5	19.3	20.1	21.0
	8							21.1	22.6	24.1	25.6	27.1	28.5	29.9	31.4	32.8	34.2	35.6

Note: Positive Moment Causes Tension on Top of Slab

Table A.4N. Maximum Negative Slab Moment in (in.-kips/ft) for 38 ft Roadway on 8[5Bxx].

Depth	Slab Thickness	Bridge Span (ft)																
		30	35	40	45	50	55	60	65	70	75	80	85	90	95	100	105	110
(in.)	(in.)																	
	4	7.8	8.9	10.1	11.2	12.4	13.5											
20	6	15.9	18.3	20.7	23.1	25.4	27.8											
	8	26.6	30.6	34.6	38.5	42.4	46.3											
	4		6.4	7.2	8.1	8.9	9.7	10.5	11.3	12.1	12.9	13.7	14.4					
28	6		13.2	14.9	16.6	18.2	19.9	21.6	23.2	24.8	26.4	28.1	29.7					
	8		21.9	24.8	27.6	30.4	33.2	35.9	38.7	41.4	44.1	46.8	49.4					
	4					6.9	7.5	8.1	8.7	9.3	9.9	10.5	11.1	11.7	12.3			
34	6					14.1	15.4	16.6	17.9	19.2	20.4	21.7	22.9	24.1	25.3			
	8					23.5	25.6	27.7	29.8	31.9	34.0	36.1	38.2	40.2	42.2			
	4							6.5	7.0	7.5	8.0	8.5	9.0	9.5	10.0	10.4	10.9	11.4
40	6							13.4	14.4	15.5	16.5	17.5	18.5	19.5	20.5	21.4	22.4	23.4
	8							22.4	24.1	25.8	27.5	29.1	30.8	32.4	34.1	35.7	37.4	39.0

Note: Negative Moment Causes Tension on Bottom of Slab

Table A.5P. Maximum Positive Slab Moment in (in.-kips/ft) for 40 ft Roadway on 5Bxx + 8[4Bxx] + [5Bxx].

Box Depth	Slab Thickness	Bridge Span (ft)																
		30	35	40	45	50	55	60	65	70	75	80	85	90	95	100	105	110
(in.)	(in.)																	
	4	6.4	7.4	8.4	9.4	10.4	11.3											
20	6	14.0	16.1	18.3	20.4	22.5	24.6											
	8	24.2	28.0	31.7	35.4	39.1	42.7											
	4		5.3	6.0	6.7	7.4	8.1	8.8	9.5	10.2	10.9	11.6	12.2					
28	6		11.6	13.1	14.6	16.1	17.7	19.2	20.6	22.1	23.6	25.1	26.6					
	8		20.0	22.7	25.3	28.0	30.6	33.2	35.8	38.4	40.9	43.5	46.0					
	4					5.7	6.2	6.8	7.3	7.8	8.3	8.9	9.4	9.9	10.4			
34	6					12.4	13.5	14.7	15.8	17.0	18.1	19.2	20.3	21.5	22.6			
	8					21.4	23.5	25.4	27.4	29.4	31.4	33.3	35.3	37.2	39.2			
	4							5.4	5.9	6.3	6.7	7.1	7.5	8.0	8.4	8.8	9.2	9.6
40	6							11.8	12.7	13.6	14.6	15.5	16.4	17.3	18.2	19.1	20.0	20.9
	8							20.5	22.1	23.7	25.2	26.8	28.4	30.0	31.5	33.1	34.6	36.2

Note: Positive Moment Causes Tension on Top of Slab

Table A.5N. Maximum Negative Slab Moment in (in.-kips/ft) for 40 ft Roadway on 5Bxx + 8[4Bxx] + [5Bxx].

Box Depth	Slab Thickness	Bridge Span (ft)																
		30	35	40	45	50	55	60	65	70	75	80	85	90	95	100	105	110
(in.)	(in.)																	
	4	9.2	10.4	11.5	12.6	13.7	14.8											
20	6	17.4	19.7	21.8	23.9	26.0	28.0											
	8	27.4	30.9	34.3	37.6	40.9	44.0											
	4		7.9	8.8	9.6	10.4	11.2	12.0	12.8	13.5	14.3	15.0	15.8					
28	6		15.0	16.6	18.2	19.7	21.3	22.8	24.2	25.7	27.1	28.5	29.8					
	8		23.5	26.1	28.6	31.1	33.5	35.8	38.1	40.4	42.6	44.8	47.0					
	4					8.2	8.9	9.5	10.1	10.7	11.3	11.9	12.4	13.0	13.6			
34	6					15.6	16.8	18.0	19.1	20.3	21.4	22.5	23.6	24.6	25.7			
	8					24.5	26.4	28.3	30.1	31.9	33.6	35.4	37.1	38.8	40.4			
	4							7.8	8.3	8.8	9.3	9.8	10.2	10.7	11.2	11.6	12.1	12.5
40	6							14.8	15.8	16.7	17.6	18.5	19.4	20.3	21.2	22.0	22.9	23.7
	8							23.3	24.8	26.3	27.7	29.2	30.6	32.0	33.3	34.7	36.0	37.4

Note: Negative Moment Causes Tension on Bottom of Slab

Table A.6P. Maximum Positive Slab Moment in (in.-kips/ft) for 42 ft Roadway on 2[5Bxx] + 6[4Bxx] + 2[5Bxx].

Box Depth	Slab Thickness	Bridge Span (ft)																
		30	35	40	45	50	55	60	65	70	75	80	85	90	95	100	105	110
(in.)	(in.)																	
	4	6.2	7.2	8.2	9.2	10.2	11.2											
20	6	13.6	15.8	18.0	20.2	22.4	24.6											
	8	23.7	27.5	31.4	35.2	39.0	42.8											
	4		5.1	5.8	6.5	7.2	7.9	8.6	9.3	10.0	10.7	11.4	12.1					
28	6		11.1	12.6	14.2	15.7	17.3	18.8	20.3	21.8	23.4	24.9	26.4					
	8		19.4	22.1	24.7	27.4	30.1	32.8	35.4	38.1	40.8	43.4	46.1					
	4					5.5	6.1	6.6	7.1	7.7	8.2	8.7	9.3	9.8	10.3			
34	6					12.1	13.3	14.4	15.6	16.8	18.0	19.1	20.3	21.5	22.6			
	8					21.1	23.1	25.2	27.2	29.3	31.3	33.4	35.4	37.4	39.5			
	4							5.3	5.7	6.2	6.6	7.0	7.5	7.9	8.3	8.7	9.2	9.6
40	6							11.6	12.6	13.5	14.5	15.4	16.3	17.3	18.2	19.2	20.1	21.0
	8							20.3	21.9	23.6	25.2	26.9	28.5	30.2	31.8	33.4	35.1	36.7

Note: Positive Moment Causes Tension on Top of Slab

Table A.6N. Maximum Negative Slab Moment in (in.-kips/ft) for 42 ft Roadway on 2[5Bxx] + 6[4Bxx] + 2[5Bxx].

Box Depth	Slab Thickness	Bridge Span (ft)																
		30	35	40	45	50	55	60	65	70	75	80	85	90	95	100	105	110
(in.)	(in.)																	
	4	8.3	9.6	10.9	12.2	13.5	14.7											
20	6	16.8	19.4	22.0	24.6	27.2	29.7											
	8	27.7	32.0	36.3	40.5	44.8	49.0											
	4		7.0	7.9	8.8	9.8	10.7	11.6	12.5	13.4	14.3	15.2	16.1					
28	6		14.1	16.0	17.9	19.7	21.6	23.4	25.3	27.1	28.9	30.7	32.5					
	8		23.2	26.3	29.4	32.5	35.5	38.5	41.6	44.6	47.6	50.6	53.5					
	4					7.6	8.3	9.0	9.7	10.4	11.1	11.8	12.5	13.2	13.9			
34	6					15.3	16.8	18.2	19.6	21.1	22.5	23.9	25.3	26.7	28.1			
	8					25.3	27.6	30.0	32.3	34.7	37.0	39.3	41.7	44.0	46.3			
	4							7.3	7.9	8.5	9.1	9.6	10.2	10.8	11.3	11.9	12.4	13.0
40	6							14.8	16.0	17.2	18.3	19.5	20.6	21.7	22.9	24.0	25.1	26.3
	8							24.4	26.3	28.2	30.1	32.0	33.9	35.8	37.7	39.5	41.4	43.2

Note: Negative Moment Causes Tension on Bottom of Slab

Table A.7P. Maximum Positive Slab Moment in (in.-kips/ft) for 44 ft Roadway on 3[5Bxx] + 4[4Bxx] + 3[5Bxx].

Box Depth	Slab Thickness	Bridge Span (ft)																
		30	35	40	45	50	55	60	65	70	75	80	85	90	95	100	105	110
(in.)	(in.)																	
	4	6.1	7.1	8.1	9.1	10.1	11.1											
20	6	13.3	15.5	17.7	19.9	22.0	24.2											
	8	23.2	26.9	30.7	34.5	38.2	42.0											
	4		5.1	5.8	6.5	7.2	7.9	8.6	9.3	10.0	10.7	11.4	12.1					
28	6		11.1	12.6	14.1	15.7	17.2	18.8	20.3	21.8	23.3	24.9	26.4					
	8		19.2	21.9	24.5	27.2	29.9	32.5	35.2	37.8	40.5	43.1	45.8					
	4					5.5	6.0	6.5	7.1	7.6	8.1	8.7	9.2	9.7	10.3			
34	6					11.9	13.1	14.2	15.4	16.5	17.7	18.8	20.0	21.1	22.3			
	8					20.6	22.7	24.7	26.7	28.7	30.7	32.7	34.7	36.7	38.7			
	4							5.2	5.6	6.1	6.5	6.9	7.3	7.7	8.2	8.6	9.0	9.4
40	6							11.3	12.2	13.2	14.1	15.0	15.9	16.8	17.8	18.7	19.6	20.5
	8							19.6	21.2	22.8	24.4	26.0	27.6	29.2	30.8	32.4	34.0	35.6

Note: Positive Moment Causes Tension on Top of Slab

Table A.7N. Maximum Negative Slab Moment in (in.-kips/ft) for 44 ft Roadway on 3[5Bxx] + 4[4Bxx] + 3[5Bxx].

Box Depth	Slab Thickness	Bridge Span (ft)																
		30	35	40	45	50	55	60	65	70	75	80	85	90	95	100	105	110
(in.)	(in.)																	
	4	8.3	9.7	11.0	12.4	13.7	15.1											
20	6	17.3	20.1	22.9	25.7	28.5	31.3											
	8	29.0	33.7	38.4	43.1	47.8	52.4											
	4		6.3	7.1	8.0	8.9	9.7	10.6	11.5	12.3	13.2	14.0	14.9					
28	6		13.0	14.8	16.6	18.4	20.2	22.0	23.7	25.5	27.3	29.1	30.9					
	8		21.8	24.8	27.8	30.8	33.8	36.8	39.8	42.8	45.8	48.8	51.8					
	4					7.4	8.1	8.8	9.5	10.2	10.9	11.6	12.3	13.1	13.8			
34	6					15.2	16.7	18.2	19.7	21.2	22.6	24.1	25.6	27.1	28.5			
	8					25.6	28.1	30.5	33.0	35.5	38.0	40.4	42.9	45.4	47.8			
	4							7.6	8.2	8.8	9.4	10.0	10.6	11.2	11.8	12.4	13.0	13.7
40	6							15.7	16.9	18.2	19.5	20.7	22.0	23.3	24.5	25.8	27.0	28.3
	8							26.3	28.4	30.5	32.6	34.8	36.9	39.0	41.1	43.2	45.3	47.4

Note: Negative Moment Causes Tension on Bottom of Slab

APPENDIX B

RECOMMENDED SLAB TRANSVERSE DESIGN MOMENTS FOR PROPOSED NEW TXDOT STANDARD BRIDGE CONFIGURATIONS

Table B.1P. Maximum Positive Slab Moment in (in.-kips/ft) for 24 ft Roadway on 5Bxx + 4[4Bxx] + 5Bxx.

Box Depth	Slab Thickness	Bridge Span (ft)																
		30	35	40	45	50	55	60	65	70	75	80	85	90	95	100	105	110
(in.)	(in.)																	
	4	5.5	6.0	6.5	6.9	7.3	7.7											
20	6	9.3	10.2	11.0	11.8	12.5	13.2											
	8	13.7	14.9	16.1	17.2	18.3	19.3											
	4		4.8	5.2	5.5	5.9	6.2	6.5	6.8	7.1	7.4	7.7	7.9					
28	6		8.2	8.8	9.4	10.0	10.6	11.1	11.6	12.1	12.6	13.1	13.6					
	8		11.9	12.9	13.8	14.6	15.4	16.2	17.0	17.7	18.5	19.2	19.8					
	4					4.9	5.2	5.4	5.7	5.9	6.2	6.4	6.6	6.8	7.0			
34	6					8.3	8.8	9.2	9.7	10.1	10.5	10.9	11.3	11.7	12.0			
	8					12.2	12.9	13.5	14.1	14.8	15.4	15.9	16.5	17.1	17.6			
	4							4.3	4.5	4.6	4.8	5.0	5.2	5.4	5.5	5.7	5.9	6.0
40	6							7.3	7.6	7.9	8.3	8.6	8.9	9.2	9.5	9.7	10.0	10.3
	8							10.6	11.1	11.6	12.1	12.5	13.0	13.4	13.8	14.2	14.6	15.0

Note: Positive Moment Causes Tension on Top of Slab

Table B.1N. Maximum Negative Slab Moment in (in.-kips/ft) for 24 ft Roadway on 5Bxx + 4[4Bxx] + 5Bxx.

Box Depth	Slab Thickness	Bridge Span (ft)																
		30	35	40	45	50	55	60	65	70	75	80	85	90	95	100	105	110
(in.)	(in.)																	
	4	7.8	8.6	9.3	10.0	10.7	11.3											
20	6	13.6	14.9	16.2	17.4	18.5	19.6											
	8	20.0	22.0	23.8	25.6	27.3	28.9											
	4		6.7	7.3	7.8	8.3	8.8	9.3	9.8	10.2	10.7	11.1	11.5					
28	6		11.6	12.6	13.5	14.4	15.3	16.1	16.9	17.7	18.5	19.2	19.9					
	8		17.2	18.6	20.0	21.3	22.6	23.8	25.0	26.1	27.2	28.3	29.4					
	4					6.9	7.3	7.7	8.1	8.4	8.8	9.2	9.5	9.8	10.2			
34	6					11.9	12.6	13.3	14.0	14.6	15.2	15.8	16.4	17.0	17.6			
	8					17.6	18.6	19.6	20.6	21.6	22.5	23.4	24.2	25.1	25.9			
	4							6.0	6.3	6.6	6.9	7.2	7.4	7.7	8.0	8.2	8.5	8.7
40	6							10.4	10.9	11.4	11.9	12.4	12.9	13.3	13.8	14.2	14.6	15.0
	8							15.4	16.1	16.9	17.6	18.3	19.0	19.7	20.3	20.9	21.6	22.2

Note: Negative Moment Causes Tension on Bottom of Slab

Table B.2P. Maximum Positive Slab Moment in (in.-kips/ft) for 26 ft Roadway on 4Bxx +4[5Bxx] + 4Bxx.

Box Depth	Slab Thickness	Bridge Span (ft)																
		30	35	40	45	50	55	60	65	70	75	80	85	90	95	100	105	110
(in.)	(in.)																	
	4	7.7	8.1	8.5	8.8	9.1	9.4											
20	6	12.6	13.2	13.8	14.3	14.8	15.3											
	8	17.8	18.7	19.5	20.3	21.0	21.7											
	4		6.3	6.5	6.8	7.0	7.2	7.4	7.6	7.8	8.0	8.2	8.3					
28	6		10.2	10.6	11.1	11.4	11.8	12.1	12.4	12.7	13.0	13.3	13.6					
	8		14.4	15.1	15.6	16.2	16.7	17.2	17.6	18.0	18.4	18.8	19.2					
	4					6.3	6.5	6.7	6.8	7.0	7.2	7.3	7.5	7.6	7.7			
34	6					10.3	10.6	10.9	11.2	11.4	11.7	11.9	12.2	12.4	12.6			
	8					14.5	15.0	15.4	15.8	16.2	16.5	16.9	17.2	17.5	17.8			
	4							6.1	6.3	6.4	6.6	6.7	6.8	7.0	7.1	7.2	7.3	7.4
40	6							10.0	10.2	10.5	10.7	10.9	11.1	11.4	11.6	11.7	11.9	12.1
	8							14.1	14.5	14.8	15.1	15.5	15.8	16.1	16.3	16.6	16.9	17.1

Note: Positive Moment Causes Tension on Top of Slab

Table B.2N. Maximum Negative Slab Moment in (in.-kips/ft) for 26 ft Roadway on 4Bxx +4[5Bxx] + 4Bxx.

Box Depth	Slab Thickness	Bridge Span (ft)																
		30	35	40	45	50	55	60	65	70	75	80	85	90	95	100	105	110
(in.)	(in.)																	
	4	7.4	8.3	9.1	9.9	10.7	11.5											
20	6	13.6	15.2	16.7	18.2	19.6	21.0											
	8	20.8	23.3	25.7	27.9	30.1	32.3											
	4		4.8	5.3	5.8	6.2	6.7	7.1	7.5	7.9	8.3	8.7	9.1					
28	6		8.8	9.7	10.6	11.4	12.2	13.0	13.8	14.5	15.3	16.0	16.7					
	8		13.5	14.9	16.2	17.5	18.7	19.9	21.1	22.3	23.4	24.5	25.6					
	4					5.7	6.1	6.5	6.9	7.2	7.6	8.0	8.3	8.7	9.0			
34	6					10.4	11.1	11.8	12.5	13.2	13.9	14.6	15.2	15.9	16.5			
	8					15.9	17.1	18.2	19.2	20.3	21.3	22.4	23.4	24.3	25.3			
	4							6.0	6.4	6.7	7.1	7.4	7.8	8.1	8.4	8.7	9.0	9.3
40	6							11.0	11.7	12.3	13.0	13.6	14.2	14.8	15.4	16.0	16.5	17.1
	8							16.9	18.0	18.9	19.9	20.9	21.8	22.7	23.6	24.5	25.4	26.2

Note: Negative Moment Causes Tension on Bottom of Slab

Table B.3P. Maximum Positive Slab Moment in (in.-kips/ft) for 28 ft Roadway on 6[5Bxx].

Box Depth	Slab Thickness	Bridge Span (ft)																
		30	35	40	45	50	55	60	65	70	75	80	85	90	95	100	105	110
(in.)	(in.)																	
	4	7.6	8.2	8.8	9.4	9.9	10.5											
20	6	13.1	14.2	15.3	16.3	17.2	18.1											
	8	19.3	21.0	22.6	24.0	25.4	26.8											
	4		6.4	6.9	7.3	7.7	8.1	8.5	8.9	9.3	9.6	9.9	10.3					
28	6		11.1	11.9	12.7	13.4	14.1	14.8	15.4	16.0	16.7	17.2	17.8					
	8		16.3	17.6	18.7	19.8	20.8	21.8	22.8	23.7	24.6	25.5	26.3					
	4					6.4	6.7	7.0	7.3	7.6	7.9	8.2	8.5	8.7	9.0			
34	6					11.0	11.6	12.2	12.7	13.2	13.7	14.2	14.7	15.1	15.6			
	8					16.3	17.2	18.0	18.8	19.5	20.3	21.0	21.7	22.4	23.0			
	4							6.0	6.3	6.5	6.8	7.0	7.2	7.4	7.7	7.9	8.1	8.3
40	6							10.4	10.8	11.3	11.7	12.1	12.5	12.9	13.3	13.7	14.0	14.4
	8							15.3	16.0	16.7	17.3	17.9	18.5	19.1	19.6	20.2	20.7	21.2

Note: Positive Moment Causes Tension on Top of Slab

Table B.3N. Maximum Negative Slab Moment in (in.-kips/ft) for 28 ft Roadway on 6[5Bxx].

Box Depth	Slab Thickness	Bridge Span (ft)																
		30	35	40	45	50	55	60	65	70	75	80	85	90	95	100	105	110
(in.)	(in.)																	
	4	7.1	8.0	8.8	9.6	10.4	11.2											
20	6	13.7	15.4	17.0	18.6	20.1	21.6											
	8	21.8	24.5	27.1	29.7	32.1	34.5											
	4		5.9	6.5	7.1	7.7	8.3	8.9	9.4	9.9	10.5	11.0	11.5					
28	6		11.4	12.6	13.8	14.9	16.0	17.1	18.2	19.2	20.3	21.3	22.3					
	8		18.2	20.1	22.0	23.8	25.6	27.3	29.0	30.7	32.3	33.9	35.5					
	4					6.1	6.5	7.0	7.4	7.8	8.3	8.7	9.1	9.5	9.9			
34	6					11.8	12.6	13.5	14.3	15.2	16.0	16.8	17.5	18.3	19.1			
	8					18.8	20.2	21.5	22.9	24.2	25.5	26.8	28.0	29.2	30.5			
	4							5.7	6.1	6.4	6.8	7.1	7.5	7.8	8.1	8.4	8.7	9.1
40	6							11.1	11.8	12.4	13.1	13.8	14.4	15.0	15.7	16.3	16.9	17.5
	8							17.7	18.8	19.9	20.9	22.0	23.0	24.0	25.0	26.0	27.0	27.9

Note: Negative Moment Causes Tension on Bottom of Slab

Table B.4P. Maximum Positive Slab Moment in (in.-kips/ft) for 30 ft Roadway on 2[5Bxx] + 3[4Bxx] + 2[5Bxx].

Box Depth	Slab Thickness	Bridge Span (ft)																
		30	35	40	45	50	55	60	65	70	75	80	85	90	95	100	105	110
(in.)	(in.)																	
	4	6.3	7.0	7.7	8.4	9.0	9.6											
20	6	11.2	12.5	13.7	14.8	15.9	16.9											
	8	16.9	18.7	20.5	22.2	23.8	25.4											
	4		5.4	5.9	6.4	6.8	7.3	7.7	8.2	8.6	9.0	9.4	9.8					
28	6		9.5	10.4	11.3	12.1	12.9	13.7	14.4	15.2	15.9	16.6	17.3					
	8		14.3	15.6	16.9	18.1	19.4	20.5	21.7	22.8	23.9	24.9	26.0					
	4					5.8	6.2	6.5	6.9	7.3	7.6	7.9	8.3	8.6	8.9			
34	6					10.2	10.9	11.6	12.2	12.9	13.5	14.1	14.7	15.2	15.8			
	8					15.4	16.4	17.4	18.3	19.3	20.2	21.1	22.0	22.9	23.7			
	4							5.3	5.6	5.9	6.2	6.5	6.8	7.0	7.3	7.5	7.8	8.0
40	6							9.5	10.0	10.5	11.0	11.5	12.0	12.4	12.9	13.4	13.8	14.2
	8							14.2	15.0	15.7	16.5	17.2	17.9	18.7	19.3	20.0	20.7	21.4

Note: Positive Moment Causes Tension on Top of Slab

Table B.4N. Maximum Negative Slab Moment in (in.-kips.ft) for 30 ft Roadway on 2[5Bxx] + 3[4Bxx] + 2[5Bxx].

Box Depth	Slab Thickness	Bridge Span (ft)																
		30	35	40	45	50	55	60	65	70	75	80	85	90	95	100	105	110
(in.)	(in.)																	
	4	8.6	9.6	10.5	11.4	12.3	13.2											
20	6	15.4	17.2	18.9	20.5	22.1	23.6											
	8	23.4	26.0	28.6	31.0	33.4	35.7											
	4		7.2	7.9	8.6	9.2	9.9	10.5	11.1	11.7	12.3	12.8	13.4					
28	6		12.9	14.2	15.4	16.5	17.7	18.8	19.9	20.9	22.0	23.0	24.0					
	8		19.5	21.4	23.2	25.0	26.8	28.4	30.1	31.7	33.2	34.8	36.3					
	4					7.7	8.3	8.8	9.3	9.8	10.3	10.8	11.2	11.7	12.1			
34	6					13.9	14.8	15.8	16.7	17.6	18.4	19.3	20.1	20.9	21.7			
	8					21.0	22.4	23.8	25.2	26.6	27.9	29.2	30.4	31.7	32.9			
	4							7.1	7.5	7.9	8.3	8.7	9.1	9.4	9.8	10.1	10.5	10.8
40	6							12.7	13.5	14.2	14.9	15.6	16.2	16.9	17.5	18.2	18.8	19.4
	8							19.2	20.4	21.4	22.5	23.5	24.6	25.6	26.5	27.5	28.5	29.4

Note: Negative Moment Causes Tension on Bottom of Slab

Table B.5P. Maximum Positive Slab Moment in (in.-kips/ft) for 32 ft Roadway on 4[4Bxx] + 5Bxx + 3[4Bxx].

Box Depth	Slab Thickness	Bridge Span (ft)																
		30	35	40	45	50	55	60	65	70	75	80	85	90	95	100	105	110
(in.)	(in.)																	
	4	8.1	9.0	9.9	10.7	11.6	12.4											
20	6	15.6	17.4	19.1	20.8	22.4	23.9											
	8	24.9	27.8	30.5	33.2	35.8	38.2											
	4		6.8	7.5	8.1	8.7	9.4	9.9	10.5	11.1	11.6	12.2	12.7					
28	6		13.2	14.5	15.7	16.9	18.1	19.2	20.4	21.4	22.5	23.6	24.6					
	8		21.0	23.1	25.1	27.0	28.9	30.7	32.5	34.2	35.9	37.6	39.3					
	4					6.9	7.4	7.9	8.4	8.8	9.2	9.7	10.1	10.5	10.9			
34	6					13.4	14.4	15.3	16.2	17.0	17.9	18.7	19.5	20.3	21.1			
	8					21.4	22.9	24.4	25.8	27.2	28.5	29.9	31.2	32.4	33.7			
	4							6.5	6.9	7.3	7.7	8.0	8.4	8.7	9.0	9.4	9.7	10.0
40	6							12.6	13.4	14.1	14.8	15.5	16.2	16.8	17.5	18.1	18.8	19.4
	8							20.2	21.4	22.5	23.6	24.7	25.8	26.9	27.9	28.9	30.0	31.0

Note: Positive Moment Causes Tension on Top of Slab

Table B.5N. Maximum Negative Slab Moment in (in.-kips/ft) for 32 ft Roadway on 4[4Bxx] + 5Bxx + 3[4Bxx].

Box Depth	Slab Thickness	Bridge Span (ft)																
		30	35	40	45	50	55	60	65	70	75	80	85	90	95	100	105	110
(in.)	(in.)																	
	4	7.9	8.9	10.0	10.9	11.9	12.8											
20	6	15.6	17.6	19.6	21.6	23.5	25.3											
	8	25.3	28.6	31.8	34.9	38.0	41.0											
	4		6.7	7.5	8.3	9.0	9.7	10.4	11.1	11.8	12.4	13.1	13.7					
28	6		13.3	14.8	16.3	17.7	19.1	20.5	21.9	23.2	24.5	25.8	27.1					
	8		21.6	24.0	26.4	28.7	31.0	33.2	35.4	37.6	39.7	41.8	43.9					
	4					7.1	7.6	8.2	8.7	9.2	9.8	10.3	10.8	11.3	11.8			
34	6					13.9	15.0	16.1	17.2	18.2	19.3	20.3	21.3	22.3	23.3			
	8					22.5	24.3	26.1	27.8	29.5	31.2	32.8	34.5	36.1	37.7			
	4							6.7	7.2	7.6	8.0	8.4	8.9	9.3	9.7	10.1	10.5	10.9
40	6							13.2	14.1	15.0	15.8	16.7	17.5	18.3	19.1	19.9	20.7	21.5
	8							21.4	22.8	24.2	25.6	27.0	28.3	29.7	31.0	32.3	33.5	34.8

Note: Negative Moment Causes Tension on Bottom of Slab

Table B.6P. Maximum Positive Slab Moment in (in.-kips/ft) for 34 ft Roadway on 2[4Bxx] + 3[5Bxx] + 3[4Bxx].

Box Depth	Slab Thickness	Bridge Span (ft)																
		30	35	40	45	50	55	60	65	70	75	80	85	90	95	100	105	110
(in.)	(in.)																	
	4	8.3	9.3	10.3	11.3	12.3	13.2											
20	6	16.8	18.9	20.9	22.9	24.8	26.7											
	8	27.6	31.1	34.5	37.7	40.9	44.1											
	4		6.6	7.4	8.1	8.7	9.4	10.1	10.7	11.3	12.0	12.6	13.2					
28	6		13.4	14.9	16.3	17.7	19.0	20.3	21.6	22.9	24.2	25.4	26.6					
	8		22.1	24.5	26.9	29.1	31.4	33.5	35.7	37.8	39.8	41.9	43.9					
	4					7.0	7.5	8.0	8.5	9.0	9.5	10.0	10.5	11.0	11.4			
34	6					14.1	15.2	16.2	17.2	18.3	19.2	20.2	21.2	22.2	23.1			
	8					23.2	25.0	26.7	28.4	30.1	31.7	33.3	34.9	36.5	38.1			
	4							6.7	7.1	7.5	7.9	8.3	8.7	9.1	9.5	9.9	10.2	10.6
40	6							13.5	14.3	15.2	16.0	16.8	17.6	18.4	19.2	19.9	20.7	21.5
	8							22.2	23.6	25.0	26.3	27.7	29.0	30.3	31.6	32.9	34.1	35.4

Note: Positive Moment Causes Tension on Top of Slab

Table B.6N. Maximum Negative Slab Moment in (in.-kips/ft) for 34 ft Roadway on 2[4Bxx] + 3[5Bxx] + 3[4Bxx].

Box Depth	Slab Thickness	Bridge Span (ft)																
		30	35	40	45	50	55	60	65	70	75	80	85	90	95	100	105	110
(in.)	(in.)																	
	4	8.1	9.2	10.3	11.3	12.4	13.4											
20	6	16.5	18.8	21.0	23.2	25.3	27.4											
	8	27.4	31.2	34.9	38.5	42.1	45.6											
	4		6.8	7.6	8.4	9.1	9.9	10.6	11.4	12.1	12.8	13.5	14.2					
28	6		13.8	15.5	17.1	18.7	20.2	21.8	23.3	24.7	26.2	27.7	29.1					
	8		23.0	25.7	28.4	31.0	33.6	36.1	38.6	41.1	43.6	46.0	48.4					
	4					7.1	7.7	8.3	8.9	9.4	10.0	10.5	11.1	11.6	12.2			
34	6					14.5	15.7	16.9	18.1	19.3	20.4	21.6	22.7	23.8	24.9			
	8					24.1	26.2	28.1	30.1	32.0	33.9	35.8	37.7	39.5	41.3			
	4							6.7	7.2	7.7	8.1	8.6	9.0	9.5	9.9	10.4	10.8	11.2
40	6							13.8	14.8	15.7	16.6	17.6	18.5	19.4	20.3	21.2	22.0	22.9
	8							22.9	24.5	26.1	27.6	29.2	30.7	32.2	33.7	35.2	36.6	38.1

Note: Negative Moment Causes Tension on Bottom of Slab

Table B.7P. Maximum Positive Slab Moment in (in.-kips/ft) for 36 ft Roadway on 2[5Bxx] + 3[4Bxx] +3[5Bxx].

Box Depth	Slab Thickness	Bridge Span (ft)																
		30	35	40	45	50	55	60	65	70	75	80	85	90	95	100	105	110
(in.)	(in.)																	
	4	7.2	8.2	9.1	10.1	11.0	12.0											
20	6	14.7	16.8	18.8	20.7	22.6	24.5											
	8	24.5	27.9	31.2	34.5	37.7	40.8											
	4		6.0	6.7	7.4	8.1	8.8	9.5	10.1	10.8	11.4	12.1	12.7					
28	6		12.3	13.8	15.2	16.6	18.0	19.4	20.8	22.1	23.4	24.7	26.0					
	8		20.5	22.9	25.3	27.7	30.0	32.3	34.5	36.8	39.0	41.2	43.3					
	4					6.3	6.8	7.4	7.9	8.4	8.9	9.4	9.9	10.4	10.9			
34	6					13.0	14.0	15.1	16.2	17.2	18.2	19.3	20.3	21.3	22.3			
	8					21.6	23.4	25.1	26.9	28.6	30.4	32.1	33.7	35.4	37.1			
	4							6.0	6.4	6.8	7.2	7.6	8.0	8.4	8.8	9.2	9.6	10.0
40	6							12.3	13.2	14.0	14.8	15.7	16.5	17.3	18.1	18.9	19.7	20.5
	8							20.5	21.9	23.3	24.7	26.1	27.5	28.8	30.2	31.5	32.8	34.1

Note: Positive Moment Causes Tension on Top of Slab

Table B.7N. Maximum Negative Slab Moment in (in.-kips/ft) for 36 ft Roadway on 2[5Bxx] + 3[4Bxx] +3[5Bxx].

Box Depth	Slab Thickness	Bridge Span (ft)																
		30	35	40	45	50	55	60	65	70	75	80	85	90	95	100	105	110
(in.)	(in.)																	
	4	8.2	9.3	10.5	11.6	12.7	13.8											
20	6	15.6	17.8	20.0	22.1	24.2	26.3											
	8	24.6	28.1	31.5	34.9	38.2	41.5											
	4		6.9	7.8	8.6	9.4	10.2	11.0	11.8	12.6	13.4	14.1	14.9					
28	6		13.2	14.8	16.4	18.0	19.5	21.0	22.5	24.0	25.5	27.0	28.4					
	8		20.9	23.5	26.0	28.4	30.9	33.3	35.6	38.0	40.3	42.6	44.9					
	4					7.5	8.1	8.7	9.4	10.0	10.6	11.2	11.8	12.4	13.0			
34	6					14.2	15.4	16.7	17.8	19.0	20.2	21.3	22.5	23.6	24.7			
	8					22.5	24.4	26.3	28.2	30.1	31.9	33.7	35.5	37.3	39.1			
	4							7.2	7.7	8.2	8.7	9.2	9.7	10.2	10.7	11.2	11.7	12.1
40	6							13.7	14.7	15.7	16.6	17.6	18.5	19.5	20.4	21.3	22.2	23.1
	8							21.7	23.3	24.8	26.3	27.8	29.3	30.8	32.2	33.7	35.1	36.6

Note: Negative Moment Causes Tension on Bottom of Slab

Table B.8P. Maximum Positive Slab Moment in (in.-kips/ft) for 38 ft Roadway on 8[5Bxx].

Box Depth	Slab Thickness	Bridge Span (ft)																
		30	35	40	45	50	55	60	65	70	75	80	85	90	95	100	105	110
(in.)	(in.)																	
	4	7.3	8.3	9.4	10.4	11.4	12.3											
20	6	15.4	17.6	19.7	21.9	23.9	26.0											
	8	26.2	29.9	33.5	37.1	40.7	44.2											
	4		5.9	6.7	7.4	8.1	8.8	9.5	10.1	10.8	11.5	12.1	12.8					
28	6		12.5	14.0	15.5	17.0	18.5	19.9	21.4	22.8	24.2	25.6	26.9					
	8		21.2	23.8	26.4	28.9	31.4	33.9	36.3	38.7	41.1	43.4	45.8					
	4					6.2	6.8	7.3	7.8	8.3	8.8	9.4	9.9	10.4	10.8			
34	6					13.1	14.3	15.4	16.5	17.6	18.7	19.7	20.8	21.8	22.9			
	8					22.3	24.2	26.1	28.0	29.8	31.7	33.5	35.3	37.1	38.9			
	4							5.9	6.3	6.7	7.1	7.5	8.0	8.4	8.8	9.2	9.5	9.9
40	6							12.4	13.3	14.2	15.1	15.9	16.8	17.6	18.5	19.3	20.1	21.0
	8							21.1	22.6	24.1	25.6	27.0	28.5	29.9	31.4	32.8	34.2	35.6

Note: Positive Moment Causes Tension on Top of Slab

Table B.8N. Maximum Negative Slab Moment in (in.-kips/ft) for 38 ft Roadway on 8[5Bxx].

Box Depth	Slab Thickness	Bridge Span (ft)																
		30	35	40	45	50	55	60	65	70	75	80	85	90	95	100	105	110
(in.)	(in.)																	
	4	7.8	8.9	10.1	11.2	12.4	13.5											
20	6	15.9	18.3	20.7	23.1	25.4	27.8											
	8	26.5	30.6	34.6	38.5	42.4	46.3											
	4		6.4	7.2	8.1	8.9	9.7	10.5	11.3	12.1	12.9	13.7	14.4					
28	6		13.1	14.9	16.6	18.2	19.9	21.5	23.2	24.8	26.4	28.0	29.7					
	8		21.9	24.8	27.6	30.4	33.2	35.9	38.6	41.4	44.1	46.7	49.4					
	4					6.8	7.5	8.1	8.7	9.3	9.9	10.5	11.1	11.7	12.3			
34	6					14.1	15.4	16.6	17.9	19.2	20.4	21.6	22.9	24.1	25.3			
	8					23.4	25.6	27.7	29.8	31.9	34.0	36.1	38.1	40.2	42.2			
	4							6.5	7.0	7.5	8.0	8.5	9.0	9.5	9.9	10.4	10.9	11.4
40	6							13.4	14.4	15.5	16.5	17.5	18.5	19.5	20.4	21.4	22.4	23.4
	8							22.4	24.1	25.8	27.4	29.1	30.8	32.4	34.1	35.7	37.3	39.0

Note: Negative Moment Causes Tension on Bottom of Slab

Table B.9P. Maximum Positive Slab Moment in (in.-kips/ft) for 40 ft Roadway on 2[4Bxx] + 5[5Bxx] + 2[4Bxx].

Box Depth	Slab Thickness	Bridge Span (ft)																
(in.)	(in.)	30	35	40	45	50	55	60	65	70	75	80	85	90	95	100	105	110
	4	7.1	8.2	9.3	10.4	11.4	12.5											
20	6	15.4	17.8	20.1	22.5	24.8	27.1											
	8	26.7	30.8	34.9	39.0	43.0	47.1											
	4		5.8	6.5	7.3	8.1	8.8	9.6	10.3	11.0	11.8	12.5	13.2					
28	6		12.5	14.2	15.9	17.5	19.1	20.8	22.4	24.0	25.6	27.2	28.8					
	8		21.8	24.6	27.5	30.4	33.2	36.0	38.8	41.6	44.4	47.1	49.9					
	4					6.1	6.6	7.2	7.8	8.3	8.9	9.4	10.0	10.5	11.1			
34	6					13.2	14.4	15.7	16.9	18.1	19.3	20.5	21.7	22.9	24.1			
	8					22.9	25.0	27.2	29.3	31.4	33.5	35.6	37.6	39.7	41.8			
	4							5.7	6.2	6.6	7.0	7.5	7.9	8.4	8.8	9.2	9.7	10.1
40	6							12.4	13.4	14.4	15.3	16.3	17.2	18.2	19.1	20.0	21.0	21.9
	8							21.5	23.2	24.9	26.5	28.2	29.8	31.5	33.1	34.8	36.4	38.0

Note: Positive Moment Causes Tension on Top of Slab

Table B.9N. Maximum Negative Slab Moment in (in.-kips/ft) for 40 ft Roadway on 2[4Bxx] + 5[5Bxx] + 2[4Bxx].

Box Depth	Slab Thickness	Bridge Span (ft)																
(in.)	(in.)	30	35	40	45	50	55	60	65	70	75	80	85	90	95	100	105	110
	4	8.5	9.7	10.8	11.9	13.0	14.1											
20	6	17.0	19.3	21.6	23.8	26.0	28.1											
	8	27.7	31.5	35.2	38.8	42.4	45.9											
	4		7.1	8.0	8.8	9.6	10.4	11.2	11.9	12.7	13.5	14.2	14.9					
28	6		14.2	15.9	17.5	19.2	20.7	22.3	23.8	25.3	26.8	28.3	29.8					
	8		23.2	26.0	28.6	31.3	33.9	36.4	38.9	41.4	43.8	46.3	48.7					
	4					7.5	8.1	8.7	9.3	9.9	10.5	11.1	11.6	12.2	12.8			
34	6					14.9	16.2	17.4	18.6	19.8	20.9	22.1	23.2	24.4	25.5			
	8					24.4	26.4	28.4	30.3	32.3	34.2	36.1	37.9	39.8	41.6			
	4							7.1	7.6	8.1	8.5	9.0	9.5	9.9	10.4	10.9	11.3	11.8
40	6							14.2	15.1	16.1	17.1	18.0	18.9	19.9	20.8	21.7	22.6	23.5
	8							23.1	24.7	26.3	27.8	29.4	30.9	32.4	33.9	35.4	36.9	38.3

Note: Negative Moment Causes Tension on Bottom of Slab

Table B.10P. Maximum Positive Slab Moment in (in.-kips/ft) for 42 ft Roadway on 4Bxx + 7[5Bxx] + 4Bxx.

Box Depth	Slab Thickness	Bridge Span (ft)																
		30	35	40	45	50	55	60	65	70	75	80	85	90	95	100	105	110
(in.)	(in.)																	
	4	7.2	8.3	9.4	10.6	11.7	12.9											
20	6	15.4	17.9	20.4	22.9	25.3	27.8											
	8	26.6	30.9	35.2	39.4	43.7	47.9											
	4		5.8	6.6	7.4	8.2	9.0	9.8	10.6	11.4	12.1	12.9	13.7					
28	6		12.5	14.3	16.0	17.7	19.4	21.1	22.8	24.5	26.2	27.9	29.6					
	8		21.6	24.6	27.6	30.5	33.5	36.4	39.4	42.3	45.2	48.1	51.0					
	4					6.2	6.8	7.4	8.0	8.6	9.2	9.8	10.4	11.0	11.6			
34	6					13.4	14.7	16.0	17.3	18.6	19.9	21.1	22.4	23.7	25.0			
	8					23.1	25.4	27.6	29.8	32.1	34.3	36.5	38.7	40.9	43.1			
	4							5.9	6.4	6.8	7.3	7.8	8.3	8.7	9.2	9.7	10.1	10.6
40	6							12.7	13.8	14.8	15.8	16.8	17.8	18.9	19.9	20.9	21.9	22.9
	8							22.0	23.8	25.5	27.3	29.0	30.8	32.5	34.3	36.0	37.8	39.5

Note: Positive Moment Causes Tension on Top of Slab

Table B.10N. Maximum Negative Slab Moment in (in.-kips/ft) for 42 ft Roadway on 4Bxx + 7[5Bxx] + 4Bxx.

Box Depth	Slab Thickness	Bridge Span (ft)																
		30	35	40	45	50	55	60	65	70	75	80	85	90	95	100	105	110
(in.)	(in.)																	
	4	8.6	9.9	11.3	12.6	13.9	15.2											
20	6	17.6	20.3	23.0	25.7	28.4	31.0											
	8	29.1	33.7	38.2	42.6	47.1	51.5											
	4		7.0	7.9	8.9	9.8	10.7	11.6	12.5	13.4	14.3	15.2	16.1					
28	6		14.3	16.2	18.1	20.0	21.8	23.7	25.6	27.4	29.2	31.1	32.9					
	8		23.7	26.9	30.0	33.1	36.2	39.3	42.4	45.5	48.5	51.5	54.5					
	4					7.7	8.4	9.1	9.8	10.6	11.3	12.0	12.7	13.4	14.1			
34	6					15.7	17.2	18.6	20.1	21.5	23.0	24.4	25.9	27.3	28.7			
	8					26.0	28.5	30.9	33.3	35.7	38.1	40.5	42.9	45.2	47.6			
	4							7.5	8.1	8.7	9.2	9.8	10.4	11.0	11.5	12.1	12.7	13.2
40	6							15.3	16.5	17.7	18.9	20.0	21.2	22.4	23.6	24.7	25.9	27.0
	8							25.4	27.4	29.3	31.3	33.2	35.2	37.1	39.1	41.0	42.9	44.8

Note: Negative Moment Causes Tension on Bottom of Slab

Table B.11P. Maximum Positive Slab Moment in (in.-kips/ft) for 44 ft Roadway on 9[5Bxx].

Box Depth	Slab Thickness	Bridge Span (ft)																
		30	35	40	45	50	55	60	65	70	75	80	85	90	95	100	105	110
(in.)	(in.)																	
	4	6.6	7.7	8.9	10.0	11.1	12.2											
20	6	14.7	17.2	19.6	22.1	24.6	27.0											
	8	26.0	30.3	34.6	38.9	43.2	47.5											
	4		5.4	6.2	7.0	7.7	8.5	9.3	10.0	10.8	11.6	12.4	13.1					
28	6		12.0	13.7	15.4	17.2	18.9	20.6	22.3	24.0	25.7	27.4	29.1					
	8		21.2	24.2	27.2	30.2	33.2	36.2	39.3	42.3	45.3	48.3	51.3					
	4					5.8	6.3	6.9	7.5	8.1	8.7	9.2	9.8	10.4	11.0			
34	6					12.8	14.1	15.4	16.7	17.9	19.2	20.5	21.8	23.0	24.3			
	8					22.6	24.8	27.1	29.3	31.6	33.8	36.1	38.3	40.6	42.8			
	4							5.4	5.9	6.3	6.8	7.2	7.7	8.2	8.6	9.1	9.5	10.0
40	6							12.1	13.1	14.1	15.1	16.1	17.1	18.1	19.1	20.1	21.1	22.1
	8							21.3	23.0	24.8	26.6	28.3	30.1	31.9	33.6	35.4	37.2	38.9

Note: Positive Moment Causes Tension on Top of Slab

Table B.11N. Maximum Negative Slab Moment in (in.-kips/ft) for 44 ft Roadway on 9[5Bxx].

Box Depth	Slab Thickness	Bridge Span (ft)																
		30	35	40	45	50	55	60	65	70	75	80	85	90	95	100	105	110
(in.)	(in.)																	
	4	8.2	9.5	10.8	12.1	13.4	14.8											
20	6	17.2	20.0	22.7	25.5	28.2	31.0											
	8	29.1	33.8	38.5	43.1	47.8	52.4											
	4		6.8	7.7	8.6	9.6	10.5	11.4	12.3	13.3	14.2	15.1	16.0					
28	6		14.2	16.2	18.1	20.1	22.0	24.0	25.9	27.9	29.8	31.7	33.6					
	8		24.1	27.4	30.7	34.0	37.3	40.6	43.9	47.2	50.4	53.7	56.9					
	4					7.3	8.0	8.7	9.4	10.1	10.8	11.5	12.2	12.9	13.6			
34	6					15.4	16.8	18.3	19.8	21.3	22.8	24.2	25.7	27.2	28.6			
	8					26.0	28.5	31.0	33.5	36.0	38.5	41.0	43.5	46.0	48.5			
	4							7.0	7.5	8.1	8.7	9.2	9.8	10.3	10.9	11.5	12.0	12.6
40	6							14.7	15.8	17.0	18.2	19.4	20.6	21.7	22.9	24.1	25.2	26.4
	8							24.8	26.8	28.8	30.8	32.8	34.8	36.8	38.8	40.7	42.7	44.7

Note: Negative Moment Causes Tension on Bottom of Slab

Table B.12P. Maximum Positive Slab Moment in (in.-kips/ft) for 46 ft Roadway on 3[5Bxx] + 3[4Bxx] + 4[5Bxx].

Box Depth	Slab Thickness	Bridge Span (ft)																
		30	35	40	45	50	55	60	65	70	75	80	85	90	95	100	105	110
(in.)	(in.)																	
	4	6.7	7.7	8.7	9.8	10.8	11.8											
20	6	14.3	16.5	18.7	20.9	23.1	25.3											
	8	24.5	28.3	32.1	35.9	39.6	43.4											
	4		5.6	6.3	7.0	7.8	8.5	9.2	10.0	10.7	11.4	12.1	12.8					
28	6		11.9	13.5	15.1	16.7	18.2	19.8	21.3	22.9	24.4	25.9	27.4					
	8		20.4	23.2	25.9	28.6	31.3	33.9	36.6	39.2	41.9	44.5	47.1					
	4					5.9	6.4	7.0	7.5	8.1	8.6	9.1	9.7	10.2	10.7			
34	6					12.6	13.7	14.9	16.1	17.3	18.4	19.6	20.7	21.9	23.0			
	8					21.6	23.6	25.6	27.6	29.6	31.6	33.6	35.6	37.5	39.5			
	4							5.5	6.0	6.4	6.8	7.2	7.7	8.1	8.5	8.9	9.3	9.8
40	6							11.8	12.8	13.7	14.6	15.5	16.4	17.3	18.2	19.1	20.0	20.9
	8							20.3	21.9	23.5	25.0	26.6	28.2	29.7	31.3	32.8	34.4	35.9

Note: Positive Moment Causes Tension on Top of Slab

Table B.12N. Maximum Negative Slab Moment in (in.-kips/ft) for 46 ft Roadway on 3[5Bxx] + 3[4Bxx] + 4[5Bxx].

Box Depth	Slab Thickness	Bridge Span (ft)																
		30	35	40	45	50	55	60	65	70	75	80	85	90	95	100	105	110
(in.)	(in.)																	
	4	8.7	10.0	11.4	12.7	14.0	15.4											
20	6	17.5	20.3	23.0	25.8	28.5	31.1											
	8	29.0	33.5	38.0	42.5	47.0	51.4											
	4		7.3	8.3	9.3	10.3	11.2	12.2	13.2	14.1	15.1	16.0	17.0					
28	6		14.8	16.8	18.8	20.8	22.8	24.7	26.7	28.6	30.5	32.5	34.4					
	8		24.5	27.8	31.1	34.3	37.6	40.8	44.0	47.2	50.4	53.6	56.7					
	4					7.9	8.7	9.4	10.2	10.9	11.6	12.4	13.1	13.8	14.5			
34	6					16.0	17.6	19.1	20.6	22.1	23.5	25.0	26.5	28.0	29.5			
	8					26.5	29.0	31.5	33.9	36.4	38.9	41.3	43.7	46.2	48.6			
	4							7.6	8.2	8.8	9.4	10.0	10.6	11.1	11.7	12.3	12.9	13.5
40	6							15.4	16.6	17.8	19.0	20.2	21.4	22.6	23.8	24.9	26.1	27.3
	8							25.4	27.4	29.4	31.4	33.3	35.3	37.3	39.2	41.2	43.1	45.1

Table B.13P. Maximum Positive Slab Moment in (in.-kips/ft) for 48 ft Roadway on 4[5Bxx] + 4Bxx + 5[5Bxx].

Box Depth	Slab Thickness	Bridge Span (ft)																
		30	35	40	45	50	55	60	65	70	75	80	85	90	95	100	105	110
(in.)	(in.)																	
	4	6.8	7.9	9.0	10.0	11.1	12.1											
20	6	14.8	17.1	19.4	21.8	24.1	26.4											
	8	25.6	29.7	33.7	37.7	41.7	45.7											
	4		5.6	6.4	7.2	7.9	8.7	9.4	10.2	10.9	11.7	12.4	13.2					
28	6		12.2	13.9	15.6	17.2	18.9	20.5	22.1	23.8	25.4	27.0	28.6					
	8		21.2	24.1	27.0	29.8	32.7	35.5	38.4	41.2	44.0	46.8	49.6					
	4					5.9	6.5	7.1	7.6	8.2	8.8	9.3	9.9	10.4	11.0			
34	6					12.9	14.1	15.4	16.6	17.8	19.0	20.2	21.5	22.7	23.9			
	8					22.4	24.5	26.6	28.8	30.9	33.0	35.1	37.2	39.3	41.4			
	4							5.6	6.0	6.5	6.9	7.3	7.8	8.2	8.7	9.1	9.5	10.0
40	6							12.1	13.1	14.0	15.0	15.9	16.9	17.8	18.8	19.7	20.7	21.6
	8							21.0	22.7	24.3	26.0	27.6	29.3	30.9	32.6	34.2	35.9	37.5

Note: Positive Moment Causes Tension on Top of Slab

Table B.13N. Maximum Negative Slab Moment in (in.-kips/ft) for 48 ft Roadway on 4[5Bxx] + 4Bxx + 5[5Bxx].

Box Depth	Slab Thickness	Bridge Span (ft)																
		30	35	40	45	50	55	60	65	70	75	80	85	90	95	100	105	110
(in.)	(in.)																	
	4	8.6	10.1	11.5	13.0	14.4	15.9											
20	6	18.1	21.2	24.2	27.3	30.3	33.4											
	8	30.7	35.8	41.0	46.2	51.3	56.5											
	4		7.1	8.2	9.2	10.2	11.3	12.3	13.3	14.4	15.4	16.5	17.5					
28	6		15.0	17.2	19.3	21.5	23.7	25.9	28.0	30.2	32.4	34.6	36.7					
	8		25.4	29.1	32.7	36.4	40.1	43.8	47.5	51.1	54.8	58.5	62.2					
	4					7.8	8.6	9.4	10.2	11.0	11.8	12.5	13.3	14.1	14.9			
34	6					16.4	18.1	19.7	21.4	23.0	24.7	26.4	28.0	29.7	31.3			
	8					27.8	30.6	33.4	36.2	39.0	41.8	44.6	47.4	50.2	53.1			
	4							7.5	8.1	8.8	9.4	10.0	10.7	11.3	11.9	12.6	13.2	13.8
40	6							15.7	17.1	18.4	19.7	21.1	22.4	23.7	25.0	26.4	27.7	29.0
	8							26.7	28.9	31.2	33.4	35.6	37.9	40.1	42.4	44.6	46.9	49.2

Note: Negative Moment Causes Tension on Bottom of Slab

Table B.14P. Maximum Positive Slab Moment in (in.-kips/ft) for 50 ft Roadway on 2[4Bxx] + 7[5Bxx] + 2[4Bxx].

Box Depth	Slab Thickness	Bridge Span (ft)																
(in.)	(in.)	30	35	40	45	50	55	60	65	70	75	80	85	90	95	100	105	110
	4	7.3	8.5	9.7	10.8	12.0	13.2											
20	6	15.7	18.3	20.9	23.5	26.0	28.6											
	8	27.2	31.7	36.2	40.6	45.1	49.5											
	4		5.4	6.1	6.9	7.7	8.4	9.2	9.9	10.7	11.4	12.2	12.9					
28	6		11.7	13.3	14.9	16.6	18.2	19.9	21.5	23.1	24.7	26.4	28.0					
	8		20.2	23.0	25.9	28.7	31.5	34.3	37.2	40.0	42.8	45.6	48.4					
	4					5.9	6.5	7.1	7.7	8.2	8.8	9.4	10.0	10.6	11.1			
34	6					12.8	14.1	15.3	16.6	17.8	19.1	20.4	21.6	22.9	24.1			
	8					22.1	24.3	26.5	28.7	30.9	33.0	35.2	37.4	39.6	41.7			
	4							5.7	6.2	6.7	7.1	7.6	8.1	8.6	9.0	9.5	10.0	10.4
40	6							12.4	13.4	14.4	15.5	16.5	17.5	18.5	19.5	20.5	21.6	22.6
	8							21.5	23.2	25.0	26.8	28.5	30.3	32.0	33.8	35.5	37.3	39.0

Note: Positive Moment Causes Tension on Top of Slab

Table B.14N. Maximum Negative Slab Moment in (in.-kips/ft) for 50 ft Roadway on 2[4Bxx] + 7[5Bxx] + 2[4Bxx].

Box Depth	Slab Thickness	Bridge Span (ft)																
(in.)	(in.)	30	35	40	45	50	55	60	65	70	75	80	85	90	95	100	105	110
	4	8.5	9.9	11.4	12.8	14.3	15.7											
20	6	18.2	21.3	24.4	27.6	30.7	33.8											
	8	31.4	36.7	42.1	47.5	52.9	58.3											
	4		6.8	7.7	8.7	9.7	10.7	11.7	12.7	13.7	14.7	15.7	16.7					
28	6		14.5	16.7	18.8	20.9	23.1	25.2	27.4	29.5	31.7	33.9	36.0					
	8		25.1	28.7	32.4	36.1	39.8	43.5	47.2	50.9	54.6	58.3	62.1					
	4					7.6	8.4	9.1	9.9	10.7	11.5	12.3	13.1	13.8	14.6			
34	6					16.3	18.0	19.7	21.4	23.0	24.7	26.4	28.1	29.8	31.5			
	8					28.2	31.0	33.9	36.8	39.7	42.6	45.5	48.4	51.4	54.3			
	4							7.5	8.1	8.7	9.4	10.0	10.7	11.3	11.9	12.6	13.2	13.9
40	6							16.1	17.4	18.8	20.2	21.6	22.9	24.3	25.7	27.1	28.5	29.9
	8							27.7	30.0	32.4	34.8	37.2	39.5	41.9	44.3	46.7	49.1	51.5

Note: Negative Moment Causes Tension on Bottom of Slab

Table B.15P. Maximum Positive Slab Moment in (in.-kips/ft) for 52 ft Roadway on 4Bxx + 9[5Bxx] + 4Bxx.

Box Depth	Slab Thickness	Bridge Span (ft)																
		30	35	40	45	50	55	60	65	70	75	80	85	90	95	100	105	110
(in.)	(in.)																	
	4	6.7	7.8	8.9	9.9	11.0	12.1											
20	6	14.6	17.0	19.4	21.8	24.2	26.6											
	8	25.4	29.6	33.8	38.0	42.1	46.3											
	4		5.5	6.2	7.0	7.8	8.6	9.3	10.1	10.9	11.7	12.4	13.2					
28	6		12.0	13.7	15.4	17.1	18.8	20.4	22.1	23.8	25.5	27.2	28.9					
	8		20.9	23.8	26.8	29.8	32.7	35.6	38.6	41.5	44.5	47.4	50.3					
	4					5.8	6.4	7.0	7.5	8.1	8.7	9.2	9.8	10.4	11.0			
34	6					12.7	14.0	15.2	16.5	17.7	19.0	20.2	21.5	22.7	24.0			
	8					22.1	24.3	26.5	28.7	30.9	33.1	35.3	37.5	39.6	41.8			
	4							5.4	5.9	6.3	6.8	7.2	7.7	8.1	8.6	9.0	9.5	9.9
40	6							11.9	12.9	13.9	14.9	15.8	16.8	17.8	18.8	19.8	20.7	21.7
	8							20.8	22.5	24.2	25.9	27.6	29.3	31.0	32.8	34.5	36.2	37.9

Note: Positive Moment Causes Tension on Top of Slab

Table B.15N. Maximum Negative Slab Moment in (in.-kips/ft) for 52 ft Roadway on 4Bxx + 9[5Bxx] + 4Bxx.

Box Depth	Slab Thickness	Bridge Span (ft)																
		30	35	40	45	50	55	60	65	70	75	80	85	90	95	100	105	110
(in.)	(in.)																	
	4	8.4	9.8	11.3	12.8	14.2	15.7											
20	6	18.1	21.2	24.3	27.5	30.7	33.8											
	8	31.1	36.5	41.9	47.4	52.8	58.3											
	4		6.9	7.9	9.0	10.0	11.0	12.1	13.1	14.2	15.2	16.3	17.3					
28	6		14.9	17.1	19.3	21.5	23.8	26.0	28.2	30.5	32.8	35.0	37.3					
	8		25.6	29.4	33.3	37.1	40.9	44.8	48.7	52.6	56.4	60.4	64.3					
	4					7.6	8.3	9.1	9.9	10.7	11.5	12.3	13.1	13.9	14.7			
34	6					16.3	18.0	19.7	21.4	23.1	24.8	26.5	28.2	29.9	31.7			
	8					28.1	31.0	33.9	36.8	39.8	42.7	45.7	48.6	51.6	54.6			
	4							7.3	7.9	8.5	9.1	9.8	10.4	11.0	11.7	12.3	13.0	13.6
40	6							15.6	17.0	18.3	19.7	21.1	22.4	23.8	25.2	26.5	27.9	29.3
	8							26.9	29.3	31.6	33.9	36.3	38.6	41.0	43.4	45.7	48.1	50.5

Note: Negative Moment Causes Tension on Bottom of Slab